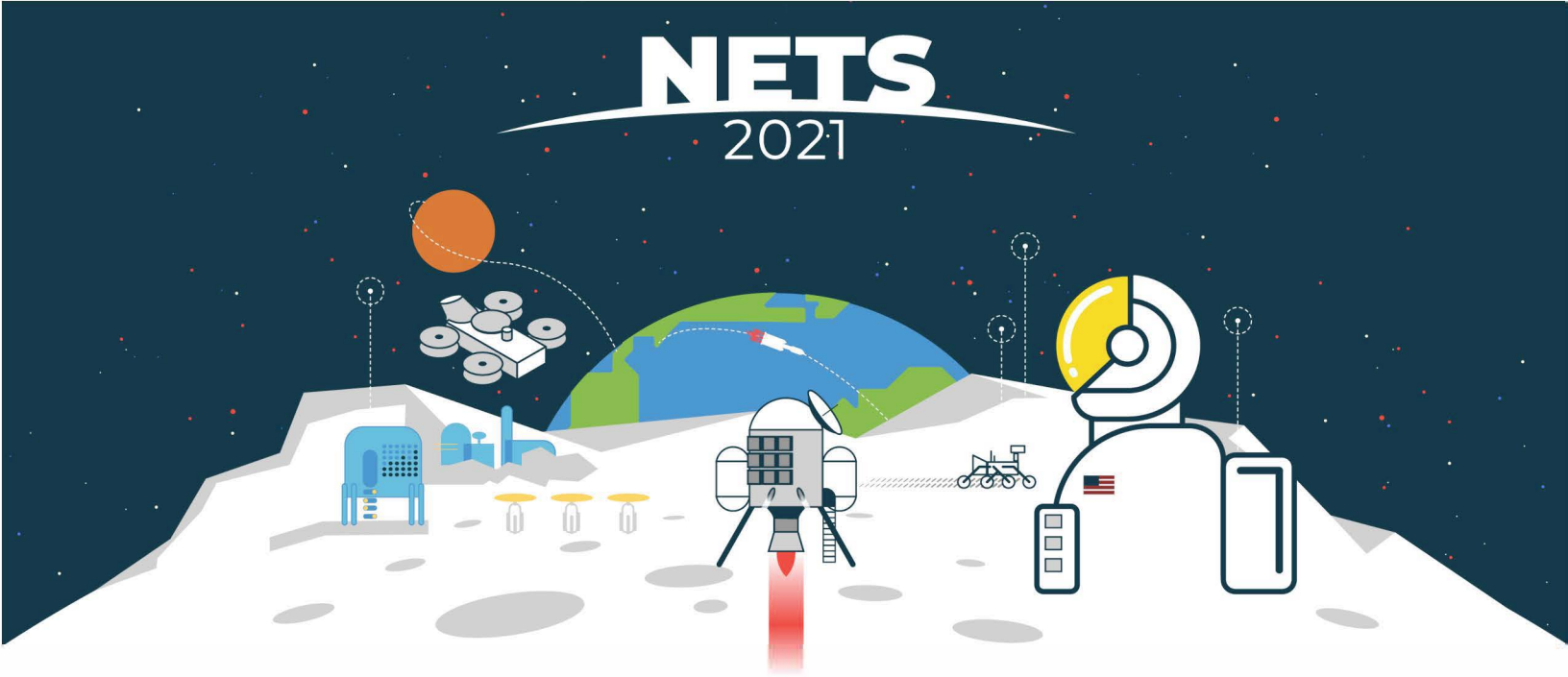

NUCLEAR and
EMERGING
TECHNOLOGIES for
SPACE

CONFERENCE PROCEEDINGS

Hosted by Oak Ridge National Laboratory

April 26th-30th, 2021

Track 1: Radioisotopes and Power Conversion Systems

Technical Track Chair(s): Scott Wilson

U.S. DEPARTMENT OF ENERGY

https://nets2021.ornl.gov

OAK RIDGE National Laboratory

Author	Title
Barco, Alessandra	Impact Studies for the ESA Radioisotope Power Systems
Barth, Christopher B.	Design of 1 KW Simplified Stirling Controller Using Capacitor-Based Power Factor Correction
Breedlove, Jeffrey J.	Turbo-Brayton Convertor for Radioisotope Power Systems
Clarke, Eric	Multi-Mission Thermoelectric Generator Assembly Testing and Launch Operations for Mars 2020
Collins, E.D.	Results, Implications, and Projections from Irradiation and Examination of Initial NpO_2 Test Targets for Improved ^{238}Pu Production
Katalenich, Jeffrey A.	Microsphere Plutonium-238 Oxide Fuel to Revolutionize New Radioisotope Power Systems and Heat Sources for Planetary Exploration
Kramer, Daniel P.	Developing Production Life Cycle (PLC) Levels Based on Production Factors and their Application in Determining the Production Readiness of a Heritage RTG Component (SiGe Thermocouples)
Lee, Young	Mission Concept Considerations for Ocean World Exploration Using RPS Inside a Pressure Vessel
Lesh, Andrew	Manufacturing Development of Chargeable Atomic Batteries, An Affordable Alternative to Plutonium-Based Radioisotope Heater Units and Thermoelectric Generators
Morrison, Christopher	Chargeable Atomic Batteries – Commercial Radioisotope Power Systems for Space and Terrestrial Missions
Overy, Robert D.	Next Generation Radioisotope Power for Space Exploration
Pierce, Jonathon	Spark Plasma Synthesis of SiGe Materials and Performance of Unicouples
Rhodes, Joshua	Mitigation of ^{208}Tl Gamma Dose from ^{236}Pu Decay Chain Via Chemical Removal of ^{232}U
Sadergaski, Luke R.	Online Monitoring of Radiochemical Processing Streams for the Plutonium-238 Supply Program
Thomas, Chris	High Energy Density Tritium Betavoltaics for MEMS and Sensor Data Gathering Applications
Zillmer, Andrew	Overview of Recent Pu-238 Production Activities at Idaho National Laboratory

Nuclear and Emerging Technologies for Space
Sponsored by Oak Ridge National Laboratory, April 26th-30th, 2021.
Available online at https://nets2021.ornl.gov

IMPACT STUDIES FOR THE ESA RADIOISOTOPE POWER SYSTEMS

Alessandra Barco[1], Richard M. Ambrosi[1], Christophe Fongarland[2], Yann Guguin[3], Pierre Brunet[3], Keith Stephenson[4]

[1]School of Physics and Astronomy, University of Leicester, LE1 7RH Leicester, UK
[2]ArianeGroup, 78133 Les Mureaux Cedex, France
[3]ArianeGroup, 91710 Vert-le-Petit, France
[4]ESA/ESTEC TEC-EP, 2201AZ Noordwijk, The Netherlands
Primary Author Contact Information: +44 (0) 116 373 6255, ab849@leicester.ac.uk

Since 2009, ESA has been conducting R&D activities leading towards the future development of a European capability in radioisotope power systems (RPSs) for space. An important aspect of the overall program is safety, and this involves ensuring that the design of these systems, in particular of the heat source (i.e. fuel and containment layers), meets a set of stringent requirements: it is fundamental to properly design them in order to avoid inadvertently releasing radioactive material into the environment in the event of an accident. Validated heat source accident models are necessary to inform the design iteration of the European ^{241}Am-based RPSs, and to construct a safety case for their launch.

The research project here presented was a collaboration, supported by ESA, between the University of Leicester and ArianeGroup. Its goal was to start the process of understanding the behavior of the fuel containment systems under the most relevant accident conditions by computer modelling, to validate them experimentally given the infrastructure, test facilities and expertise of ArianeGroup in this field, and to characterize the different materials. The data obtained will help to iterate and improve the design of the European RPS heat sources by focusing on the fuel containment systems.

I. INTRODUCTION

Radioisotope power systems have been employed in space missions since the beginning of spaceflight[1,2,3]: they can provide heat and electricity to the spacecraft subsystems thanks to the radioactive decay of the fuel element, without any moving part or need for maintenance. RHUs (radioisotope heater units) provide localized heat to keep critical components in their operating temperature range, while RTGs (radioisotope thermoelectric generators) supply electrical power thanks to the thermoelectric effect. Being capable of generating substantial amounts of heat for long periods of time, independently of the solar flux, they can be the most viable energy source for some space missions, such as the exploration of outer planets or the exploration of a planetary surface with long day/night cycles (Moon).

Since 2009, ESA has been developing its own RPS program, aiming towards a European capability for the independent design, production and management of RPSs [4]. This R&D program is focused on the use of americium-241, due its availability and relatively cost-effective production in the European context. The University of Leicester is leading the development of a 10 W_{el} RTG (with a specific electric power of around 1 W_{el}/kg) and a 3 W_{th} RHU. The ^{241}Am-based RHU is currently baselined for the ESA lunar mission EL3 (Ref. 5).

An activity supported by the ESA Networking/Partnering Initiative (NPI) started in May 2018, as a collaboration between the University of Leicester and ArianeGroup. This activity, which ended in October 2020, had three main tasks:

- Study of the impact mechanics of European RTG and RHU heat sources;
- Characterization of the different materials and structures under impact conditions;
- Analysis of the data to iterate and improve the European heat source designs.

II. DESIGN OF ESA HEAT SOURCES

Safety must be a fundamental part of an RPS program from the earliest phases, not only in relation to safety policies and management, but also for the system concept and design.

All heat source designs to date, both from the USA (the General Purpose Heat Source - GPHS, and the Light Weight RHU - LWRHU[1]) and Russia (Angel-RHU[2]), have focused on a multilayer architecture: this minimizes the probability of release of a radioisotope into the environment in case of accident (such as launch pad explosion, or Earth re-entry), while ensuring that heat and electricity can be distributed to the spacecraft as required. The different layers of the heat source architecture can have slightly different primary functional requirements (impact survival, or thermal protection from re-entry high temperatures and heat flux), but they all act as redundant and diverse containment structures.

The same approach has been followed in the ESA program (Figure 1). All the materials currently in use for the ^{241}Am-based flight design are available in Europe. The same material philosophy has been applied to both the RHU and the RTG heat source:

- An outer C-C (carbon-carbon) composite aeroshell. Its main purpose is for re-entry thermal

protection and, to a lesser extent, impact protection in case of accident. A number of 2.5D and 3D C-C composites have been evaluated, and the current design includes Sepcarb 3D (supplied by ArianeGroup);

- An insulation layer having very low thermal conductivity, to protect the fueled clad from the high temperatures associated with accident scenarios. Initially based on a rigid CBCF material, it is now a compressible graphite felt;
- A clad made of Pt-20Rh. This inner containment layer acts as a final safety barrier in the event that the aeroshell is breached. Pt-based alloys seem to be the most compatible, stable and least reactive materials that could meet the safety requirements for RPS. The current clad design includes threaded components for ease of sealing and welding, and a vent hole covered by a porous frit.

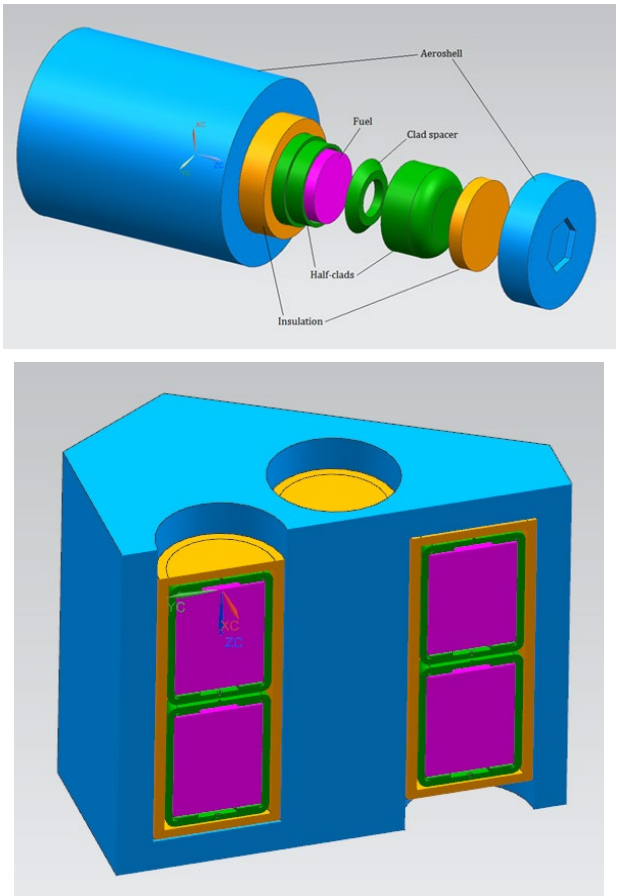

Fig. 1a (top) and 1b (bottom). CAD models for the ^{241}Am-based RHU (top) and RTG (bottom) heat source, not in scale: C-C composite for the aeroshell (blue), graphite felt for insulation (orange), Pt-20Rh for cladding (green), ^{241}Am-based fuel (purple)

III. IMPACT TESTS

To verify and certify the ability of radioisotope heat sources to survive different accident scenarios, in addition to software modelling, destructive and non-destructive safety tests are performed in representative environments. The first impact tests for the ESA heat sources were performed in March 2019 in France, at ArianeGroup's Research Center (Vert-Le-Petit); a second testing campaign took place at the same site in November 2019.

III.A. Testing configuration

The samples were accelerated through a He-pressurized gas gun, and they impacted on a concrete slab positioned at the opposite end of the gun in a dedicated test chamber. Concrete was chosen as impact surface to simulate the ground, but other potential options for future tests can include granite and steel. Sensors were placed at the exit of the gas gun and on the first impact plate in front of the concrete slab, in order to measure the time of contact with the projectile assembly. By knowing these instants and the distances between the various components of the set-up, it was then possible to calculate the velocity of the sample shot. The gas gun pressure was regulated to have an impact velocity in the same range as the terminal velocity calculated in the preliminary re-entry studies (whenever possible). However, it is important to highlight that the terminal velocity does not coincide with the maximum velocity that can be reached by the heat source: if the accident environment (e.g., explosion) pushes it downward or towards another target, it is possible for the heat source to hit the ground or the target much faster.

III.B. First testing campaign

The samples were tested in different orientations, as demanded by the safety requirements compiled by the University of Leicester. Five simulant-fueled clads were used during the first testing campaign: molybdenum was chosen as a mass dummy for the fuel (since it has a similar density to americium oxide). The 4 RTG clads were made of stainless steel, but they were representative of the flight design in terms of dimensions. The fifth sample was a smaller version of the RHU clad from a previous phase of the project, made of Pt-30Rh, and without the thread to join the two parts (only the TIG-welding).

TABLE 1. Impact tests results from the first campaign.

Shot	Sample	Orientation	Speed [m/s]	Gas gun pressure [bar]
1	RTG1	End-on	140	7.4
2	RTG2	End-on	109	6.2
3	RHU	End-on	129	4.7
4	RTG3	Side-on	117	4.8
5	RTG4	Side-on	144	7.4

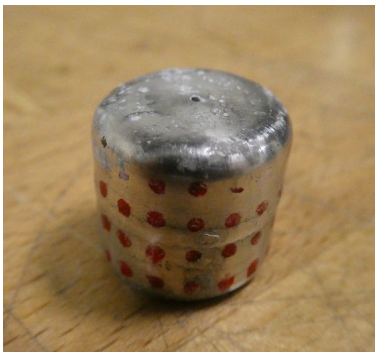

Fig. 2. Pt-30Rh RHU clad, end-on impact

III.C. Second testing campaign

Four samples were tested during the second campaign:

- Cylinder of C-C composite, with the aeroshell dimensions and previously subjected to laser testing;
- Full RHU, previously subjected to laser testing;
- RHU clad, made of Pt-20Rh and previously impacted inside the RHU, with a glass ceramic as fuel simulant;
- A second RHU clad, made of Pt-20Rh, with molybdenum as fuel simulant.

Although the final velocities calculated in the re-entry studies were lower, it was decided to keep the speed in nearly the same range of the first campaign, in order to have a more direct comparison of the results. Additionally, if the samples could sustain an impact at higher speeds than those expected, the design would provide more confidence in case of accident.

Fig. 3. Pt-20Rh RHU clad, impacted twice end-on

IV. POST-TEST INVESTIGATIONS

The choice of the right materials and design features is mandatory in order to have a safe and reliable nuclear heat source. Therefore, post-tests investigations of the samples were conducted at ESA/ESTEC and at the University of Leicester, to characterize the behavior of both the materials and the whole design of the heat sources.

Only the three Pt-Rh samples were studied in detail.

While two of the clads showed only negligible erosion on the rounded edges, preliminary stereomicroscopy analyses on the RHU clad impacted twice showed a crack in the weld area. Additional SEM analyses on the sectioned clad revealed that the "crack" was simply the joint between the two parts of the clad (the lid and the longer sleeve), right at the base of the thread: based on the shape of the grains visible after etching, it appears that the welding depth was not enough to guarantee a perfect joint of the clad parts.

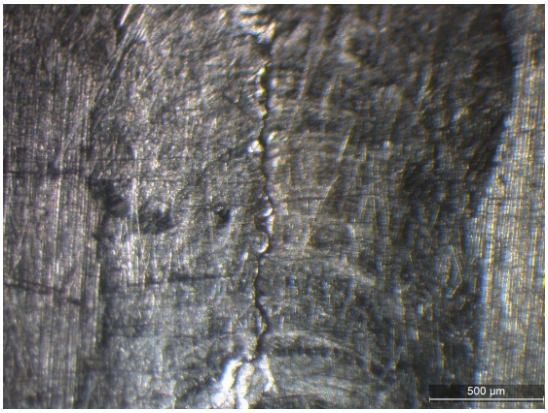

Fig. 4. Detail of the weld area for the RHU clad impacted twice (stereomicroscopy).

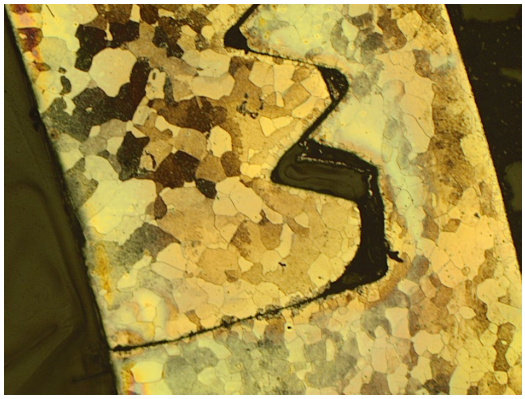

Fig. 5. Detail of the weld area for the RHU clad impacted twice (optical microscope).

Some porosity inclusions around the weld region were also detected: they had been likely caused by some particulate contamination on the weld areas surfaces, or by inadequate gas shielding in the weld process.

These analyses are giving a first indication that the Pt-20Rh clads can survive impacts at speeds higher than their final velocities. However, the welding parameters

should be analysed, and potentially changed, to improve the ability of the clad weld to survive impacts.

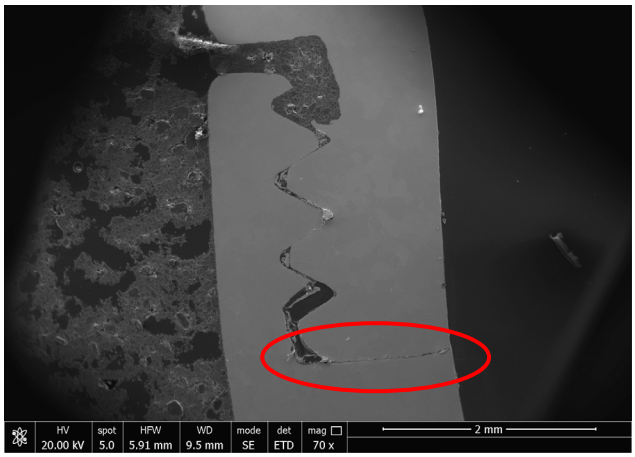

Fig. 6. Detail of the weld area for the RHU clad impacted twice (SEM).

V. IMPACT MODELLING

In addition to experimental campaigns, software modelling is an essential part of the design process, since it allows studying a wide range of scenarios with different boundary conditions and assumptions, without relying on expensive samples and tests.

The software used for the impact modelling is the hydrocode LS-Dyna. Hydrocodes are computer programs for the study of very fast, very intense loading on materials and structures; the name derives from the hydrodynamic behavior of the materials, assumed when the loading conditions exceed the material strength properties by several order of magnitude.

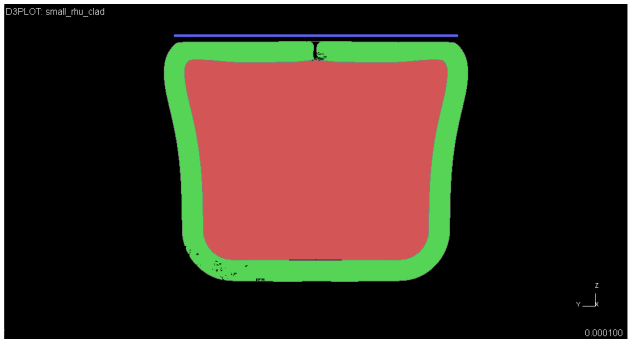

Fig. 7. After-impact deformation of the Pt-30Rh clad from the first testing campaign (FE model)

Preliminary simulations where the Pt-Rh alloys and molybdenum have been modelled as elasto-plastic hydrodynamic materials show the same deformation present in the impacted samples, although the "bell" shape is highly emphasized. This could be caused by the choice of boundary conditions (rigid wall instead of concrete); or, the behavior of the materials might be at the lower boundary of the hydrodynamic field. Therefore, other material models are being considered for the Pt-Rh, including the Johnson-Cook model: this model is an experimentally-based visco-plastic constitutive equation, and can provide a fairly realistic representation of the material behavior especially in case of subsonic impact velocities.

VI. CONCLUSIONS

The NPI activity here presented was the first step in the safety studies for the ESA ^{241}Am-based heat sources, and it is closely related to other ongoing activities that will allow to achieve TRL5 for the development maturity of the encapsulation systems. While the focus of this activity was on the fuel inner containment systems, the next step will be to properly model the nuclear fuel in ceramic form and the carbon-based materials.

Since Europe and ESA currently do not have an operational launch safety framework, this project is also closely related to the ongoing definition of a launch safety and authorization process (LSAP) for European missions with radioisotope power systems.

The collaboration between France and the UK will be a fundamental step to build further and deeper collaborative links in the European space nuclear power program, especially when the ESA RPS program is at a stage to transition from an R&D phase to an industry activity.

REFERENCES

[1] NASA Radioisotope Power Systems website, https://rps.nasa.gov/ (accessed 21/03/2019).

[2] G.L. Bennett, *Mission interplanetary: Using radioisotope power to explore the solar system*. Energy Conversion and Management, 49 (2008), 382–392.

[3] N.N. Ponomarev-Stepnoi et al., *Russian space nuclear power and nuclear thermal propulsion systems*. Nuclear News, 43 (13) (2000), 33-46.

[4] R.M. Ambrosi et al., *Radioisotope power systems for the European space nuclear power program*, 40th IEEE Aerospace Conference, Big Sky (MT, USA), March 2019.

[5] K. Stephenson and M Landgraf, *Hybrid radioisotope-solar power systems as a key to sustained lunar exploration*. 12th European Space Power Conference, Juan-les-Pins, France, 30 September - 4 October 2019.

Nuclear and Emerging Technologies for Space
Sponsored by Oak Ridge National Laboratory, April 26th-30th, 2021.
Available online at https://nets2021.ornl.gov

DESIGN OF 1 KW SIMPLIFIED STIRLING CONTROLLER USING CAPACITOR-BASED POWER FACTOR CORRECTION

Christopher B Barth, Donguk Max Yang, and Max F Chaiken

[1]*NASA Glenn Research Center, Cleveland, Ohio, 44135*

Primary Author Contact Information: Christopher.b.barth@nasa.gov, 216-433-2678

Free-piston Stirling convertors provide efficient, reliable thermal to electric power conversion, provided they are paired with a reliable controller. This paper outlines work underway on design concepts for kilowatt-class controllers. Using passive power factor correction (PFC) this design explores the possibility of reducing programmatic risk through system simplification. Efficiency is maximized through incorporating wide-bandgap gallium nitride (GaN) switches, and passive PFC volume is minimized through the use of polymer multi-layer capacitors. This work is aimed at exploring new approaches for future Stirling controllers.

I. Project Background and State of the Art

Free-piston Stirling convertors are capable of converting heat energy into electricity at 3-4 times higher efficiency than radioisotope thermoelectric generator (RTG) systems and have a higher power density than Brayton systems in the 1 to 10 kW power range. This characteristic has made them appealing for space power applications, but Stirling engines also require a controller to maintain stable operation. The implementation of controllers has proven to require significant development and this work seeks to identify strategies for controller simplification.

I.A. Stirling and Controller Optimization

The NASA Glenn Research Center (GRC) has made steady progress with corporate partners on the development of both Stirling convertors and controllers for Dynamic Radioisotope Power Systems (DRPS). Specifications have been guided by historical precedent in the design of 75 W convertors and the needs of 28 V spacecraft power buses. The development of 1 kW space-qualified Stirling convertors and controllers for the Fission Surface Power (FSP) project will benefit from a system-level optimization.

There are a few key differences between Stirling control for FSP and prior DRPS systems. The most prominent is that DRPS systems are required to remain operational from fueling through end of mission, necessitating that the Stirling control system operate through launch. FSP mission concepts call for the system to be activated after landing on the moon alleviating the launch requirements. Another simplification of the FSP system arises from the introduction of centering springs into most of the candidate Stirling engine concepts. This change will likely make the engines self-starting and eliminate the need for extended motoring at startup. The design proposed here capitalizes on these characteristics.

I.B. Power Factor Correction

The control of free-piston Stirling convertors has historically been complicated by high winding inductance in the alternator. This inductance, and the resulting reactive impedance, limit the flow of power from the Stirling alternator and prevent an energy balance between thermal energy flowing into the convertor and electrical energy leaving the alternator. The difference between the thermal energy input and the electrical load results in excess mechanical energy in the piston, causing over-stroke and damaging the convertor. In order to maintain control of the engine, the winding inductance must be negated using power factor correction (PFC).

PFC can be accomplished actively using an H-bridge to emulate capacitive reactance by enforcing a phase shift between the Stirling alternator current and voltage. Active PFC control can be implemented using a digital controller. The Dual Convertor Controller (DCC) and Advanced Stirling Convertor Control Unit (ACU), are two prior designs developed with oversight from GRC to control 75 W Stirling convertors, which employed an FPGA with relatively complex control for PFC functionality.

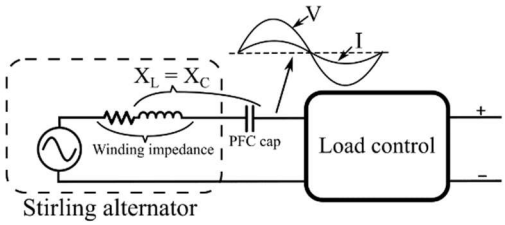

Figure 1: Capacitor-based PFC

An alternative to active PFC is the use of a series-connected capacitor which reduces controller complexity as well as voltage stress on the main power switches. The capacitor-based PFC controller approach, as shown Figure 1, has been demonstrated in breadboard-form as the 75 W NASA Analog Controller (NAC). Historically, the use of PFC capacitors for flight designs has been avoided because of their large size and unverified reliability. Polypropylene

capacitors following the MIL-PRF-83421/2 specification are the most appropriate legacy devices for this application, and 1 kW class Stirling convertors anticipated for FSP will require approximately 36 parallel devices resulting in a volume of 1.2 L, and a mass of 0.7 kg (1.5 lbs). for each convertor. This volume is challenging for large arrays of 8 or more engines in fission applications, and more so when redundancy is considered.

II. System design methodology and core strategy

The high radiation environment and high engine count (8, 12 or 24) required for the FSP project motivates the consideration of a simplified controller which minimizes development risks in cost and schedule. All electronic components, the circuit topology, and thermal management demonstrated in this research are being selected to have a path to flight within the timeframe of the FSP project or are representative of existing flight components.

II.A High-density NanoLam capacitors

To address the need for high-density capacitors for Stirling controllers, NASA has awarded an FY21 Small Business and Innovation and Research (SBIR) Phase I contract to Sigma Technologies/Polycharge of Tuscon, AZ, to adapt their polymer nanolaminate or "NanoLam" capacitors for use in Stirling controllers. NanoLam capacitors are fabricated via vacuum deposition and comprised of 1000s of nano-capacitors formed from polymer dielectrics and aluminum electrodes. The nano-laminate material is formed in sheets then cut and stacked to form capacitors with voltage ratings from 10-10,000 V.

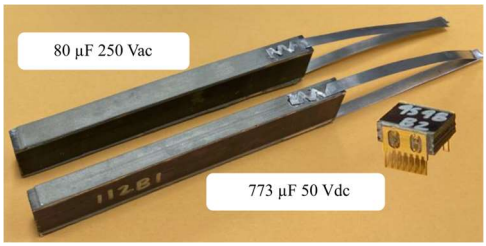

Figure 2: Unencapsulated NanoLam capacitors

The NanoLam technology replaces the process of film extrusion, metallization, and winding used in film capacitors with a simplified process in which aluminum wire and a monomer liquid are introduced into a machine that converts them into a large "mother capacitor" of nanolaminate material. This manufacturing simplification combined with the use of low-cost radiation-cured monomers used to form the cross-linked dielectrics makes NanoLam technology highly cost competitive when compared to film and multi-layer ceramic capacitors (MLC). NanoLam devices have demonstrated an energy density (J/cc) four times higher and a specific energy density (J/kg) 10 times higher than dc multilayer ceramic MLC capacitors. Additionally a capacitance density nearly two orders of magnitude higher than legacy mil-spec devices suitable for PFC applications has been achieved in unpackaged devices. NanoLam capacitors also do not exhibit voltage bias derating but do offer self-healing, open-mode failure, and superior radiation hardness to polypropylene devices. Figure 2 shows two of the prototype NanoLam capacitors developed by Sigma Technologies/Polycharge.

II.B Active Device Selection

Wide bandgap devices such as Gallium Nitride (GaN) and Silicon Carbide (SiC) have promised advances in space power for some time because of their general resilience to ionization and higher figures of merit than silicon devices, however challenges related to device quality and single event effects (SEEs) have limited their use in space power to commercial applications in near-earth orbit. To motivate further adoption of these devices in space power, this work is evaluating the use of GaN devices from two suppliers of high-reliability devices targeting the space market. While these devices do not have flight heritage with NASA, discussions with industry representatives and NASA radiation and quality experts have indicated that they are representative of GaN devices which could feasibly be brought to flight within the timeframe of the FSP project.

II.C. Stirling control strategy

Achieving high power factor requires minimal phase shift between line current and voltage as well as minimal distortion in the current waveform. With the challenge of phase shift being handled directly by a capacitor, the remaining functionality of the Stirling controller is to provide a low total harmonic distortion, unity power factor load to the Stirling. This functionality is common in terrestrial applications with one common topology being the totem-pole bridgeless PFC converter shown in Figure 3. The line frequency switches of the totem-pole converter perform rectification at the engine frequency and the high frequency switches perform boost functionality with alternating polarity.

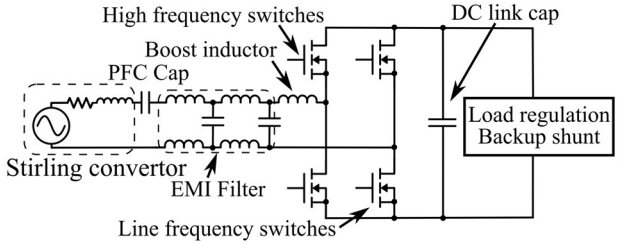

Figure 3: Schematic of Stirling PFC controller stage implemented with totem-pole bridgeless boost

While continuous conduction mode (CCM) is historically the most frequent strategy for boost PFC control, hardware and control can be simplified through the use of boundary conduction mode (BCM) or discontinuous conduction mode (DCM). In these approaches, the inductor

current either instantaneously reaches zero each switching cycle (BCM) or returns to zero for a percentage of each switching cycle (DCM). Neither BCM nor DCM requires the accurate measurement of inductor current. Under BCM it is sufficient to sense the inductor current zero crossing by means of a sense winding on the boost-inductor coil and no sensing is required for DCM operation. Figure 4 shows a comparison of the inductor current waveforms for CCM and DCM.

The DCC and ACU controller designs have implemented using CCM-type control, however in an effort to explore a simplified control system, this work has pursued the use of DCM control. Under DCM, the high-frequency control loop regulating the inductor current amplitude is eliminated and the boost converter runs at a constant frequency and duty ratio with the system designed to ensure that the inductor current returns to zero each switching cycle [1]. This control is easily accomplished using radiation-tolerant analog ICs. The average line current flowing into the boost circuit is in phase with the line voltage due to the changing volt-second balance on the inductor resulting from the changing input voltage. A properly designed DCM boost stage can maintain efficiency on par with CCM control despite the higher RMS inductor current under DCM as shown in Figure 4. This is partially due to the elimination of switching losses in the boost diode during DCM operation [1].

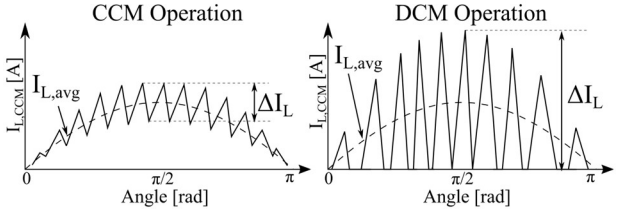

Figure 4: Comparison of CCM and DCM waveforms

Using the DCM approach, there is no control needed at the switching frequency and only minimal changes in duty ratio over the line cycle to optimize power factor and control the piston stroke to the proper amplitude. Flyback, Cuk, and SEPIC converters can produce unity power factor as PFC circuits operating in DCM, however a boost-style converter will exhibit distortion in the current waveform as the peak line voltage approaches the dc link voltage [2] [3]. For this reason, the design is constrained such that a minimum boost ratio of 15% is required between the peak ac amplitude and the dc link voltage.

During CCM operation, the boost converter raises voltage between input and output as a function of duty ratio (d) according to the relationship,

$$V_{out} = \frac{1}{1-d} V_{in}. \quad (1)$$

In DCM operation, the voltage conversion ratio is more complex. The approximate duty ratio needed to load the Stirling may be calculated based on the impedance conversion which must take place between the Stirling and the dc link at the output of the controller. The input and output impedance of the boost stage is simply calculated as,

$$R_{in} = \frac{V_{Stirling}}{I_{Stirling}} \ \ and \ \ R_{out} = \frac{V_{dc\,link}^2}{P_{dc\,link}}. \quad (2)$$

The required gain (M) between the input and output voltage can be stated in terms of impedance as,

$$R_{in} * M^2 = R_{out} \quad \rightarrow \quad M = \sqrt{\frac{R_{out}}{R_{in}}}. \quad (3)$$

The dimensionless parameter K is an indication of the range of conditions over which a boost converter will operate in DCM. For $K > K_{crit}$ the converter will run in CCM and for $K < K_{crit}$ the converter will run in DCM [4]. K and K_{crit} are calculated in terms of the boost inductance (L), the switching frequency (f_{switch}) and the duty ratio for the boost converter as,

$$K = \frac{2\,L\,f_{switch}}{R_{out}} \ \ and \ K_{crit} = d(1-d)^2. \quad (4)$$

The gain for a boost converter in DCM is [4],

$$M = \frac{1+\sqrt{1+\frac{4d^2}{K}}}{2}. \quad (5)$$

Constraining the system to operate in DCM, the duty ratio required to load the Stirling can be calculated as,

$$d = \sqrt{K * (M^2 - M)}. \quad (6)$$

The boost duty is tuned at low bandwidth to maintain the appropriate alternator loading and voltage amplitude.

II.D. System-level optimization

Mass and loss minimization is important for flight applications, but a tradeoff often exists between these two design goals. Additionally, circuit components for flight are limited by reliability and radiation hardness requirements, and semiconductor switches, inductors and capacitors are available with discrete values and limitations. This makes solving a continuous optimization for the best trade between efficiency and power density very challenging and minimally beneficial. Instead of a continuous optimization, a random process can be used to develop a Pareto design front indicating the optimized trade space [5]. The optimization is accomplished using a script to generate a large number of feasible circuit designs based on an available parts library and acceptable limitations for variables such as alternator current/voltage, switching frequency, and conducted EMI [6].

In this work, a script has been created in Matlab to generate and evaluate the performance of a large number of plausible circuit designs. After each selection, following selections were restricted to ensure the system would function as designed. The selections made for each design iteration include:

- Number of parallel interleaved boost stages
- Primary switch
- DC link voltage

- Boost diode
- Stirling alternator voltage and resulting impedance
- DC link capacitor size
- PFC capacitor size
- Switching frequency
- Inductor selection
- DCM duty ratio
- Input differential mode filter stage count and sizing

After the design is formulated, linear loss and mass models (objective functions) are used to evaluate the design performance. Simplified linear loss estimates are used for the Pareto optimization because the ability to quickly iterate over a large number of candidate designs and calculate their relative merit is more important than knowing the precise efficiency. After analysis, the efficiency and mass of each design is then plotted as shown in Figure 5. In this example the trade front is relatively sharp, and choosing the design closest to the lower left corner will result in the best trade between efficiency and power density.

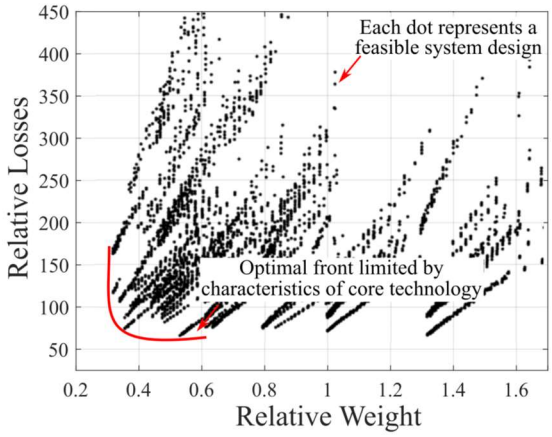

Figure 5: Pareto plot of feasible system designs showing relative weight and losses

III. Control simulation results

Simulations have been conducted using LT Spice with a Stirling model to validate the concept of DCM boost control of a Stirling engine. Assuming the use of self-centering engines in the FSP application, the engine temperature and piston amplitude will rise with reactor start-up. During this interval, the controller will present a small constant impedance load to the engine. As the piston amplitude increases the controller PI control will adjust the boost duty ratio to limit engine voltage and piston motion to the designed amplitude.

Figure 6 shows the plot of regulated engine operation with the PI control nearly constant throughout the ac cycle of the engine. This is the only dynamic control required for the DCM boost controller strategy and is implemented using simple analog operational amplifiers widely available as high-reliability, SEE tolerant devices.

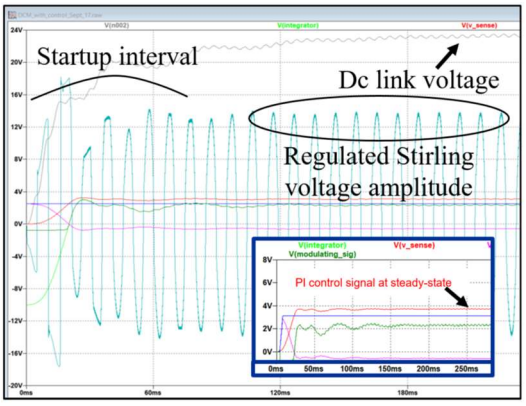

Figure 6: Plot of simulated Stirling and controller waveforms

III. Conclusions and next steps

This work has motivated a simplified Stirling control strategy focused on multi-engine fission applications. The development of NanoLam PFC capacitors was discussed as well as the active devices and DCM control strategy being used. The design optimization strategy is outlined as well as preliminary simulation results showing control functionality. Hardware and experimental results will be presented in future work.

ACKNOWLEDGMENTS

Special thanks to Dr. Tomas Modeer of SCiBreak, Stockholm, Sweden for the use of his Pareto front template script.

References

[1] K. Raggl, T. Nussbaumer, G. Doerig, J. Biela and J. Kolar, "Comprehensive Design and Optimization of a High-Power-Density Single-Phase Boost PFC," *IEEE Transactions on Industrial Electronics,* vol. 56, no. 7, pp. 2574-2587, 2009.

[2] L. Rossetto, G. Spiazzi and P. Tenti, "Control Techniques for Power Factor Correction Converters," in *Power Electronics, Motion Control and associated applications (PEMC)*, Warzawa, Poland, 1994.

[3] K.-H. Liu and Y.-L. Lin, "Current Waveform Distortion in Power Factor Correction Circuits Employing Discontinuous-mode Boost Converters," in *20th Annual IEEE Power Electronics Specialist Conference*, Milwaukee, WI, 1989.

[4] P. T. Krein, Elements of Power Electronics, New York: Oxford University Press, 1998, pages 117-124.

[5] J. Kolar, J. Biela, S. Waffler, T. Friedli and U. Badstuebner, "Performance Trends and Limitations of Power Electronic Systems," in *6th International Conference on Integrated Power Electronics Systems*, Nuremberg, Germany, 2010.

[6] T. Modeer, N. Pallo, T. Foulkes, C. B. Barth and R. C. N. Pilawa-Podgurski, "Design of a GaN-Based Interleaved Nine-Level Flying Capacitor Multilevel Inverter for Electric Aircraft Applications," *IEEE Transactions on Power Electronics,* vol. 35, no. 11, pp. 12153-12165, 2020.

[7] T. Nussbaumer, K. Raggi and J. Kolar, "Design Guidelines for Interleaved Single-Phase Boost PFC Circuits," *IEEE Transactions on Industrial Electronics,* vol. 56, no. 7, pp. 2559-2573, 2009.

Nuclear and Emerging Technologies for Space
Sponsored by Oak Ridge National Laboratory, April 26th-30th, 2021.
Available online at https://nets2021.ornl.gov

TURBO-BRAYTON CONVERTER FOR RADIOISOTOPE POWER SYSTEMS

Jeffrey J. Breedlove[1], Thomas M. Conboy[1], and Mark V. Zagarola[1]

[1]*Creare LLC, 16 Great Hollow Road, Hanover, NH 03755*

Jeffrey J. Breedlove: 603-643-3800, jfb@creare.com

Creare has teamed with Aerojet Rocketdyne, the University of New Mexico Institute for Space and Nuclear Power Studies (UNM ISNPS), Sest Incorporated (Sest), and West Coast Solutions to develop a turbo-Brayton power converter for future National Aeronautics and Space Administration (NASA) missions that use radioisotope heat sources. NASA has considered the closed Brayton cycle attractive for spaceflight applications since the 1960s, and Creare has developed miniature Brayton technology for over 40 years. Key characteristics include high specific power, high efficiency, long-life operation without wear, undetectable vibration, and flexible packaging. Detailed design results indicate a 300 We-class converter with a turbine inlet temperature of 730°C will have a thermal-to-electric conversion efficiency of nearly 25% and a specific power greater than 20 We/kg. Prototype converter testing is scheduled to begin in April to verify these predictions.

I. INTRODUCTION

Future NASA space missions require advanced systems to convert thermal energy into electric power for long durations. Closed-loop Brayton converters are attractive for these applications because they enable high reliability, long life, and high specific power (W/kg). They also consist of discrete components that can be packaged to fit optimally with other subsystems, and their continuous gas flow can communicate directly with remote heat sources and heat rejection surfaces without heavy conductive links or intermediate flow loops.

Prior closed Brayton cycle work at Creare has focused on cryogenic refrigerators for spaceflight applications. This experience provides critical expertise, which is now being leveraged to develop power converters for space. The resulting technology is readily scalable for power levels from tens of watts to hundreds of kilowatts and beyond. Potential near-term NASA applications include Radioisotope Power System (RPS) devices, "Kilopower" reactor concepts, Nuclear Electric Propulsion (NEP), and Surface Power missions.

Creare, Aerojet Rocketdyne, UNM ISNPS, Sest, and West Coast Solutions form a complementary team. Creare is designing, fabricating, and testing the converter; Aerojet Rocketdyne performed preliminary system design integration activities; UNM ISNPS evaluated thermal performance for the heat source assembly; Sest assessed converter reliability and robustness; and West Coast Solutions designed spaceflight power conversion and control electronics. The combined efforts of our team enable development of a prototype converter with a path to a complete generator system that is practical and attractive for future space missions.

II. TECHNOLOGY DESCRIPTION

Figure 1 is a schematic representation of a closed-loop Brayton converter. In this configuration, the compressor pressurizes the cycle gas and forces it to pass through the system in a continuous loop of steady flow. The temperature of the cycle gas increases as it flows through the recuperator and the hot interface heat exchanger. The hot, high-pressure gas then produces mechanical power as it expands through the turbine. The turbine exhaust stream transfers most of its heat to the high-pressure flow stream via the recuperator. The precooler then transfers waste heat to the heat rejection system before the gas is re-pressurized. The compressor impeller and turbine impeller are attached to a common shaft with a permanent-magnet alternator between them. As a result, the mechanical power produced by the turbine drives the compressor directly, and excess shaft power generates electric power via the alternator. The power conversion electronics transform the high-frequency, three-phase, alternator output into regulated DC power for general use. A heat rejection system transfers waste heat from the precooler, turbomachine housing, and electronics to space via radiator surfaces.

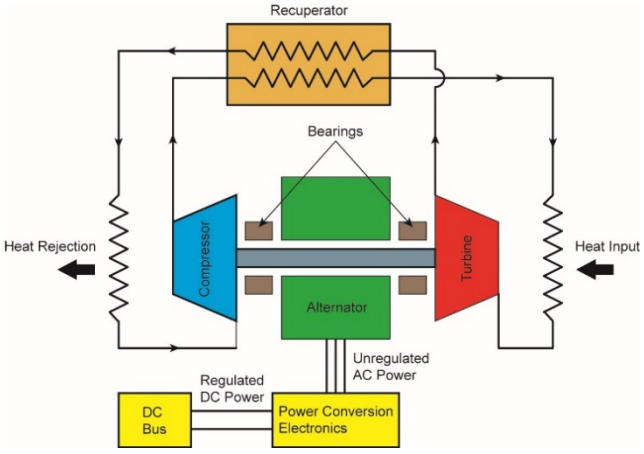

Fig 1. Schematic for closed-loop Brayton converter.

The only moving part in the converter is a miniature turbomachine rotor. Hydrodynamic gas bearings and clearance seals eliminate mechanical contact between moving surfaces. This lack of contact permits high rotational speeds, which is important for high efficiency and specific power; and it also enables extremely long maintenance-free life. Creare has performed several reliability and endurance tests, including a 14-year life test and over 10,000 start/stop cycles with no maintenance, wear, or performance degradation.[1]

III. HERITAGE

The converter builds on proven technology for miniature turbo-Brayton systems Creare has developed for long-duration space missions. These systems have satisfied rigorous NASA and Department of Defense requirements for reliability, endurance, vibration emittance, space launch tolerance, electromagnetic interference and susceptibility, and environmental cycling.[1,2] One such system is a turbo-Brayton cryocooler that operated on the Hubble Space Telescope for over 6.5 years without maintenance or performance degradation while meeting all mission requirements.[3] Subsequently, Creare made significant improvements in manufacturing,[4] and is continuing advanced component and system development for several emerging applications.[5,6] Creare began applying turbo-Brayton technology toward the development of miniature power converters for NASA in 2001,[7,8] and this work is continuing today. These projects have demonstrated fundamental technologies required at the sizes, power levels, temperatures, and rotational speeds needed for radioisotope power system converters.

IV. TURBOMACHINE

A single turbomachine assembly contains the turbine, alternator, and compressor. It has a hot end and cold end, joined together by relatively thin metal features. These thin features provide adequate structural rigidity for mechanical loads while minimizing conductive heat transfer. The compressor, alternator, and bearings are located at the cold end of the assembly. The rotor shaft extends from the cold end to the hot end, where the turbine is located. The turbine is the only major component at the hot end of the assembly.

The turbomachine includes a small high-speed rotor with a mass of only 39 grams. The rotor has a compressor impeller and a turbine impeller attached to a common shaft, and a permanent magnet is installed inside the hollow shaft to provide the rotating magnetic field for the alternator. The impeller diameters are 19 mm (0.75 inch), and the shaft diameter is 9.53 mm (0.375 inch). Figure 2 is a photograph of the rotor assembly with compressor impeller and thrust bearing disk (left) and turbine impeller (right).

The turbomachine is designed to operate during launch, consistent with RPS program requirements. Prior Creare Brayton systems have completed vibration qualification tests and spaceflight launches. Most notably, the Creare cryocooler on the Hubble Space Telescope endured qualification testing, two Space Shuttle launches, and one landing. Several other programs have also conducted vibration tests with Creare turbomachines. However, none of these tests were performed while the turbomachines were operating because none of the applications required operation during launch. Consequently, extensive computational fluid dynamics analyses have been completed to assess rotordynamic operation during launch, and a risk-reduction vibration test will be performed with a representative rotor assembly to corroborate the results.

Fig 2. Rotor assembly with compressor impeller and thrust bearing disk (left) and turbine impeller (right).

V. RECUPERATOR

The recuperator is a microtube heat exchanger with counter current flow. It is an advanced adaptation of traditional shell and tube technology commonly used for industrial heat exchangers. The RPS embodiment is significantly lighter and smaller than conventional shell and tube heat exchangers and plate fin units with the same performance characteristics. High performance is achieved by utilizing thousands of very small tubes. Small length scales enable extremely high heat transfer area per unit volume without the need for secondary surfaces (i.e., fins). The result is very high heat transfer density with very low pressure losses. Longitudinal conduction from the hot end to the cold end is also very low, which is important when high thermal effectiveness is desired.

The RPS recuperator is very similar to five units Creare recently built for a turbo-Brayton refrigerator to enable cryogenic propellant storage in space for NASA missions.[9] The cryocooler version passed NASA General Environmental Verification Specification launch vibration qualification testing, and analyses indicate the RPS version has greater design margin.

The recuperator is an all-welded stainless steel assembly. There are no braze joints. The tubes are 304 stainless steel (UNS S30400), and all of the other components are 316L stainless steel (UNS S31603).

Stainless steel has acceptable strength and creep resistance for the specified operating conditions. The predicted stress in the microtubes is only 8.9 MPa (1,300 psi) due to their small diameter. Stresses in the outer shell and headers are greater because of their larger sizes; however, material thicknesses in these areas have been specified to achieve acceptable creep life with desired reliability.

Creare developed the microtube heat exchanger technology and associated manufacturing processes collaboratively with Mezzo Technologies Incorporated and Edare LLC. Several units have been built, and the required fabrication processes have been demonstrated. The supply chain, manufacturing process, and quality control are well established and have demonstrated consistently high quality. Figure 3 is a photograph of the recuperator built for the RPS prototype converter.

Fig 3. Recuperator for RPS prototype converter.

VI. LIFE AND RELIABILITY

Long life with high reliability is critical for spaceflight power systems. Consequently, Sest was recruited to conduct an objective life and reliability assessment with assistance from Creare. The results from this work formed the basis for further independent review currently being conducted by a Risk-Informed Life Testing team led by the Johns Hopkins University Applied Physics Laboratory.

Long life is straightforward to achieve since there is no lubrication or sliding contact during operation, and axisymmetric rotation produces negligible reciprocating forces to initiate fatigue. The life-limiting factor for the converter is centrifugal creep of the turbine rotor. Although high temperature and high speed are desired to maximize efficiency and specific power, both factors are limited to maintain centrifugal creep growth within acceptable limits. Detailed finite element analyses indicate that the RPS life goal of 20 years of operation time (3 years of ground storage and 17 years of operation in space) can be achieved with a turbine inlet temperature of 730°C, using Inconel 718 (UNS N07718) for the turbine impeller. However, creep tests with samples from the selected material lot are required to validate these predictions.

VII. GENERATOR SYSTEM CONCEPT

Creare and Aerojet Rocketdyne worked together to develop a conceptual design for a generator system with a spaceflight configuration. A key requirement is that the assembly must fit within the USA/9904/B(U)F-85 Radioisotope Thermoelectric Generator Transportation System. The resulting design is very similar to the design Rockwell International Corporation (forerunner to Aerojet Rocketdyne) developed previously for the 500 We Dynamic Isotope Power System for the JPL Mariner Mark 2 spacecraft.[10] Figure 4 shows two Creare converters integrated with two electronics assemblies, six General Purpose Heat Source Step 2 modules, and a heat rejection system. This configuration enables both converters to operate at approximately half power, or one converter to operate at full power. The two converters are hermetically isolated from each other with independent gas charges, so they do not interact directly with each other.

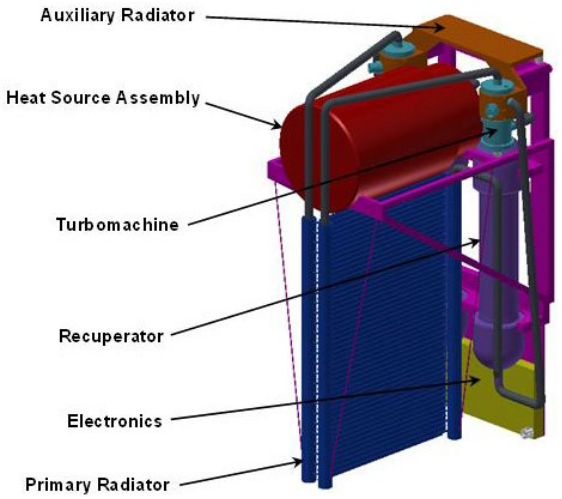

Fig 4. Baseline design for generator system.

Figure 5 illustrates an alternative power system design that replaces the planar radiator in our baseline configuration with a curved radiator. Although the curved radiator increases system mass, it is attractive because its larger surface area reduces the compressor inlet temperature to improve power conversion efficiency. The planar radiator discharges heat from both of its surfaces, with a total area of 0.80 m^2; while we have assumed single-sided heat transfer for the curved radiator, with a total effective area of 1.19 m^2. The primary drawback associated with the curved radiator is that it requires more fabrication development effort.

We predicted the performance of our power system for nine potential missions identified by NASA. The prototype converter we are developing is expected to produce 337 W of AC electric power with a turbine inlet temperature of 730°C and a compressor inlet temperature of 100°C. The corresponding thermal to electric conversion efficiency is 24.9%, and the power density is 20.4 W/kg. At the generator-system level, our baseline design has an overall conversion efficiency of 21.3% and a specific power of 2.40 W/kg for reference operating conditions with a 4 K

vacuum environment, while the alternative design with the curved radiator is at 26.7% and 2.60 W/kg for the same conditions. In both systems, the two converters and electronics modules are cross-connected to provide full power when either converter and/or either controller fail completely.

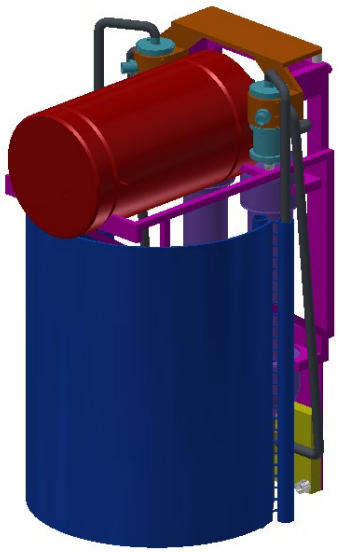

Fig 5. Alternative design for generator system.

VIII. STATUS AND PLANS

We have fabricated a prototype converter configured for testing with electric heaters and a laboratory heat rejection system. Mechanical verification tests are presently under way, and performance testing is scheduled to begin in April.

IX. CONCLUSIONS

Creare and its partners are developing a turbo-Brayton power converter to support future NASA RPS missions. This converter leverages extensive closed Brayton cycle technology developed at Creare over several decades with emphasis on cryogenic refrigerators for long-life spaceflight applications. This technology is now being adapted to create a converter that is designed to produce 337 W of electric power with a predicted thermal to electric conversion efficiency of 24.9% and a predicted specific power of 20.4 W/kg.

ACKNOWLEDGMENTS

The information presented in this paper is based upon work supported by the National Aeronautics and Space Administration under Contract Number 80GRC17C0028.

REFERENCES

1. J. J. BREEDLOVE, M. V. ZAGAROLA, G. F. NELLIS, J. A. GIBBON, F. X. DOLAN and W. L. SWIFT, Life and Reliability Characteristics of Turbo Brayton Coolers, pp. 489-498, R. G. ROSS, JR., Ed., Kluwer Academic/Plenum Publishers, New York, NY (2001).
2. F. X. DOLAN, W. L. SWIFT, LT. B. J. TOMLINSON, A. GILBERT and J. BRUNING, A Single Stage Reverse Brayton Cryocooler: Performance and Endurance Tests on the Engineering Model, pp. 465-474, Plenum Press, New York (1997).
3. W. L. SWIFT, F. X. DOLAN and M. V. ZAGAROLA, The NICMOS Cooling System – 5 Years of Successful On Orbit Operation, pp. 799-806, Trans Cryogenic Engineering Conference – CEC, 52, AIP Conference Proceedings, 985 (2008).
4. M. V. ZAGAROLA, J. J. BREEDLOVE, C. S. KIRKCONNELL, J. T. RUSSO and T. CHIANG, Demonstration of a Two Stage Turbo Brayton Cryocooler for Space Applications, pp. 461-469, S. D. MILLER and R. G. ROSS, JR., ICC Press (2008).
5. J. J. BREEDLOVE, K. J. CRAGIN and M. V. ZAGAROLA, Testing of a Two Stage 10 K Turbo Brayton Cryocooler for Space Applications, S. D. MILLER and R. G. ROSS, JR., ICC Press (2014).
6. M. V. ZAGAROLA, J. J. BREEDLOVE and K. J. CRAGIN, Demonstration of a High Capacity Cryocooler for Zero Boil Off Cryogen Storage in Space, International Cryocooler Conference 17, Los Angeles, CA (9-12 July 2012).
7. L. S. MASON, Realistic Specific Power Expectations for Advanced Radioisotope Power Systems, 4th International Energy Conversion Engineering Conference and Exhibit (IECEC), Paper AIAA 2006 4193, San Diego, CA (2006).
8. M. ZAGAROLA, M. G. IZENSON, J. BREEDLOVE, G. M. O'CONNOR, A. C. KETCHUM, R. L. JETLEY and J. K. SIMONS, An Advanced Turbo Brayton Converter for Radioisotope Power Systems, pp. 632-640, Space Technology and Applications International Forum—STAIF 2005, Publ. AIP Conf Proc 746, American Institute of Physics, Melville, NY (2005).
9. D. DESERRANNO, M. V. ZAGAROLA, D. CRAIG, R. GAREHAN, T. GIGLIO, J. SMITH, J. K. SANDERS and M. DAY, Performance Testing of a High Effectiveness Recuperator for High Capacity Turbo-Brayton Cryocoolers, 19th International Cryocooler Conference (ICC 19), San Diego, CA (2016).
10. OTTING, W., NASA [National Aeronautics and Space Administration] low power DIPS [Dynamic Isotope Power System] conceptual design study; Final report. United States: N. p., 1990. DOI: 10.2172/721000.

Nuclear and Emerging Technologies for Space
Sponsored by Oak Ridge National Laboratory, April 26th-30th, 2021.
Available online at https://nets2021.ornl.gov

MULTI-MISSION THERMOELECTRIC GENERATOR ASSEMBLY TESTING AND LAUNCH OPERATIONS FOR MARS 2020

Eric Clarke, Joe Giglio, Kendall Wahlquist, Craig Dees, Kevin Geddes, Jaymon Birch, Shad Davis, Brandon Horkley, Hannah Usher, and Lucas Rich

Idaho National Laboratory 1955 Fremont Ave., Idaho Falls, ID, 83415

Primary Author Contact Information: 208-533-7050 and Eric.Clarke@inl.gov

The Space Nuclear Power and Isotope Technologies (SNPIT) division at Idaho National Laboratory (INL) fuels, performs acceptance testing, and provides spacecraft integration support of Radioisotope Power Systems (RPS) in support of National Aeronautics and Space Administration (NASA) missions. Recently the SNPIT team completed assembly, testing and launch support of the Multi-Mission Radioisotope Thermoelectric Generator (MMRTG) for the Mars 2020 Perseverance Rover mission.

I. INTRODUCTION

The production of Radioisotope Power Systems (RPS) has been an ongoing endeavor for the U.S. Department of Energy (DOE) and its predecessor agencies for the past six decades. DOE has contracted the Idaho National Laboratory (INL) to provide RPS in support of National Aeronautics and Space Administration (NASA) missions. The overall mission of the RPS program is to develop, demonstrate, and deliver compact, safe nuclear power systems and related technologies for use in remote, harsh environments (e.g., space) where more conventional electrical power sources cannot provide sufficient power. Recently the INL team completed assembly, testing and launch support of the Multi-Mission Radioisotope Thermoelectric Generator (MMRTG) for the Mars 2020 Perseverance Rover mission. The efforts described herein represent five years of preparation and execution by a 60-member team from INL.

II. ASSEMBLY

Assembly consisted of fuel assembly and preparation of the GPHS module and generator fueling whereby an MMRTG is configured to the fueled configuration.

II.A. Fuel Assembly and Preparation

A collaboration between Oakridge National Laboratory (ORNL) and Los Alamos National Laboratory (LANL) produced the fueled clads that provide the heat the MMRTG used to produce electrical power. The fueled clad is a plutonium-238 oxide pellet contained in an Iridium alloy capsule. Each fueled clad produce approximately 62-watt thermal output. INL received the fueled clads and assembled them into the graphite components that provide the primary impact protection in the remote chance of a mission incident. Two fueled clads are placed in a Graphite Impact Shell (GIS) and two GIS are placed into a General Purpose Heat Source (GPHS) module creating a heat source with approximately 250 watts thermal at the beginning mission.

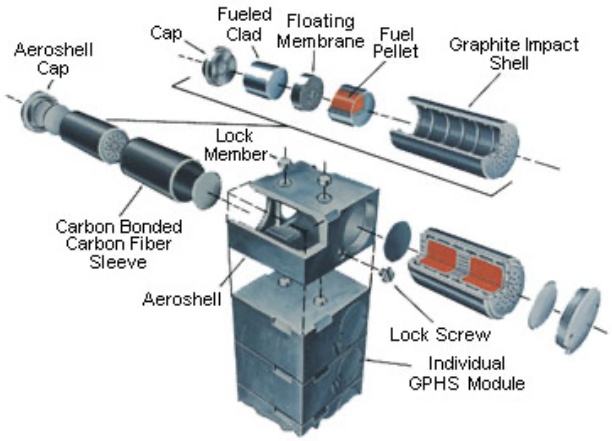

Fig. 1. GPHS module assembly [2].

Two GPHS modules were welded into each hermetically sealed can and placed on the module reduction and monitoring (MRM) system. The MRM process reduces the oxygen of the fuel by elevating the fuel temperature combined with an oxygen and carbon reaction of the graphite components. Weekly gas measurements were taken to monitor the reactant gases to determine when the fuel was reduced within specified limits. Eight completed GPHS modules were stored in four MRM cans until generator fueling began.

II.B. Generator Fueling

An unfueled MMRTG was delivered to INL as an electrically heated unit that had undergone extensive acceptance testing by the supplier team, Aerojet Rocketdyne and Teledyne Energy Systems. INL performed room temperature electrical acceptance testing to ensure the generator did not sustain any damage during shipping.

INL requested concurrence from the Mars 2020 mission to fuel the MMRTG approximately one-year before launch. Fueling began with placement of the generator in the Inert Atmosphere Assembly Chamber (IAAC). The electrical heat source was removed and the

interior of the MMRTG was inspected. The air inside the IAAC was then replaced with argon and controlled within specified limits. GPHS modules were individually removed from MRM cans, cleaned, and inspected for damage in an adjacent inert glovebox. The GPHS modules were then transferred into the IAAC and stacked on a water-cooled fixture in preparation for fueling. Eight GPHS modules were stacked, lifted, and lowered slowly into the MMRTG to minimize thermal transients to the thermoelectrics.

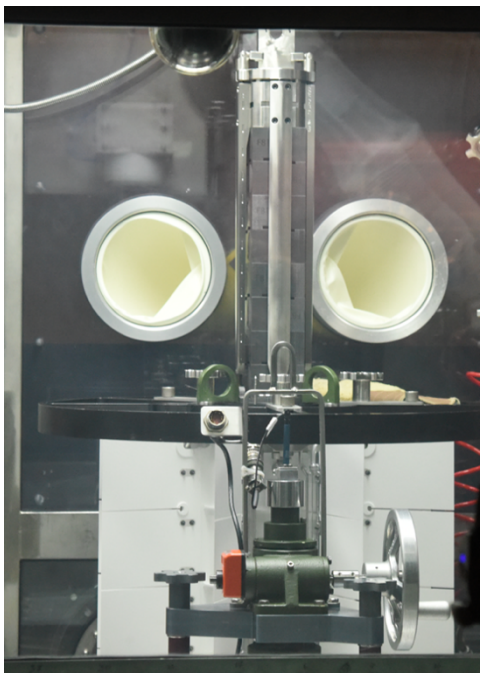

Fig. 2. GPHS module stack insertion into the MMRTG housing.

A piece of Min-K insulating material was then placed on the GPHS stack to constrain it during dynamic events such as launch, entry decent and landing. The Min-K was trimmed to a specified thickness so that when the MMRTG end cover is installed, it applies a predefined load through the Min-K to the GPHS stack thereby constraining its movement. A hose was attached to a port on the end cover allowing the argon inside the MMRTG to be removed and exchanged with helium. When the gas exchange was complete, the port was welded shut. A leak test was performed on the weld as well as the end cover seal. When the MMRTG was thermally stable, simple electrical checks were performed to verify the electrical output. The MMRTG was removed from the IAAC, radiation dose rate measurements were taken at various distances from the MMRTG, and more in-depth electrical checks were performed before transferring the MMRTG to the acceptance test stations.

III. ACCEPTANCE TESTING

Acceptance testing consisted of vibration, mass properties, and thermal vacuum tests. Electrical checks were performed between each test to ensure that the test did not cause damage to the MMRTG.

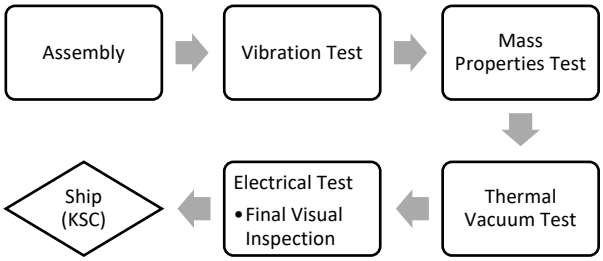

Fig. 3. INL MMRTG Assembly and Testing Flow Chart.

III.A. Vibration

The MMRTG was subjected to random spectrum and sine burst vibrational testing to verify the unit will survive the conditions experience during launch and reentry to Mars.

The MMRTG was mounted to a test fixture which incorporates accelerometers and force transducers. Accelerometers and force transducers were placed on each corner of the fixture to monitor the X, Y, and Z axis acceleration and force at the mounting end (bottom) of the MMRTG. Two triaxial response accelerometers were mounted near the fueling end (top) of the MMRTG.

Fig. 4. MMRTG mounted on the vibration test fixture.

The data collected was compared to the MMRTG provided for Mars Science Laboratory. The data showed that the two RPS were consistent with each other.

III.B. Mass Properties

Mass properties testing started by measuring the mass of the MMRTG on a precision scale. The MMRTG was then installed on the mass properties instrument which rotates about the machine axis. A fixture precisely

positions the MMRTG in two orientations to measure the composite center of gravity in the X-Y, and X-Z orientations. The measured values were provided to Teledyne Energy Systems to analytically subtract non flight components and calculate the actual center of gravity and mass moments of inertia.

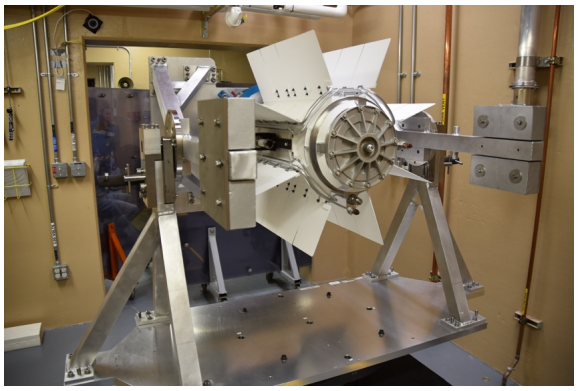

Fig. 5. MMRTG mounted on the mass properties instrument turned to measure the X-Z center of gravity.

III.C. Thermal Vacuum Testing

The MMRTG was subjected to a final power level verification where the heat transfer boundary conditions were fully controlled. This is done by testing in the INL thermal vacuum chamber where gas convection and conduction are eliminated, and radiant heat transfer is well characterized. Testing was performed to verify final power output across the generator design load voltage range. The data generated was used to validate numerical models for the life power output prediction of the fueled flight unit.

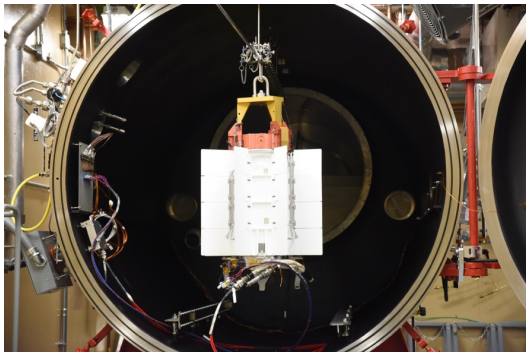

Fig. 6. MMRTG mounted inside the thermal vacuum chamber.

III.D. System Certification and Acceptance

The MMRTG was certified for flight following successful assembly and testing at INL. The flight data package included the record of assembly, radiation dose rate survey, vibration testing, mass properties testing, thermal vacuum chamber testing, electrical testing and visual inspection results. Any nonconformance that occurred during assembly and testing was documented on the certificate. The completed data package was presented to the Mars 2020 mission team for acceptance and verification of all interface requirements.

IV. LAUNCH SUPPORT OPERATIONS

After flight acceptance, the MMRTG was ready for transportation and integration with the Mars 2020 rover at Kennedy Space Center (KSC).

IV.A. Transportation

INL transported the MMRTG to KSC approximately four-months before launch. A series of pre-shipment electrical checks were performed to ensure the health of the MMRTG prior to shipment. These tests included a ground conductor resistance check, isolation resistance check (power and instrumentation circuits), and an ambient air electrical output performance test.

The MMRTG was loaded into the certified DOT type-B shipping cask (9904) after successful pre-shipment electrical checks were performed. The 9904 cask required active cooling to prevent MMRTG damage from overheating. Cooling was provided using a chilled water jacket on the exterior of the 9904 cask. Chilled water was provided by portable chillers during loading.

Fig. 7. 9904 Cask inside the RTGTS.

The cask with MMRTG was loaded into the Radioisotope Thermoelectric Generator Trailer System (RTGTS), a specially designed transportation trailer to support the transport of a loaded 9904 cask. A team of INL employees followed the RTGTS during transport to provide monitoring support and response to out of tolerance conditions.

The 9904 cask was unloaded at KSC and the MMRTG removed at KSC. Post-shipment health checks were compared to the pre-shipment health checks to ensure no damage occurred during shipment.

IV.B. Integration

The flight mechanical and electrical adapters were installed onto the MMRTG three months prior to the launch. INL conducted integrated operations with Jet Propulsion Laboratory (JPL) personnel to install the flight hardware, which provides the mechanical and electrical interface between the MMRTG and the Mars 2020 rover.

The hot-fit check, a mission risk reduction operation, was performed three-months in advance of launch.

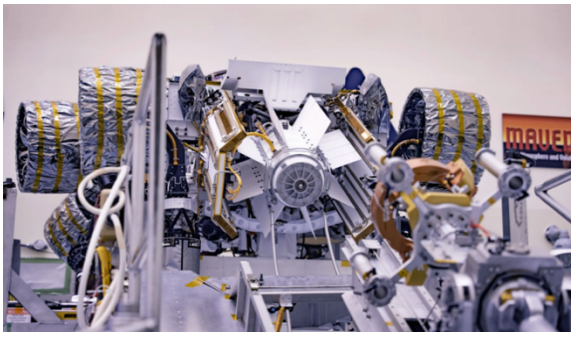

Fig. 8. MMRTG hot-fit check to Mars 2020 rover.

The hot-fit check was the first electrical and mechanical mating of the fueled MMRTG to the Mars 2020 rover and is a key milestone in the overall mission integration workflow. INL was responsible for delivering the MMRTG and supporting the electrical and mechanical integration at the Payload Hazardous Servicing Facility (PHSF) at KSC. JPL performed several integrated functional tests after the MMRTG was mechanically and electrically mated. The MMRTG was de-mated from the rover after testing was completed and stored until final integration at the Vertical Integration Facility (VIF).

The MMRTG was transported to the VIF ten-days before launch. INL and JPL worked together to perform mechanical and electrical integration.

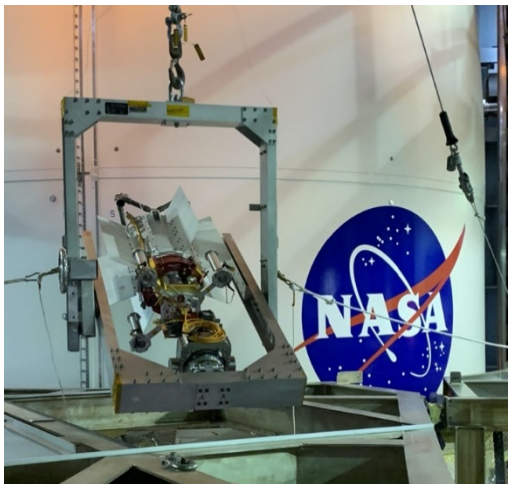

Fig. 9. Final MMRTG integration operations to the Mars 2020 Perseverance Rover at the VIF.

II. CONCLUSIONS

The MMRTG for the Mars 2020 rover was the second MMRTG assembled, tested, and integrated. There were several challenges that the INL, Aerojet Rocketdyne and Teledyne Energy System team had to systematically work through to support launch of the Mars 2020 rover.

The Mars 2020 Perseverance Rover, aboard an Atlas V-541 rocket, was launched from Launch Complex 41 located at the Cape Canaveral Air Force Station (CCAFS) in Florida on July 30th, 2020. INL played a key role in the successful launch of the rover through execution of the MMRTG mechanical and electrical integration operations with JPL mission system integrators and NASA's launch service program organization.

ACKNOWLEDGMENTS

The authors would like to acknowledge Dr. Stephen Johnson and Ms. Kelly Lively from Idaho National Laboratory for their leadership in assembly, testing, and launch operations for the MMRTG. The authors also would like to acknowledge Bill Otting and Andrew Lane from Aerojet Rocketdyne and Josh Wojcik from Teledyne Energy Systems for their technical support fueling and testing the MMRTG. The authors also acknowledge the efforts of Oakridge National Laboratory and Los Alamos National Laboratory for supplying the fueled clads. This work was funded through Department of Energy contract DE-AC07-05ID14517.

REFERENCES

1. Kenneth Rosenberg and Stephen G. Johnson, "Assembly and Testing of a Radioisotope Power System for the New Horizons Spacecraft," *AIAA 4th International Energy Conversion Engineering Conference and Exhibit (IECEC)*, San Diego, California, 6/26/2006, ISBN: 978-1-62410-041-3.
2. James Werner, Kelly Lively and Drake Kirkham, "A Multi-Mission Radioisotope Thermoelectric Generator (MMRTG) for Mars 2020," 2017 IEEE Aerospace Conference, Big Sky, Montana, 4/11/2017, p. 989, ISBN: 978-1-5090-1614-3.

Nuclear and Emerging Technologies for Space
Sponsored by Oak Ridge National Laboratory, April 26th-30th, 2021.
Available online at https://nets2021.ornl.gov

RESULTS, IMPLICATIONS, AND PROJECTIONS FROM IRRADIATION AND EXAMINATION OF INITIAL NpO_2 TEST TARGETS FOR IMPROVED ^{238}Pu PRODUCTION

E.D. Collins, R.N. Morris, J.L. McDuffee, P.L. Mulligan, J.S. Delashmitt, S.R. Sherman, R.J. Vedder, and R.M. Wham

Oak Ridge National Laboratory 1 Bethel Valley Road, Oak Ridge, TN 37830-6423

collinsed@ornl.gov

An alternative target design with potential improvements—including a major increase in ^{238}Pu production rate and annual capacity; fewer targets to be fabricated, irradiated, and processed; and a significant elimination of aluminum-bearing, radioactive liquid waste—has been conceived and evaluated using reactor physics and thermal hydraulics analyses. The alternative target design uses pressed pellets of $^{237}NpO_2$ stacked inside a Zircaloy-4 cladding tube. Four test targets were fabricated, irradiated, and examined. No potential problems were indicated. Projections from measured constituents indicated annual production could be increased by a factor of ~2, and the number of targets required to be fabricated, irradiated, and processed could be reduced by a factor of ~5.

I. INTRODUCTION

The production of ^{238}Pu by irradiation of ^{237}Np targets comprises a four-step rotating sequence, which is used repeatedly.[1] These four steps, illustrated in Fig. 1, include (1) target fabrication; (2) neutron irradiation; (3) postirradiation chemical processing to recover and purify the plutonium product, separate it from unconverted ^{237}Np and fission product waste, convert it to heat source PuO_2, and purify the ^{237}Np; and (4) conversion to NpO_2 for target fabrication.

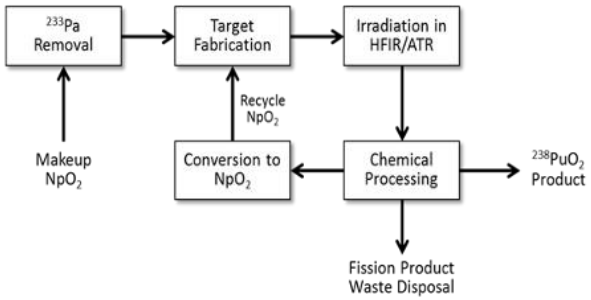

Fig. 1. Sequential ^{238}Pu production process steps.

The heat source PuO_2 product specification requires the plutonium to contain at least 82.5% ^{238}Pu. Therefore, the target irradiation step is limited to transmute less than 15% of the ^{237}Np into plutonium. This limitation minimizes the production of other plutonium isotopes, primarily ^{239}Pu, that are produced by neutron capture of ^{238}Pu with a cross section that is ~3 times greater than the cross section for production of ^{238}Pu from ^{237}Np. Thus, for the annual production goal of 1.5 kg of heat source PuO_2, multi kilograms per year of ^{237}Np must be purified, converted to NpO_2, fabricated into targets, irradiated, and chemically processed each year.

A significant limitation that constrains the production steps and, therefore, the timing of completion of the production sequence is the safeguards limit on the amount of purified ^{237}Np which can be in the production inventory. Other limitations, such as those on disposal of transuranic waste, or delays that can occur in any of the four steps, can reduce the annual capacity for production of ^{238}Pu.

II. CURRENT TARGET DESIGN

Aluminum-clad, aluminum-matrix–NpO_2 cermet pellets were selected as the initial pin-type target design. Each target contains 52 pressed pellets within the ~20-in. active length of the target. Each pellet volume contains 20% oxide, 70% aluminum, and 10% void space for fission gas expansion. The total weight of ^{237}Np in each target is 30.7 g.

This type of target design was chosen for ^{238}Pu production because it has been successfully used for many years for irradiation of plutonium, americium, and curium in the transuranium element production program at Oak Ridge National Laboratory. However, only 5–50 targets per year have been required for the transuranium element production rate needed; however, for production of kilogram amounts of ^{238}Pu per year, with the conversion of ^{237}Np limited to <15% per irradiation cycle, multikilogram quantities of ^{237}Np must be irradiated each year, requiring several hundred targets to be fabricated, transported to and from the reactors, irradiated, and processed each year.

In addition, for the ^{238}Pu production process, the production rate is limited by the research reactor's operating time, the volume of available irradiation space in the reactors, and the $^{237}NpO_2$ loading per target, which is limited by heat transfer and the 660 °C melting point of

aluminum. Thus, achieving the needed production rate of ^{238}Pu is challenging, and both the High Flux Isotope Reactor (HFIR) at Oak Ridge National Laboratory and the Advanced Test Reactor at Idaho National Laboratory will be required.

III. ALTERNATIVE TARGET DESIGN

An alternative target design with potential improvements has been conceived and evaluated using reactor physics and thermal hydraulics analyses. This design is expected to result in a major increase in ^{238}Pu production rate and annual capacity, fewer targets to be fabricated, irradiated, and processed, and a significant elimination of aluminum-bearing, radioactive liquid waste. The alternative target design uses pressed pellets of $^{237}NpO_2$, stacked inside a Zircaloy-4 (Zr-4) cladding tube.

Modeling analyses using codes described in Refs. 2 and 3 compared irradiation of a 7-target array of oxide targets with a 5-target array of targets containing pellets of larger diameter. Zircaloy cladding for the larger pellets is commercially available. The model determined time and spatially dependent heat generation rates, neutron flux, ^{237}Np burnup, ^{238}Pu yields, and Pu isotopic concentrations over the course of multiple HFIR cycles. Also, self-shielding effects were modeled. Analyses indicated that the heat generation rates are predominantly a surface effect, and the rates diminish with distance into the pellet.[4,5]

III.A. Phase 1 Test Target Design

Four test targets, each containing four NpO_2 pellets, were fabricated (Fig.2) and irradiated in Phase 1. Based on experience with the existing cermet pellet targets, one oxide target was irradiated in a HFIR ISVXF position for two cycles, two test targets were irradiated for three cycles (thought to be the optimum irradiation time), and one target was irradiated for four cycles to see if excess heat generation might cause internal melting. The 2-cycle target was designated as NP01, the two 3-cycle targets as NP02 and NP03, and the 4-cycle target as NP04.

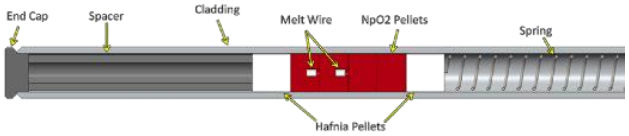

Fig. 2. Assembly of test target.

Because of the uncertainties in the neutron capture cross section for ^{237}Np and a lack of knowledge about the thermophysical properties of irradiated NpO_2 (thermal conductivity, swelling/shrinking, estimated melting point of >2,500 C for NpO_2), there was a concern that the pellets could melt near their centerline sometime during the 2- to 4-cycle irradiation, especially the 4-cycle irradiation. Small Pt–Ir melt wires (melting point of ~2,100 °C) were placed inside two of the four pellets within each target to provide an indication of internal temperature as a backup to MET examination of the post irradiation microstructure..

To avoid possible reactor safety issues, the four NpO_2 pellets were sandwiched between hafnium oxide (hafnia) pellets to suppress neutron flux on either end of the pellet stack, mitigating fission peaking in the top and bottom pellets. Additional precautions were taken to accommodate possible NpO_2 melting by placing refractory metal tungsten crucibles above and below the pellet stack. Highly absorbing hafnium metal shields were placed over the tungsten crucibles to prevent further fission of ^{238}Np if the pellets were to melt into these regions. Finally, the entire assembly was placed into an aluminum capsule as a secondary containment. The design also included a semicircular hafnium metal shield to simulate the neutron flux self-shielding caused by additional NpO_2 pellets targets anticipated in the future production design.

IV. POSTIRRADIATION EXAMINATION (PIE) RESULTS

All four targets were intact after irradiation. Fission gas puncture tests were made and ^{85}Kr evolutions were measured. The results showed a general increase with increasing irradiation time. There was a significant difference in the evolution measurements from the two 3-cycle targets, although subsequent chemical analyses showed less difference in yields of ^{239}Pu.

Radial and longitudinal microstructure analyses were made of all target pellets except the 2-cycle target (NP01) which was too friable to be made into a material-graphic (MET) mount. The radial MET mount of a 4-cycle (NP04) target clad pellet is shown in Fig. 3 as an illustration.

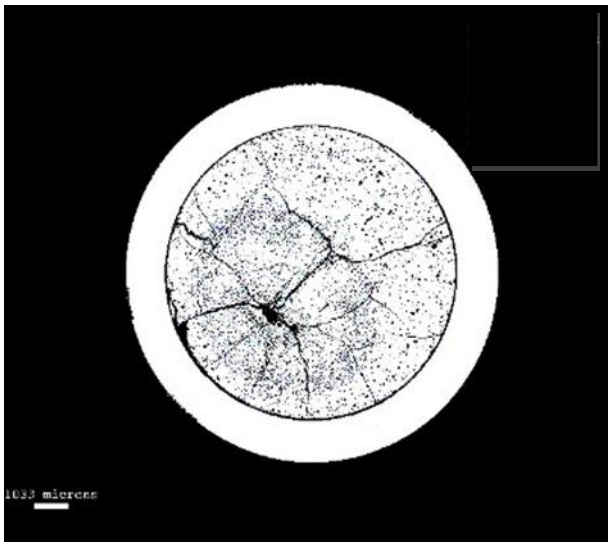

Fig. 3. Radial MET mount of 4-cycle target NP04 clad pellet

Similar MET mounts of the two 3-cycle target pellets (NP02 and NP03) also showed internal, off-centered heat effect zones in the side of the pellet with greatest neutron exposures. No evidence of melting was observed in the microstructure. The small Pt–Ir melt wires may have melted or were lost during handling, and thus could not be examined. Pellet-gap measurements showed no swelling but slight shrinkage. The maximum shrinkage appeared to be in the surface beneath the heat-affected zone, although the heat affected zone was significantly internal from the pellet surface.

The behavior seen in the MET mounts was typical of that expected for dense oxide that has been irradiated and temperature-cycled. The pellets were quite fragile and easily broke up into small pieces during handling and polishing, resulting in less than desirable polishing. Pellet-clad gaps were observed in both the 3- and 4-cycle targets and inferred in the 2-cycle target by the fact that it fell apart.

Three observed features were important: (1) lack of melting, (2) off-center power peaking, and (3) lack of swelling of the pellets into the claddings to strain them. Overall, no deleterious effects were noted that threaten the concept or create difficult irradiation conditions. A potential issue may be the fission gas release, as it may be sensitive to unknown fabrication or irradiation conditions.

A portion of the four pellets from each target was dissolved in nitric acid, and the dissolved components were analyzed to determine actual ^{237}Np burnup, ^{238}Pu yields, and Pu isotopic quality, as well as key fission product radioactivity concentrations (Table 1). The measurements of dissolved components clearly showed increasing yields of ^{238}Pu and fission products plus decreasing ^{238}Pu quality with increasing irradiation time.

Table 1. NpO2 Test Targets PIE Radiochemical and Mass Analyses

Target Number	NP01	NP02	NP03	NP04
No. of HFIR cycles	2	3	3	4
ICPMS				
238Pu, mg/g sample	40.6	53.1	59.1	72.9
Total Pu, mg/g sample	43.4	58.0	65.1	81.9
Np, mg/g sample	794	794	751	789
Np/total Pu ratio	18.3	13.7	11.5	9.6
238Pu isotopic quality,%	93.48	91.50	90.73	89.01
Gamma Spec, Ci/g sample @ Rx Dischg.				
95Zr	0.935	0.909	1.09	1.435
144Ce	0.188	0.263	0.342	0.373
106Ru	0.087	0.116	0.113	0.142
134Cs	0.00069	0.0015	0.00164	0.0023
137Cs	0.0072	0.0113	0.0116	0.0135
155Eu	0.00053	0.00061	0.00097	0.00103

V. OXIDE DISSOLUTION RATES

The shear-leach method of oxide dissolution of irradiated targets is planned. The use of fluoride as a catalyst will not be possible because of corrosion-susceptible equipment in the processing facility. During the PIE dissolution of a portion of the 4-cycle (NP04) irradiated clad-oxide, dissolution rates of the ^{238}Pu and key fission products were measured (Fig. 4).

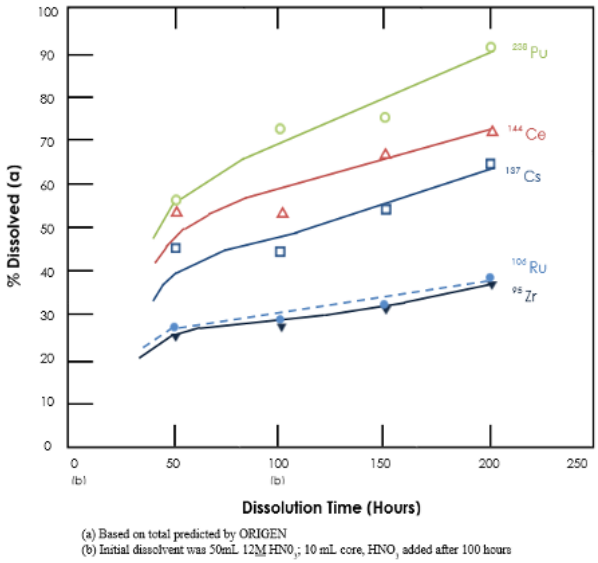

(a) Based on total predicted by ORIGEN
(b) Initial dissolvent was 50mL 12M HNO_3; 10 mL core, HNO_3 added after 100 hours

Fig. 4. Dissolution rates for 4-cycle irradiated target (NP04).

The dissolution rates were much faster during the first 50 hours when the nitric acid concentration and oxide surface area were the highest. Fresh acid was added after 100 hours of dissolution time, and the dissolution rates of Pu, Ce, and Cs continued at a lower rate. An even lower rate was measured for Ru and Zr, which are known to have more resistant forms. The optimum dissolution procedure will need to be developed in future tests.

VI. PROJECTIONS TO FULL SCALE TARGETS

Calculations were made using conservative assumptions to enable an annual comparison of (1) the number of targets to be fabricated, irradiated, and processed; (2) the yields of heat source PuO_2 containing a plutonium mass isotopic purity of 82.5%; and (3) the amount of unconverted ^{237}Np to be recycled. The conditions and assumptions were as follows:

1. The projection of the oxide test target yield and conversion data to a full-length target is proportional to the ratio of the average axial neutron flux to the peak neutron flux (where the test target pellets were located). This ratio was calculated by graphical integration of the area underneath the HFIR thermal and epithermal neutron flux cosine curves, which is shown in Ref. 6.

2. The average/peak ratio used was 81% for both thermal and epithermal flux cur

3. Nine HFIR ISVXF irradiation positions are used for either cermet or oxide targets.

4. Seven HFIR cycles are performed each year. Therefore, 3.5 two-cycle targets, 2.33 three-cycle targets, or 1.75 four-cycle targets can be irradiated annually.

5. Each ISVXF position contains seven cermet targets or five oxide targets.

6. The 3-cycle oxide target data are the average of the data measured for NP02 and NP03 test targets.

Table 2 shows that both HFIR and the Advanced Test Reactor will be required to produce the goal of 1.5 kg heat source PuO_2 per year, whereas the projected performance of oxide targets can be made in HFIR. Conversions of ^{237}Np to Pu are lower for oxide targets than for cermet targets, but yields are higher because the ^{237}Np loading is much greater. The largest yield is for 2-cycle irradiations because more irradiations can be made each year, but both 3-cycle and 4-cycle irradiations can achieve the production goal. Also, the amount of unconverted ^{237}Np to be recycled is smaller for the 4-cycle irradiation, which requires less effort and time for chemical processing. Therefore, the 4-cycle irradiation of oxide targets appears to be optimum.

TABLE 2. Comparison of cermet target and projected oxide target performance.

Target Type	Cermet	Cermet	Oxide	Oxide	Oxide
No. of HFIR cycles	2	3	2	3	4
g initial Np per target	30.7	30.7	225	225	225
Adjusted for whole target					
% conversion to Pu	10.0	12.6	4.02	5.70	7.58
% unconverted Np	88.8	80.9	91.0	89.0	91.3
%Pu-238/Total Pu	88.5	85.0	93.48	91.12	89.01
g Pu (82.5% Pu-238) per target	3.29	3.98	10.25	14.12	18.41
Number targets in each ISVXF	7	7	5	5	5
Yield Pu/ISVXF position	23.03	27.02	51.25	70.60	92.03
g Pu/year per ISVXF position	80.6	63.0	179	164	161
g/Pu/year per 9 ISVXF positions	725	567	1,611	1,476	1,449
g PuO2/year per 9 ISVXF positions	823	643	1,829	1,675	1,695
Maximum no. targets per year	220	142	157	105	79
kg residual Np per year	5.28	3.11	32.2	21.0	16.2
No. tgts for 1.5 kg PuO2/y	401	332	129	94	72
kg residual Np per year	9.6	7.3	26.4	18.8	14.8

VII. CONCLUSIONS

PIE results on the initial $^{237}NpO_2$ test targets showed no evidence of melting and no deleterious effects that would threaten the proposed use to improve production rate, annual yield, and ^{238}Pu isotopic purity of the heat source PuO_2. Projection calculations indicate the annual yield can be improved by a factor of ~2, and the number of targets required can be reduced by a factor of ~5. In addition, the generation of aluminum-bearing radioactive liquid waste would be eliminated. Used Zircaloy cladding could be disposed directly as solid waste.

ACKNOWLEDGMENTS

Funding for this work was provided by the National Aeronautics and Space Administration through the US Department of Energy, Office of Nuclear Energy.

REFERENCES

1. E.D. COLLINS and R.M. WHAM, “Converting Research and Development facilities and Operations into a ^{238}Pu Production Process,” *Transactions of ANS NETS* (2018).
2. X-5 MONTE CARLO TEAM, “MCNP-A General Monte Carlo N-Particle Transport Code, Version 5,” Los Alamos National Laboratory, LA-UR-03-1987, (2003).
3. B.T. REARDEN and M.A. JESSEE, Eds, “SCALE Code System,” Version 6.2.3, Oak Ridge National Laboratory, ORNL/TM-2005/39, (2018).
4. C.R. DAILY and J.L. MCDUFFEE, “Design Optimization Studies for NpO_2 targets Irradiated in the High Flux Isotope Reactor,” *Transactions of ANS NETS* (2019).
5. J.L. MCDUFFEE, P.L. MULLIGAN, K.R. SMITH, and R.M. WHAM, “Design and Analysis of a NpO2 Target for the Production of ^{238}Pu,” *Transactions of ANS NETS 2019*.
6. S. MIRZADEH, R.E. SCHENTER, A.P. CALLAHAN, and F.F. KNAPP, “Production Capabilities in U.S. Nuclear Reactors for Medical Isotopes,” Oak Ridge National Laboratory, ORNL/TM-12010, Figure 3.5.9, (November 1992)

Nuclear and Emerging Technologies for Space
Sponsored by Oak Ridge National Laboratory, April 26th-30th, 2021.
Available online at https://nets2021.ornl.gov

MICROSPHERE PLUTONIUM-238 OXIDE FUEL TO REVOLUTIONIZE NEW RADIOISOTOPE POWER SYSTEMS AND HEAT SOURCES FOR PLANETARY EXPLORATION

Jeffrey A. Katalenich[1], Joseph A. Sholtis, Jr.[2], Bill Nesmith[3], and Jean-Pierre Fleurial[3]

[1]*Pacific Northwest National Laboratory (PNNL), Richland, WA 99354*
[2]*Sholtis Engineering & Safety Consulting, Tijeras, NM 87059*
[3]*Jet Propulsion Laboratory, California Institute of Technology (JPL-CALTECH), Pasadena, CA 91109*

jeffrey.katalenich@pnnl.gov (509) 375-2244

Microsphere $^{238}PuO_2$ fuels have potential to provide performance and safety enhancements for future radioisotope heat and power systems (RPS) as well as enable more flexible and compact RPS designs. Improvements in RPS specific power and more flexible geometries were recently investigated by JPL and PNNL as part of a study on cryobot devices for exploring Ocean Worlds. Missions to penetrate ice and explore oceans, such as on Europa, will require RPS with high specific power within the vehicle to provide both heat and power. Such missions will be mass-constrained, and the energy required to penetrate the ice is highly dependent on cryobot size. Therefore, compact RPS geometries are needed to maximize heat and power while minimizing ^{238}Pu inventory. Microsphere-based heat sources are an attractive way to obtain flexible geometries and high volumetric power loadings because they can fill a region of any size and shape provided fuel temperatures are kept below a threshold and launch/re-entry safety are not compromised. The sol-gel technique to produce $^{238}PuO_2$ microsphere particles for heat sources has the benefit of preventing dust generation, as opposed to the current $^{238}PuO_2$ powder/pellet processing method, reducing hazards in the fuel fabrication line. Microspheres can also be individually coated to enhance thermal conductivity, and/or reduce the likelihood of $^{238}PuO_2$ fuel dispersal in an accident. Although PNNL has produced $^{238}PuO_2$ microspheres using the sol-gel method, the application of coatings and their integrity over time has yet to be investigated. Continued R&D could demonstrate the feasibility of advanced, microsphere-based heat sources and provide baseline data for planning future missions requiring new RPS with different heat source configurations.

I. BACKGROUND

RPS are necessary for a variety of space missions. The U.S. is unique in the R&D and deployment of RPS in space, which came at a considerable expense. We have been rewarded with many long-lived space vehicles providing major discoveries and insights across and beyond our solar system. Through the 1960s and 1970s, many radioisotope heat source designs were developed and flown. The performance, and safety, of these devices and the launch vehicles that transported them to space guided design changes. RPS transitioned from low-power systems designed to burn up in the atmosphere on re-entry to designs containing many kilograms of $^{238}PuO_2$ contained in robust, engineered containment structures. Since the development and qualification of the general purpose heat source (GPHS) module in the 1980s, few changes have been made to the fuel production and containment technology, largely due to the cost of conducting safety testing and the cost of modifying the procedures and equipment used for fuel fabrication and RPS assembly.

I.A. Existing Heat Sources

Current U.S. radioisotope heat sources include the 250-W_t GPHS module and the 1-W_t Light-Weight Radioisotope Heater Unit (LWRHU). Los Alamos National Laboratory (LANL) maintains the capability for processing $^{238}PuO_2$ into clad heat sources in the U.S. Although this processing line is effective and has been recapitalized, worker dose and fine particulate contamination increase the cost and risk for $^{238}PuO_2$ processing at the LANL PF-4 facility. The current $^{238}PuO_2$ processing flowsheet requires powder ball milling and pellet slugging that generate small, dispersible particles which increase radiological backgrounds and equipment failure rates. Historically, releases of these particles occur infrequently, but result in radiological uptake in workers present which is a major event. Steps in the flowsheet also require hands-on activities that, together with accumulated buildup, result in worker dose rates requiring workers to be rotated to prevent exceeding dose limits.

$^{238}PuO_2$ pellets are clad with a ductile, refractory alloy (DOP-26 iridium alloy for the GPHS, and platinum 30% rhodium for the LWRHU). These cladding materials are only ductile within a specific temperature range [1]. Insulation is used to ensure clads don't get too hot or too cold during accident scenarios and remain ductile upon impact to prevent $^{238}PuO_2$ release. Additionally, the clad pellets are contained within a graphite impact shell (GIS) and carbon aeroshell to provide additional protection against impact and re-entry. The fine-weave pierced-

fabric (FWPF) carbon composite used for the GIS and GPHS module aeroshell is no longer produced commercially and has anisotropic properties, which provides motivation to identify an alternative aeroshell material with improved performance and reduced raw material cost [2, 3].

I.B. Sol-Gel Microspheres

$^{238}PuO_2$ microspheres, shown in Fig. 1 and Fig 2, were produced at the Pacific Northwest National Laboratory (PNNL) in 2017 using the internal gelation sol-gel process [4]. Sol-gel methods allow for aqueous solutions containing ^{238}Pu to be converted directly into microspheres of the desired size without generating dust in the process. Conceptually, these microspheres can be pressed into conventional pellets, encapsulated as packed spheres, or individually coated to enhance thermal conductivity and reduce contamination risks during accidents. CeO_2 microspheres, produced as a non-radioactive surrogate, were successfully hot-pressed into LWRHU-sized pellets by the University of Dayton Research Institute to demonstrate the potential of using microspheres as a powder substitute for pellet fabrication. PNNL currently maintains a glove box capability for producing plutonium microspheres in batches of 1-10g. The potential to scale to larger batch sizes has been demonstrated recently with non-radioactive materials.

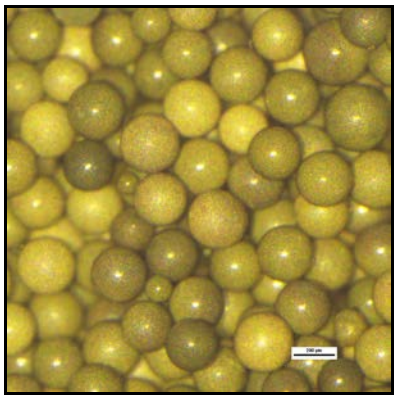

Fig. 1. $^{238}PuO_2$ sol-gel microspheres produced by the Pacific Northwest National Laboratory in 2017.

PNNL's successful production of $^{238}PuO_2$ microspheres offers new possibilities for the near and distant future. In the near-term, such microspheres, which are both non-inhalable and non-respirable, can be used as a feed material to press $^{238}PuO_2$ fuel pellets for subsequent cladding. Sol-gel processing produces virtually no dust contamination, which would reduce deterioration of LANL glove boxes, equipment, and worker exposure. In the long-term, coated $^{238}PuO_2$ microspheres would enable the production of revolutionary radioisotope heat sources for RPS with improved design integration, performance, flexibility, and safety [5]. Compared to granules produced by powder processing, microspheres are smooth

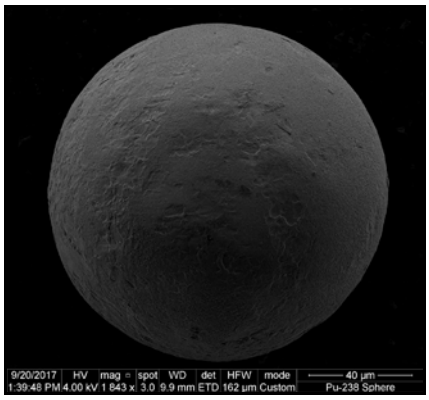

Fig. 2. $^{238}PuO_2$ sol-gel microsphere imaged using scanning electron microscopy to resolve surface features.

and round, promoting coatings with a thin compatibility layer(s) (e.g., porous and/or pyrolytic graphite) and a strong, high-temperature containment barrier (e.g., ZrC or WC). Although microsphere coating technology is demonstrated for tristructural isotropic (TRISO) uranium reactor fuels, the lifetime and performance of coatings on $^{238}PuO_2$ oxide microspheres remains to be determined.

I.C. Next Generation Systems

Future exploration missions are likely to require RPS that differ from those currently available. For example, missions to penetrate thick layers of ice to explore ocean worlds beneath them require vehicles with constrained size and aspect ratios. Such missions require heat and power sources integral to the vehicle, contrary to most probes to date with RPS external to the vehicle. Compact heat sources designed to fit inside the vehicle, possibly with flexible geometries to facilitate use in different-sized craft, could be advantageous or even enabling given size, mass, and mission duration requirements.

Since microspheres can fill a void of any shape, sol-gel microspheres are an attractive choice to enable more flexible RPS and RHU geometries. As an example, consider a Europa cryobot mission. Aside from producing heat sources meeting the unique length to diameter ratios required for such missions, microspheres could enable tailored heat source geometries to fit inside drill bits and shafts to allow melting whether or not the drill is functioning. This design flexibility could enhance the large RPS inside the cryobot main body and/or smaller RPS being deployed behind the cryobot to enable a communication link back to the surface. Additionally, microspheres could be loaded onto trays of horizontal K-1100 type graphite fibers to maximize radial heat flow, a major consideration for cryobots, and minimize centerline temperatures in the fuel that typically limit the dimensions of fueled regions.

II. CRYOBOT USE CASE

The exploration of ocean worlds such as Enceladus and Europa is an ambitious goal that may involve a phased approach. Analogous to the approach to explore Mars, which used increasingly large and sophisticated exploration craft over time, missions to ocean worlds will likely grow in complexity and scope as we learn more about these planetary bodies and how to operate there. JPL is currently investigating the feasibility of an ice penetrator mission, called PRIME (Probe using Radioisotopes for Icy Moons Exploration). PRIME uses heat from the decay of ^{238}Pu to melt through ice, power onboard systems, and to power communication relays that are left in the ice as the vehicle descends.

The power density of a radioisotope heat source is very important for a cryobot because the physical size of the heat source strongly influences the size of the cryobot, which in turn drives the thermal inventory required. Due to this circular relationship, bulkier heat sources drive up power requirements and increase the amount of ^{238}Pu required. Minimizing the size and mass of the probe is also necessary because long probes would be more difficult to land on Europa and the mass we can deliver to the surface is limited. Increasing the power of the heat source also reduces risk by decreasing the mission duration, which is largely dictated by the transit time to Europa and the time required to melt through ice.

To support PRIME, JPL and PNNL generated conceptual designs for a high-power density radioisotope heat source to minimize probe size and the time required for ice penetration [6, 7]. Initially, a variety of GPHS configurations within the cryobot were considered, as shown in Fig. 3 and Fig. 4.

Fig. 3. Various configurations of GPHS module stacks were evaluated.

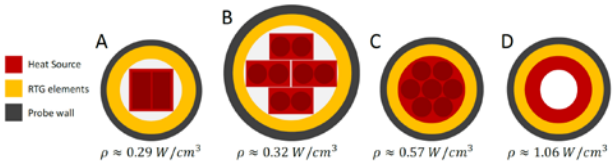

Fig. 4. New configurations yielded higher specific power than those using GPHS modules.

However, as shown in Fig. 5, the cryobot mass and melt speed based on a stack of GPHS modules are undesirable compared to alternative configurations.

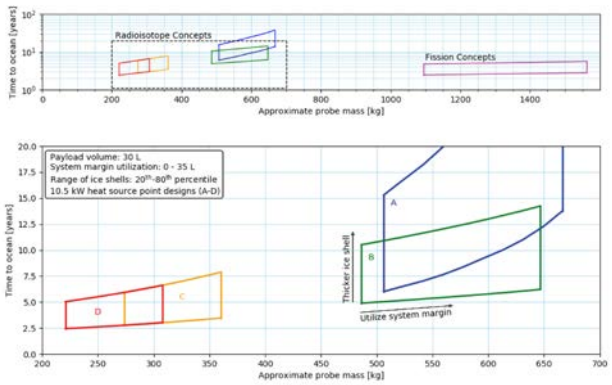

Fig. 5. Assessments indicate that cryobot configurations based on GPHS modules (blue/A and green/B) are slower and heavier than non-GPHS configurations such as those that place GIS modules into a common aeroshell (yellow/C) or microsphere-based heat sources (red/D).

Alternative heat source configurations, such as placing pellet-fueled GIS assemblies into a common aeroshell, shown in Fig. 6, or a microsphere-based heat source, as in

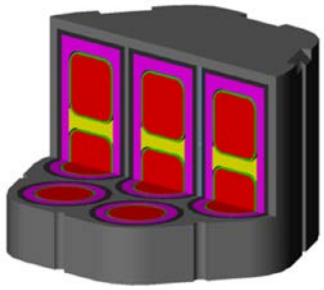

Fig. 6. Notional aeroshell containing 7 GIS.

Fig. 7 (left), provided geometries tailored to the cryobot optimal diameter and enabled more desirable melt speeds and system masses. A very preliminary modular microsphere configuration concept is also depicted in Fig. 7 (right). The microsphere-based heat source design resulted in a cryobot with the lowest system mass, smallest size, and fastest time to penetrate the ice, as shown in red in Fig. 5.

Although using a common aeroshell containing $^{238}PuO_2$ pellets in multiple GIS is likely more expedient than developing and qualifying a microsphere-based design for a first cryobot mission, JPL envisions many future missions that require a power-dense heat source using microsphere-based fuel. Moreover, microspheres facilitate development of future heat sources with flexible, modular geometries anticipated for exploration of icy moons and planets where the heat source must be integrated inside the vehicle.

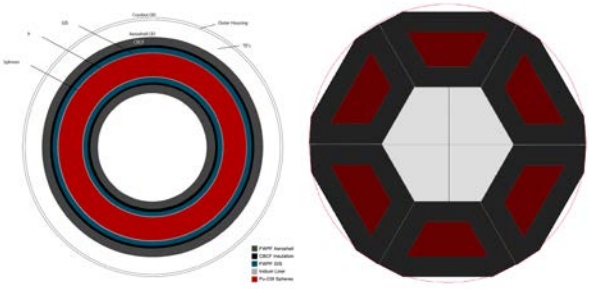

Fig. 7. Microsphere configuration cross sections for preliminary assessment of specific power and fuel temperature (left) and a modular design concept enabled by microspheres (right).

III. R&D NEEDS

Despite potential benefits of sol-gel processing and microsphere-based heat sources, changing heritage processes and systems poses technical and safety risks that must be addressed. In addition to converting portions of the PF-4 processing line to accommodate sol-gel and coating processes, qualification testing will be required to validate safety. The investment required merits a detailed assessment of the improvements expected, and an evaluation of whether sol-gel processing and coating operations could be successfully deployed at PF-4.

While sol-gel technology is mature for TRISO fuel, making $^{238}PuO_2$ microspheres has been limited to the gram scale. Although work to date has demonstrated the feasibility of sol-gel methods to produce microspheres of $^{238}PuO_2$, additional efforts are needed to answer questions regarding microsphere and coating stability.

More work is needed to address issues regarding the use of sol-gel at Los Alamos as well as the use of microsphere-based heat sources for future NASA science missions. For example, pellet pressing tests are needed to confirm that sol-gel microspheres can produce an acceptable hot pressed GPHS pellet. A sol-gel flowsheet and hardware design is also needed to estimate worker dose during processing activities. Further, an evaluation whether $^{238}PuO_2$ microspheres can be successfully coated, and the stability of those coatings, would help answer questions regarding thermal conductivity and fuel containment robustness in launch accidents.

Pursuing sustained heat source R&D would allow uncertainties and risks to be reduced; development could proceed at a pace commensurate with the likelihood of successfully implementing sol-gel at PF-4 as well as NASA's schedule requirements. Obtaining priority information in the near-term would help inform ongoing NASA planning activities and feasibility studies.

IV. CONCLUSIONS

Use of $^{238}PuO_2$ microspheres for future RPS poses advantages for fabrication as well as device performance. The sol-gel method vastly reduces the production of hazardous fines while microspheres may be coated for improved safety and thermal conductivity. Additionally, microspheres enable ideal and flexible geometries for some of the most challenging upcoming missions.

Based on the trades and constraints for a cryobot, development of radioisotope heat source configurations with a higher power density than a stack of GPHS modules is highly desirable. Attractive near-term options include 1) a common, cylindrical aeroshell that accepts 6-7 GISs containing $^{238}PuO_2$ pellets, as depicted in Figure 4, or 2) a similar aeroshell configuration with $^{238}PuO_2$ microspheres to increase power density.

Considering the perceived benefit of a new microsphere-based heat source and the lead time required to develop and qualify it, an effort should be initiated to develop a roadmap and budget, as well as perform priority experiments to answer key questions and reduce risks. Such information is needed soon to improve JPL's insights into the feasibility and cost of a microsphere-based heat source as well as when it could be available.

ACKNOWLEDGMENTS

Information presented about future power system and mission concepts is pre-decisional and is provided for planning and discussion purposes only. A portion of this research was carried out at the Jet Propulsion Laboratory, California Institute of Technology, under a contract with NASA (80NM0018D0004).

REFERENCES

1. Schock A (1980) Design Evolution and Verification of the General-Purpose Heat Source. Fairchild Space and Electronics Company, Germantown, MD
2. Romanoski GR, Pih H (1995) Impact Test Characterization of Carbon-Carbon Composites for the Thermoelectric Space Power System. Vancouver, Canada
3. Zee R, Romanoski G (2000) A filament wound carbon-carbon composite for impact shell application. AIP Conf Proc 504:1488–1493. https://doi.org/10.1063/1.1290970
4. Katalenich JA (2017) Production of PuO_2 and NpO_2 Microspheres
5. Sholtis J, Lipinski R, El-Genk M (1999) Coated particle fuel for radioisotope power systems (RPSs) and radioisotope heater units (RHUs). AIP Conf Proc 458:1378–1384. https://doi.org/10.1063/1.57532
6. Hockman B, Smith M, Nesmith B, et al (2020) Heat Sources for a Europan Melt Probe
7. Katalenich JA, Carstens NA, Lanza MS, Prichard AW (2019) Cryobot Microsphere Heat Source - PNNL Final Report, Rev. 1. Pacific Northwest National Laboratory, Richland, WA

Nuclear and Emerging Technologies for Space
Sponsored by Oak Ridge National Laboratory, April 26th-30th, 2021.
Available online at https://nets2021.ornl.gov

DEVELOPING PRODUCTION LIFE CYCLE (PLC) LEVELS BASED ON PRODUCTION FACTORS AND THEIR APPLICATION IN DETERMINING THE PRODUCTION READINESS OF A HERITAGE RTG COMPONENT (SIGE UNICOUPLES)

Daniel P. Kramer

University of Dayton, Dayton, Ohio, 45469

(937) 229-1038 / daniel.kramer@udri.udayton.edu

The development of a process that takes into account the Production Life Cycle (PLC) of a component as a function of time is constructed. PLCs can be utilized to estimate the current production readiness status of a component that is no longer in production, and for which there is a need to estimate the activities required to achieve a production re-start. Re-starting a production capability can be complex, especially if a significant amount of time has elapse since the cessation of a production activity.

In an effort to better identify the status of heritage SiGe unicouple production, a set of Production Factors were developed and utilized to estimate its PLC level. PLC values range from 1 to 9 as actual production readiness increases, while also taking into account the time since the last production unit or campaign. Since PLC values are developed at a particular time, they are a "snapshot" of the production readiness of a component at that date, which also needs to be specified. The first-order analysis shows that the current PLC for the production of heritage SiGe unicouples is PLC 2-4/June-2020, dependent on the current availability of heritage manufacturing articles from the 1990s.

I. BACKGOUND

I.A. NASA TRL - Technology Readiness Levels

Attempts to develop a structure for describing the status of a technology program has some of its early origins in a 1989 paper by S.R. Sadin, et al.[1] While not employing the later concept of TRL (Technology Readiness Levels), the paper does propose the concept of seven Readiness or Technology Levels. Over the years, NASA has developed variations of program readiness levels in further endeavors to achieve a comprehensive agency-wide accepted description and definition of the levels. This eventually resulted in the development of NASA Technology Readiness Levels (TRL). A NASA sponsored Technology Readiness Assessment (TRA) Study Team in 2016 was tasked to investigate the then current internal TRA process with input from across NASA.[2] Their report contains a NASA Technology Readiness Assessment chart that lists nine TRLs with descriptions of various aspects of each of the levels. The Radioisotope Power Systems (RPS) program (NASA/GRC) also recognizes the importance of Technology Readiness Levels as it supported the development of TRL definitions specifically for determining the status of thermoelectric technologies.[3]

I.B. DoD MRL - Manufacturing Readiness Levels

Since the U.S. Department of Defense (DoD) also has program and procurement needs for very high-quality critical components/systems similar to NASA, the DoD has adapted aspects of Technology Readiness Levels. However, in a number of areas the ultimate mission needs of the DoD can significantly differ compared to NASA's mission needs. One major difference is in the quantities of manufactured components routinely procured by the DoD. In order to accurately assess a component's manufacturing readiness, and in order to evaluate acquisition and delivery risks, the DoD has developed formal detailed Manufacturing Readiness Levels (MRL).[4] MRL definitions take into account various "treads" related to manufacturing including; Process Capability and Control, Technology/Industrial Base, Design, Cost and Funding, Materials, Quality Management, Personnel, and other factors.

II. DEVELOPMENT OF PRODUCTION LIFE CYCLE (PLC) LEVELS EMPLOYING PRODUCTION FACTORS (PF)

While NASA's Technology Readiness Levels (TRL) and the DoD's developed Manufacturing Readiness Levels (MRL) provide a process for evaluating the overall status of a component/systems development from concept to manufacturing, they generally lack the concept of time. In general, both do not address the potential detrimental influence of a time gap between production campaigns. TRL and MRL values are very useful for helping to determine the current readiness level of a component/system. Generally, this is most useful for components/systems that are in active development, in current production, or are or have been fielded. However, in reality TRL/MRL values tend to decrease over time

once development and/or manufacturing ends. This is true since deviations in materials availability, declining personnel experience, availability of equipment resources, etc. will tend to degrade TRL and MRL values as a function of time. To resurrect a development effort or to re-start a previously manufactured component requires that several critical production factors be re-established. Component/system production "re-starts" can have many challenges in that a technical community or management usually significantly underestimates the required time and/or resources needed to re-establish a robust, high quality, high yield production capability.

II.A. List of Developed Production Factors (PF):

Experience on a number of critical defense components/systems from initial concept to production has demonstrated that the re-manufacturing of "heritage" components is not easy. This experience includes the resurrection of components that were once in full production and fielded, but whose production ended due to no anticipated future needs. This has helped the author to identify several critical factors for the manufacturing of new and especially the production restart of heritage components.[5] Below are seven identified production factors that can easily degrade as a function of time recognizing that this may not be an all-inclusive list:

Materials – Are the raw materials, metals, ceramics, plastics, etc. still obtainable from qualified suppliers? Have the composition/purity of the raw materials changed over time? How quickly can it be fully demonstrated that any replacement materials are truly equivalent?

Tooling – Critical mechanical set-ups required for fabrication of component pieceparts required for manufacturing. Was hard tooling designed and/or built or only soft tooling used during component development or production? Are tooling prints or tooling still available?

Fixturing – Critical assembly devices employed in the dimensional alignment and actual fabrication of sub-components/components. Was hard fixturing designed (e.g. fully documented signed-off prints), or only soft fixturing used during component development or production (e.g. sketches or prototypes)? Are prints or the soft/hard fixturing still available?

Processing – General unit operations employed during development/production of components. Could include furnace time-temperature profiles, cleaning and assembly processes, and in-process quality assurance tests. Are any original process manuals still available?

Documentation – Status of the written quality control/assurance manuals, specifications, certifications, etc. required to fully support the development and production of the components? Documentation is utilized to ensure that materials traceability and component quality can be certified and the information archived.

Personnel – Are trained technicians, development and production engineers, and scientists available who are knowledgeable and/or experienced in the actual development and production of the components? Are personnel available with direct hands-on experience in the production of the particular component of interest?

Equipment – Has all of the equipment required to perform development through manufacturing identified? Is original equipment in-place and/or usable? If the original equipment is available, how reliable is it, and what is its expected life span versus the length of the new production campaign? Is in-process test equipment required and available? If new equipment is required, can it be designed/fabricated/purchased? Time required to purchase and make operational any necessary equipment?

II.B. Production Life Cycle (PLC) Levels for a Component

By estimating a numeral value for each of the production factors, it is possible to quantify the production status of a component at a point in time. TRL and MRL values are typically discussed in terms of levels 1 to 9. So numerical values of 1 to 9 are employed for PLC levels. Below are the developed PLC levels based on past component development, fabrication, production, and re-start experience. These levels are an attempt to describe the full life cycle of a component from concept to production with a heavy emphasis on the previously discussed production factors. Re-starting a production capability after it has been idle or disbanded in order to produce additional needed components has a unique set of difficulties. PLC levels can be employed for estimating the production readiness of a component/system that has not been continuously manufactured.

PLC 1: Initial component/system needs identified with, without, or by potential customer including basic performance criteria and operating environment

Discussion: R&D personnel identify a specific need and may interface with potential customer. Basic component/system specifications identified including: general dimensions and volume envelope, materials selections and constraints, and performance requirements. Typically R&D personnel.

PLC 2: Preliminary component/system design/fabrication analysis

Discussion: Identified performance criteria employed to initiate component/system design and fabrication. Applied research and scientific principles employed to ensure specific concepts are in alignment with outlined requirements. Limited pieceparts may be obtained for initial design and processing trials with laboratory equipment. If customer driven, their input should be obtained at appropriate times to ensure that what is being developed meets their criteria. Typically R&D personnel.

PLC 3: Initial component/system fabrication and processing development

Discussion: Larger acquisition of component/system pieceparts for design and process validation. May consist of numerous process and design iterations each mainly based on the fabrication of a limited number of processed articles and testing. Design and process improvements made with support of analytical and laboratory studies. Focus is on the demonstration of potential component/system success. Typically R&D personnel.

PLC 4: Component/system design/processing validation within a laboratory environment

Discussion: Open set-ups are still viable, but soft fixtures/tooling are to be used at later segments of this event. Processing experiments should be essentially complete. Component design tests should identify any potential deficiencies with appropriate countermeasures employed to reduce or eliminate them. Demonstration of high likelihood component can be successfully fabricated and meet all requirements. R&D personnel with Production members as appropriate.

PLC 5: Component/system development essentially completed including performance verification

Discussion: Development agency completes component/system design, process verification, and prototype fabrication. Some design and process changes are expected in the solving of realistic problems that are likely to occur. Performance testing of prototypes are employed in a thoughtful iterative process to enhance design and development. Technical development personnel will interface with appropriate production agency representatives at development meetings. Some of these activities may include the application of production agency equipment. R&D personnel with Production employees input.

PLC 6: Component/system final development and handoff to production agency

Discussion: Development agency completes design, process verification, prototype fabrication, and testing. Development agency responsible for fully demonstrating that the component/system designed will meet all performance criteria, and appraises the production agency of all known potential roadblocks. Production agency personnel are now informed of all late-stage development initiatives, and now have substantial input into final designs and processes. A go/no-go decision for the hand-off from development to production is made jointly. At the end of this PLC level, Production agency becomes the lead with R&D personnel letting go of the component/system as they are no longer the main contributors.

PLC 7: Component/system prototype demonstration production batch/lot

Discussion: Final development batch/lot employing soft or hard fixtures and tooling. Process and quality documentation nearly complete but open to moderate editing and changes. Process production equipment identified and employed as much as possible at this time. Upper management commitment to production with allocation of all needed resources. Production personnel training nearly completed and documented. Production personnel lead with R&D personnel available as needed.

PLC 8: Component/system successfully completes initial Production Test Lot (PTL)

Discussion: PTL performed employing qualified raw materials, hard fixtures and tooling, final process manuals, and dedicated processing equipment, all of which are employed during the PTL campaign. Personnel training has been completed, and trained personnel are dedicated to the PLT manufacturing effort. Manufactured PTL product is extensively tested to conclusively demonstrate that performance meets all required operating criteria. Any process documentation changes are very minor. All vendors fully qualified. Production personnel.

PLC 9: Component/system in full production, meets all operating performance requirements, and mission fielded

Discussion: Component/system is in production. Quality assurance program fully employed to ensure production units continue to meet performance criteria in operational environments. All design/process documentation is signed off, hard fixtures and tooling approved for use, and vendors qualified. Production rate (either continuous or batch) is high and frequent enough to sustain the complete maintenance and availability of production equipment as well as the personnel knowledge and skill base related to all production related activities. Production personnel.

III. ESTIMATING CURRENT PRODUCTION LIFE CYCLE (PLC) LEVEL OF HERITAGE SiGe UNICOUPLES

SiGe unicouples have been successfully employed for over four decades; from the two Voyager spacecraft launched in 1977 (powered with MHW/Multi-Hundred Watt RTGs) to New Horizons launched in 2006 (powered with a GPHS/General Purpose Heat Source RTG). Unfortunately, U.S. space qualified SiGe thermoelectric unicouples for RTGs have not been manufactured since the late 1990s, when the production capability was discontinued and the equipment, know-how, and personnel were not cohesively preserved. Recently, there has been increasing interest in heritage SiGe (hSiGe) based thermoelectrics (Figure 1) due to their mission proven capabilities.

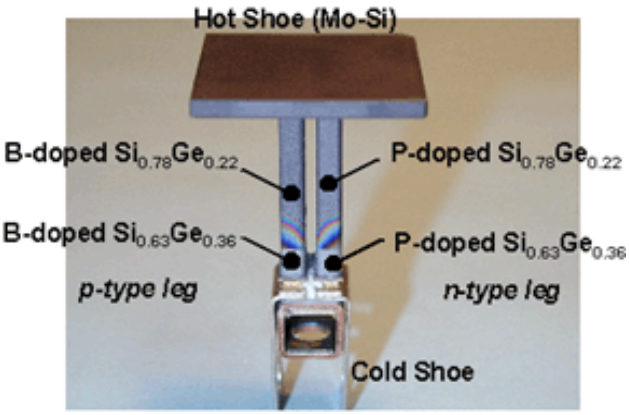

Fig 1. Example of a Heritage SiGe Unicouple.[6]

Employing NASA TRL descriptions, it would be expected that heritage SiGe unicouples are TRL 9 as they were successfully employed in a number of long-term space missions. However, since heritage SiGe unicouples have not been produced since the late 1990s does a TRL 9 fairly represent their current actual readiness status? In reality since heritage SiGe unicouples have not been produced for decades, their actual production readiness level has been dramatically diminished. By applying the discussed Production Factors, a Production Life Cycle (PLC) level can be estimated. One of the anticipated strengths of a PLC analysis is that it can provide a "snapshot" of the production readiness of a component/system at a specific date. This capability can enhance how a program can more accurately determine the actual production status of a component. Combining the discussed Production Factors in conjunction with the PLC levels, it is now possible to estimate a current manufacturing status of the heritage SiGe unicouples.

III.A. List of Production Factors with Current Estimated PLC Levels for Heritage SiGe Unicouples:

Materials – Si, Ge, dopant powders, brazes, copper alloys, alumina, etc. are still being commercially produced. However, there are likely differences in elemental compositions, powder characteristics, impurities, etc. that could complicate further required processing endeavors. Even slight differences in powder surface morphology, average particle size, particle size distributions, etc. can significantly change the properties of the final product. Therefore, there is real risk in obtaining or processing the required materials as represented in the range of the estimated PLC values presented.

PLC 2 – If the required materials are not available or are only similar to heritage materials.

PLC 4 – If the required materials are very similar to heritage materials.

Tooling – The fabrication of pieceparts that meet dimensional design specifications is critical in obtaining high-quality heritage SiGe unicouples. During most component production activities, specialized tooling needs to be designed and fabricated, sometimes for each individual piecepart. SiGe unicouple production requires tooling critical to ensure that bonded sub-assemblies meet all specifications. This would include tooling for the fabrication of the copper heat shunts, pedestals, and electrical connectors, in addition to the molybdenum, tungsten, and stainless steel pieceparts. If actual heritage SiGe unicouple tooling or hard drawings of the various tooling are available, it would significantly reduce overall risk. If they are not available, it will likely require an iterative design, fabrication, and testing process to re-develop tooling. Therefore, the risks if tooling is available or is not available is represented in the range of the estimated PLC values presented.

PLC 2 – If tooling or drawings are not available

PLC 3/4 – If tooling or drawings are available

Fixtures – Similar to tooling, fixturing is also critical for obtaining high-quality SiGe unicouples. Fixtures are used to ensure that sub-assemblies will meet all dimensional design specifications. They are employed to position individual pieceparts in an aligned "stack" during a bonding/brazing furnace operation. If fixtures are not correctly designed and fabricated, then next assembly operations in the process flow will most likely not result in dimensionally accurate high-quality components. Most component production activities require specialized tooling to be designed and fabricated, sometimes for each assembly furnace operation. Similar to tooling, if heritage SiGe unicouples fixturing or hard drawings are available it will reduce risk. If not available, it will increase risk and require an iterative design, fabrication, and testing process to re-develop the fixtures. The risks if fixtures are or are not available are represented in the range of the PLC values below.

PLC 2 – If fixtures or drawings are not available

PLC 3/4 – If fixtures are available

Processes – Many of the various unit operations require the precise control of critical processing parameters such as gas atmospheres and flow, furnace time-temperature ramps/soaks crucial for various bonding or brazing operations, etc. Processing parameters were defined originally during development activities with some likely changes even occurring during production. Production process manuals were employed during production of the heritage SiGe unicouples. If these process manuals are available it would greatly ease the re-establishment of a production capability. The risks if production process manuals are available or are not

available are represented in the range of the estimated PLC values below.

PLC 2 – If process manuals are not available

PLC 4/5 – If process manuals are available

Documentation – Production of hSiGe unicouples required certifications, quality control/assurance manuals, etc. to be generated, and very likely archived. If documentation could be readily located it would assist in the re-establishment of production capability.

PLC 2 – If full production documentation such as quality assurance/control, flow sheets, etc. are not available

PLC 4/5 – If full production documentation such as quality assurance/control, flow sheets, etc. are available

Personnel – The last production run of flight-qualified heritage SiGe unicouples was during the late 1990s. While knowledgeable thermoelectric production personnel could be employed to help re-establish unicouple production, it is very unlikely that they will have significant direct hands-on RTG flight-quality hSiGe unicouple production experience. It is significant that despite all of the extensive production documentation generated during the Cassini program, there was substantial undocumented "art" imbedded within the knowledge base of the production personnel.

PLC 1 – If hands-on heritage SiGe unicouple personnel are not available

PLC 3 – If several hands-on heritage SiGe unicouple personnel are available

Equipment – While the need for critical processing equipment such as hot presses and brazing furnaces can be readily identified, necessary "smaller" items such as assembly clean benches, process microscopes, piecepart cleaners, etc. need to be identified/obtained. Specific in-process test equipment for quality control/assurance may need to be re-designed and/or fabricated/purchased. It is probable that the design and construction of a fully functional facility for fabricating flight-quality hSiGe unicouples will need to be organized/equipped. Any delay could impact the fabrication and delivery time required for the production of high-quality components.

PLC 2 – Equipment and facility space will need to be identified, obtained, and made operational

PLC 3 – If some equipment/facility is available

By assigning a PLC numerical value to each production factor (PF) and then dividing the total of the assigned values by the number of factors considered, a "snapshot" of the current status of the manufacturability of heritage SiGe unicouples can be estimated based on the previous discussions. This method also allows for a range in the PLC to be estimated based on the discussed uncertainties that may be associated with individual PFs.

TABLE I. Estimate of current PLC levels of RTG flight-quality heritage SiGe unicouples employing the various Production Factors for High and Low Risk Scenarios.

Production Factor	High Risk Scenario	Low Risk Scenario
Materials	2	4
Tooling	2	3.5
Fixtures	2	3.5
Processes	2	4.5
Documentation	2	4.5
Personnel	1	3
Equipment	2	3
Total/# Factors	13/7	26/7
PLC	**2**	**3 to 4**

IV) SUMMARY

A process based on the development of Production Factors is employed to construct Production Life Cycle (PLC) levels of a component or system as a function of time. PLC values may provide a real benefit to a program that needs to estimate the current manufacturability status of a heritage component or system no longer in production. PLCs can be employed to estimate the current production readiness status of a component for which there is a need to estimate the activities required to achieve a production re-start. Re-starting a production capability can be complex, especially if a significant amount of time has elapse since the cessation of a production activity. Similar to TRL/MRL, the proposed PLC values also progress from 1 to 9 as actual production readiness increases and, most importantly, they are designed to take into account the usual detrimental time lapse since last production unit.

A first-order analysis of the current PLC value for RTG heritage SiGe unicouples based on the various production factors is determined. Since PLC values are developed at a particular time, they are a "snapshot" of the production readiness of a component at a particular date, which also needs to be specified. The analysis determined that the current PLC for the production of heritage SiGe unicouples is PLC 2-4/Jun-2020, depending on the current availability of various heritage manufacturing, documentation, etc. from the 1990s.

REFERENCES

1. S.R. SADIN, et al., "The NASA Technology Push Towards Future Space Mission Systems," Acta Astronautica, vol. 20, p.73-77, Pergamon, 1989.
2. S. HIRSHORN and S. JEFFRIES, *Final Report of the NASA Technology Readiness Assessment (TRA) Study Team*, NASA Office of Chief Engineer and NASA Office of Chief Technologist, March 2016.
3. *Thermoelectric RTG Technology Readiness Levels*, Radioisotope Power Systems (RPS) Program, NASA/GRC, RPS-DOC-0152, May 21, 2020, 22p.
4. *Manufacturing Readiness Level (MRL) Deskbook*, OSD Manufacturing Technology Program in collaboration with The Joint Service/Industry MRL Working Group, Version 2.0, 81 p., May 2011.
5. D.P. KRAMER, *Developing Production Life Cycle (PLC) Levels Based on Production Factors and their Application in Determining the Production Readiness of a Heritage RTG Component (SiGe Unicouples)*, UDR-TR-2020-134, University of Dayton Research Institute, Dayton, OH, July 2020, 16pp.
6. P. Beatty, https://commons.wikimedia.org/wiki/File: SiGe_Unicouple_Assembly.png, 2015.

Nuclear and Emerging Technologies for Space
Sponsored by Oak Ridge National Laboratory, April 26th-30th, 2021.
Available online at https://nets2021.ornl.gov

MISSION CONCEPT CONSIDERATIONS FOR OCEAN WORLD EXPLORATION USING RPS INSIDE A PRESSURE VESSEL

Young H. Lee[1], Tibor S. Balint[1], Brian Bairstow[1], Benjamin Donitz[1]

[1]*Jet Propulsion Laboratory, California Institute of Technology, 4800 Oak Grove Dr., Pasadena, CA, 91109*
818-354-13426, young.h.lee@jpl.nasa.gov

The National Aeronautics and Space Administration (NASA) has identified six ocean worlds according to the NASA Roadmap to Ocean Worlds, namely: Earth, Europa, Ganymede, Callisto, Enceladus, and Titan. In addition to this set, there are a number of identified potential worlds (e.g., Triton, Ceres, Pluto, Ariel, Miranda)[1]. Accessing into and through the ice shells of ocean worlds will enable compelling science set out in the Decadal Survey[2], including the search for evidence of extinct or extant life.

This paper describes the Ocean Worlds Concept of Operations Study that was conducted by the RPS Mission Analysis Team and A-Team at the Jet Propulsion Laboratory (JPL) for the Radioisotope Power Systems (RPS) Program. The main objective of this study was to investigate a concept of operations of the RPS within a PV over the end-to-end life of a mission. Most past mission concept studies have focused on the novel mission stages within the ice or within the ocean, while this study was focused on identifying considerations needed for developing the RPS within a PV (pressure vessel), examining each mission phase from an end-to-end mission operations perspective.

I. INTRODUCTION

Exploring Ocean and Ice Worlds below the ice-surface could help us to understand the origin and evolution of life in the universe, and how these planetary bodies form and evolve. Accordingly, there has been significant science community interest in subsurface exploration of ocean worlds, recognizing Europa, Enceladus, Ganymede, Callisto, Titan, Dione, Triton, and Pluto as potential scientific exploration targets. To carry out a subsurface ice and ocean access mission, key capability challenges revolve around the power source and around mitigation of extreme environmental conditions, including high pressures and low temperatures. Numerous concepts have been studied that are enabled by the use of RPS power and heat for operations, survival, melting, and mobility. Also, some mission concepts considered a mission architecture in which the probe and RPS were inserted within a PV to separate and protect the system from the extreme environments, for example, to withstand the high external pressures within the ice-shell and in the ocean below it.

The RPS Program's Mission Analysis Team and JPL's A-Team conducted an Ocean Worlds Concept of Operations (ConOps) Study, focusing on identifying key considerations needed for managing the RPS within a PV, examining each of the mission phases from an end-to-end mission operations perspective. In this paper, we address how the ConOps of a subsurface ice mission would influence mission design considerations, such as mission architectures, RPS accommodation requirements through all mission phases, and related planetary protection (PP) aspects. These design considerations would respond to environmental constraints, launch and landing constraints (e.g., g-load tolerance), as well as the sizing of the power and thermal systems for needed science measurements.

II. OCEAN WORLDS CONOPS STUDY

II.A Ocean Worlds Science

To identify the science requirements for the study, the scientists from the study team brainstormed science objectives, accompanying investigations and instruments required for science measurements targeting Ocean Worlds destinations. The five considered science objectives were

1. Search for and characterization of life within the ice shell and ocean
2. Investigate the habitability of the ice shell and ocean
3. Characterize the physical properties within the ice shell and ocean
4. Characterize the chemical state and processes within the ice shell and ocean
5. Investigate the ice-ocean interface, including chemical and physical processes and material exchange

Considering the use of the Mars Curiosity mission payload mass and power allocation as an analogy and a starting point for the study, the total mass and power for considered payloads were 75 kg ±25 kg and 64 W ±16 W, respectively. The study focused on Europa and Enceladus as baseline cases for ice-shell and ocean explorations with an RPS inside a PV. Considerations for and sensitivities to other destinations were also examined.

II.B RPS Inside a PV

There are many science and technology drivers that could impact the design of the RPS inside a PV. Power, mass, and volume requirements of required instruments

would influence both the RPS and PV sizing. As RPS could assist with melting the ice during traversing or swimming in the ocean while providing heat for keeping them warm, the desired thermal heat would also influence both the RPS and PV sizing. Equally, the Ocean Worlds environments and the concept of operations could control the mission architecture and design of the RPS inside a PV.

II.C PV Considerations

The melt-probe consists of a PV, which protects and houses the RPS, the payload, and subsystems. To enable Ocean Worlds exploration, this novel configuration requires a dedicated capability development effort where the PV design must be customized and optimized for all mission phases and target environments.

Ocean Worlds environments may contain sulfuric acid (<40% mol) near the surface, and high concentrations of salts (<~25% in ice-shell, <~2% in ocean) causing corrosion concerns. At the ice-ocean interface, the pressure could be as high as ~50 MPa at Europa, and up to ~1 MPa at Enceladus. Under these conditions, an ill-designed PV could easily fail—the most likely failure mode would be buckling. Thus, material selection for strength, weight, and thermal performance will be important. All feedthroughs for electrical wiring, sample acquisition, and windows need to be safe against pressure and fluid. Endcaps options are expensive from both mass and volume aspects. Sealing surfaces for closeout will require additional fixturing and mounting surfaces.

A smaller RPS could reduce both PV volume requirement and mass, but would necessitate low-powered subsystems and instruments and may not provide sufficient excess heat for melting or component heating.

II.D RPS Considerations

The study approach was taken to be agnostic to RPS designs. For this study, the considered RPS was 75 kg, generating ~50–300 W_e, and 1500–4000 W_t power. The excess heat not converted to electric power would be used for component heating, or rejected through the PV walls, where it could be used for ice melting. Fitting the RPS inside a PV would pose a design challenge. A compact design could situate the radiation source near the instruments. This could impact the performance and lifetime of the instruments, and would need to be mitigated through a separation distance, or shielding. Either mitigation option would increase the overall mass, and separation could also increase the volume, which would be especially undesirable for the configuration. The assumed RPS dimensions were 20–35 cm (finless diameter) and 90–110 cm (length), to be accommodated inside the PV. Existing RPS designs might not be suitable to fit inside the PV, since the PV has specific geometric constraints.

Currently, the RPS design lifetime is 17 years from the beginning of life (BOL) at fueling to the end of life (EOL) at decommissioning. Launch is typically assumed to occur within 3 years after the BOL. Ocean Worlds missions with long cruise times to the outer planets (that could take 10 years or more) and the multi-year in-situ subsurface operation may necessitate a reassessment of the design lifetime for the RPS inside a PV configuration.

The RPS could be designed to operate in vacuum (requiring an evacuated PV), or in a fill-gas “atmosphere” (which would be used inside a pressurized PV). The RPS would also need to be g-load tolerant to account for launch and landing loads. In addition, requirements for assembly, test and launch operations (ATLO), space environment (e.g., during a Venus Gravity Assist, VGA, maneuver), subsurface conditions and PP should all be considered.

III. CONCEPT OF OPERATIONS

Ocean Worlds ConOps phases were divided into two main parts: 1) transport phases comprising of ATLO, cruise to the destination, orbit insertion, and descent and landing, and 2) exploration phases including on-surface operations, subsurface operations while traversing in the ice, in-ocean operations and decommissioning at the end of the mission (EOM), that corresponds to EOL. Key considerations needed for developing the RPS within a PV over the end-to-end mission phases are highlighted in the following subsections.

III.A Considerations During ATLO

Two to three years before the launch, the power system related ATLO would begin at the Idaho National Laboratory (INL)—a Department of Energy facility—for fueling, testing, transportation, and storage. Fueling would involve loading the Pu-238 into the GPHS modules, performing acceptance testing for the RPS, shock and vibration, and environmental testing. At 12 months prior to launch, the fueled RPS would then be inserted into the pressurized or evacuated PV and sealed. All these activities would occur at INL. If pressurized, the fill-gas would need to be non-corrosive to the equipment. If other spacecraft components share the PV, those components would need to be integrated at the INL facility. A fueled system would likely require active cooling from storage through launch. The cooling method would depend on the size and thermal output of RPS. The system would go through acceptance testing and must meet PV integrity standards. About six months prior to launch, the RPS inside a PV would be transported using an RTG 9904 Type B shipping container to the launch site. This special container could bound the size of the RPS within a PV. After the delivery, the system may be

integrated with other flight hardware to allow performing integrated functional checks. A modular PV design would allow for easier access to the RPS. After integration into the launch vehicle fairing, the system could still require continuing cooling, which would require access to the RPS through the fairing. Each RPS is designed for launch shock and vibration loads (up to ~20 g), and also to mitigate launch failure risk.

III.B Considerations During Cruise and Insertion

If the trajectory involves a Venus flyby (VGA), the thermal design would need to account for a higher heat input from the Sun on spacecraft surfaces. It would reduce radiator efficiency to reject the excess heat from the RPS to space, compared to rejecting it to the 4K deep space temperature during nominal cruise to the outer planets. The deep space cruise phase could take up to 10 years or more. Earth flyby is considered a critical event for an RPS-enabled mission. It is related to safety and should be assessed for the probability of impacting the Earth in an event of failure. The PV would also need to undergo a breakdown and breakup analysis to verify that in the event of a failure at launch or re-entry, the radioactive material would not be exposed to the environment.

The radiation environment around the targeted planetary system may determine the chosen orbit and target arrival. The orbit insertion vibration and shock loads would be expected to be below launch loads.

III.C Considerations During Descent and Landing

After decoupling from the carrier, the RPS may need to provide its own thermal control during the short 1-hour descent and landing sequence. Autonomous hazard avoidance and soft landing would be implemented to minimize g-loads below the launch levels. Contamination by the descent thrusters on the target surface should be avoided, as it could bias post-landing sample analysis.

III.D Considerations During On-Surface Operations

The amount of time allowed on the surface would be driven by the radiation environment (highest at Europa). Salt and ammonia deposits might create an acidic layer on the surface, requiring corrosion resistant materials. During initial melting, most of the RPS heat would be focused to the nose (the front end in the traversing direction), while the PV-probe would need to be oriented vertically (to minimize the cross-sectional interface with the ice, and focus the weight on this point). The melt-probe would be designed to withstand tectonic-, pressure-, and tidal-forces. The melt-probe would likely have to be anchored during various phases of its traverse, where surface hardness would drive the anchoring method. Melting techniques could include drilling, melting, and/or water jetting. Due to the low gravity environment, if the melted water does not sublimate and develops a liquid pocket, the probe may become buoyant, preventing further descent. This may become an increasing challenge on Enceladus or on other smaller moons, and thus traversing may require mechanical methods.

III.E Considerations During Subsurface Operations

The probe's geometry—including front- and side-wall-thermal designs—would be closely coupled with the environmental conditions, and would impact its traversing speed and ultimately the duration to reach the ocean. For example, warmer pure ice would be softer than contaminated cold ice. A compact probe would be more desirable. For example, a 20 cm-diameter RPS inside the PV and a few meters length could traverse the ice efficiently. Miniaturization of the payload and subsystems could reduce the energy requirements, as well as allow for a compact PV design. Doubling the length of the probe would provide more volume, but more than double the power requirements, increase mass, impact landing configuration, and influence the thermal design for heat distribution. The probe may need a dedicated heat rejection system, instead of being directly tied to the PV wall. For a segmented PV design, the segment housing the RPS would need to provide both electric and thermal power to other segments. Thermal control and power-source safety would be important considerations for all types of RPS. Variable thermal power to the walls would control the melt speed and sample acquisition, and allow for freezing into the ice, while performing science investigations at the ice-water interface. Alternatively, a suitable anchoring system could be used that is designed not to interfere with mobility, and could mitigate positive buoyancy in a melted ice pocket.

III.F Considerations During In-Ocean Operations

The probe could either move freely in the ocean or could be tethered to the point of entry. This decision will have implications on the disposal at the end of mission. A tethered non-buoyant design lowered from the entry point would differ from a swimmer configuration, which would need to be buoyant and have a dedicated propulsion system. Unknown currents would further complicate the design. The PV mass would depend on the depth of the ice shell. The mission duration, combined with the ocean composition would impact corrosion mitigation efforts, material selections, probe mass, and overall design.

III.G Considerations During EOM Decommissioning

In the ice over time, the RPS may melt a liquid pocket, inducing an environment with standing water. While the decaying Pu-238 would naturally reduce its heat output to safe levels over a timeline of decades, corrosion of the PV in the ocean or ice shell could expose the heat, radioactive material or non-sterilized components to the ocean. Further study is needed to determine the appropriate time-frame for disposal in line with PP guidelines.

IV. PP CONSIDERATIONS

An Ocean Worlds subsurface and ocean explorer mission at Europa or Enceladus would be considered Category IV under PP[*3*]. This would impact the design and placement of the instruments, driving whether they would be outside the PV and directly in contact with the environment or inside with the RPS. During launch operations, contamination control (from launch vehicle materials) would need to be analyzed. Further PP considerations would be required to assess the probability of any gravity assisted maneuvers targeting the destination, or impacting a potential astrobiology target during orbit insertion, descent and landing. PP considerations would likely be similar to that of the Europa Lander during descent and landing and on the surface. While traversing in the ice and the subsurface ocean, PP would be impacted by how water is sampled and moved inside the PV. At the end of the mission, if instruments were not sterilized prior to flight (due to sensitive equipment), sterilization would need to be performed prior to disposal, for example, by baking out the components in-situ.

V. KEY FINDINGS

In this paper, we highlighted considerations needed for an RPS inside a PV mission architecture that could enable Ocean Worlds exploration of ice-shells and oceans. We discussed the complex challenges and considerations that science, technology, and mission development communities must overcome, and need to address while considering this mission architecture.

The corrosive environment (e.g., from salts in the ice) might drive the design and material selections of the PV and other surfaces exposed to this environment. For low-gravity destinations (e.g., at Enceladus), anchoring to the surface might be a significant challenge. Design considerations on anchoring methods and stability could be influenced by the unknown environments, in connection to surface hardness and porosity.

The study found that the payload would likely not be the driving factor for RPS sizing or power level. Instead, the design would be driven by the thermal power required to melt-traverse through the ice. The physical size of the RPS would be driven by the PV diameter, and the arrangements and configuration of the GPHS modules and thermal convertors. The current standardized shipping container dimensions could further constrain the design.

Ocean Worlds missions with long cruise times to the outer planets (Cruise to the Saturn and beyond can take over 10 years) and the multi-year in-situ subsurface operation may necessitate a reassessment of the design lifetime for the RPS inside a PV configuration.

During ice traversal, most of the heat would need to be directed to the front of the PV. Mission operations may require a variable heat distribution design, to serve initial melting into the ice, guided melting for obstacle avoidance, and slow melting or stopping during science investigations and sampling. Successful melt-driven traversing in the ice shell could require as much as 6–8 kW_t. This translates to 24–32 GPHS modules even at their nominal heat output at BOL. Further assessments are needed to find innovative solutions for PV designs that could minimize the RPS excess heat for successful ice-melting operations.

PP will inform developers and mission designers about the requirements for operating near planetary bodies (e.g., Earth, flybys, in-ice, and in-ocean operations, sampling and decommissioning). PP considerations would be expected to play key roles throughout all mission phases. For Ocean Worlds exploration**,** Category IV requirements should be carefully considered.

During future development steps**,** these considerations could lead to guidelines, then to accommodation requirements for RPS. Such development is expected to take years and requires a focused effort. One of the study goals was to inform the science, technology, and mission development communities about mission design and operational considerations for these types of in-situ exploration mission concepts.

ACKNOWLEDGMENTS

This work was performed at JPL, California Institute of Technology, under a contract with NASA. The authors would like to acknowledge the valuable contributions from members of Ocean Worlds ConOps A-Team Study at JPL, including participants from the Applied Physics Laboratory, Glenn Research Center (GRC), Goddard Space Flight Center, and INL. This study was funded by the RPS Program at GRC. The information presented about potential future mission concepts and notional power systems is pre-decisional and is provided for planning and discussion purposes only.

REFERENCES

1. Hendrix, A.R., et al., (2019). *The NASA Roadmap to Ocean Worlds*. Astrobiology. Jan 2019. 1-27. http://doi.org/10.1089/ast.2018.1955
2. National Academies of Sciences, Engineering, and Medicine. (2018). *Visions into Voyages for Planetary Science in the Decade 2013-2022: A Midterm Review*. Washington, DC: The National Academies Press. https://doi.org/10.17226/25186.
3. NASA, Office of Safety & Mission Assurance. (2021). *Planetary Protection*, Website: https://sma.nasa.gov/sma-disciplines/planetary-protection, Accessed: January 4, 2021.

Nuclear and Emerging Technologies for Space
Sponsored by Oak Ridge National Laboratory, April 26th-30th, 2021.
Available online at https://nets2021.ornl.gov

MANUFACTURING DEVELOPMENT OF CHARGEABLE ATOMIC BATTERIES, AN AFFORDABLE ALTERNATIVE TO PLUTONIUM-BASED RADIOISOTOPE HEATER UNITS AND THERMOELECTRIC GENERATORS

Andrew Lesh[1] and Christopher Morrison[2]

[1]*Stanford University, California, aclesh@stanford.edu*
[2]*Ultra Safe Nuclear Corporation — Technologies, Seattle, Washington, c.morrison@usnc-tech.com*

Plutonium-fueled radioisotope heater units and thermoelectric generators have enabled a variety of space missions where use of solar power alone is infeasible. While their excellent performance justifies their expense for government projects, the logistical and legal complexity of plutonium use makes them commercially unavailable. Ultra Safe Nuclear Corporation — Technologies (USNC-Tech) is developing an alternative device called a Chargeable Atomic Battery (CAB). CABs contain a nonradioactive precursor isotope that becomes a desired radioisotope via neutron capture in a fission reactor. This means that CAB units are only radioactive after neutronic charging and can be assembled in conventional facilities from relatively inexpensive materials. Prototype uncharged CAB units have been successfully manufactured and indicate the viability of this cost-effective, proliferation-safe radioisotope power source for both space and terrestrial applications.

I. INTRODUCTION

I.A. RTGs and RHUs

In circumstances where photovoltaics is not suitable to supply a space mission's power requirements, electricity has often been provided by radioisotope thermoelectric generators (RTGs). These devices employ a thermocouple to produce electricity from radioactive decay heat according to the Seebeck effect. They have been used for situations where power is required during periods of complete darkness (such as with the Apollo Lunar Surface Experiment Packages which operated throughout the lunar night) and where spacecraft are too far from the sun for sufficient solar irradiance (such as with the Pioneer, Voyager, and New Horizons interplanetary missions).[1] The current Mars rovers, *Curiosity* and *Perseverance*, likewise meet their electricity needs (110 W) and heat needs (2000 W) from RTGs, which allow them to operate at higher latitudes where weather is colder and sunlight is dimmer than at the Martian equator.[2]

Fig 1. Photograph of watt-scale RHU components with penny for scale.[1]

In other cases, solar power can provide sufficient electrical power and charge batteries for operations in intermittent darkness, but supplementation with continuous heat production is required. In this case, radioisotope heater units (RHUs), which are essentially equivalent to RTGs minus heat-electricity conversion, are used to provide survival heat for critical systems when an environment is too cold or energy-poor for operations with electric heaters alone. For example, the twin rovers *Spirit* and *Opportunity* both used RHUs to provide 8 W of baseline heating with electric heaters providing further heating when required.[3]

I.B. Need for an Alternative to Plutonium

The standard radioisotope for use in RTGs and RHUs is plutonium-238. With a thermal power density of 0.57 W/g due to its strong alpha emissions and a half-life of 87.7 years, this isotope is clearly an excellent choice for such use cases.[4] Unfortunately, there are many obstacles that preclude its widespread adoption.

$$^{238}_{93}\mathrm{Np} \rightarrow {}^{238}_{94}\mathrm{Pu} + \mathrm{e}^{-} + \overline{\nu}_{\mathrm{e}} \quad (1)$$

$$^{238}_{92}\mathrm{U} + {}^{2}_{1}\mathrm{H} \rightarrow {}^{238}_{93}\mathrm{Np} + 2\mathrm{n} + \mathrm{e}^{+} + \nu_{\mathrm{e}} \quad (2)$$

$$^{237}_{93}\mathrm{Np} + \mathrm{n} \rightarrow {}^{238}_{93}\mathrm{Np} \quad (3)$$

Plutonium-238 is sourced from the precursor isotope neptunium-238, which rapidly converts to it via beta decay with a half-life of 2.12 days (equation 1).[5] While the required neptunium-238 can be produced by bombarding uranium-238 with deuterons (equation 2), most has historically been produced from neptunium-237 via neutron capture (equation 3), which is itself a byproduct of plutonium-239 production.[6] While plutonium-238 is not used to make weapons, plutonium-239 certainly is. Uranium processing would still be required otherwise, and the produced plutonium-238 could nonetheless be converted to weapons-grade plutonium-239 via neutron capture.

The technical and logistical complexity of plutonium production, along with appropriate concerns about nuclear proliferation, result in only 400 g of plutonium-238 being produced per year in the United States, with preparations underway to increase this production to 1.5 kg per year by 2025.[7] With an initial power density of 0.57 W/g, this means our best-case scenario for total RTG/RHU output per year is a maximum of 860 W if using plutonium-238. This limited supply greatly constrains the development of technologies that could be enabled by RTGs and RHUs. Furthermore, due to proliferation concerns, the United States government only allows for the use of plutonium-238 power sources in NASA spacecraft, meaning potential terrestrial uses in arctic, subterranean, or deep ocean environments cannot be explored. Regardless, even if a company could afford the cost of the requisite plutonium, there is no regulatory pathway to obtaining it for commercial use.

NASA's Artemis program and Commercial Lunar Payload Services program are facilitating a boom in commercial lunar activity. As such, a lack of commercial RTGs and RHUs has generally restricted commercial missions to operating for one lunar day before permanently failing upon sunset due to the brutal cold and duration of the lunar night. For longer survival, it is necessary to operate in a lunar polar environment where sunlight persists for longer than at the equatorial regions.

A viable commercial alternative would not only support current lunar mission profiles, but allow for entirely new ones, opening up the entire lunar surface for long-term exploration and utilization. An alternative could also enable commercial operations in deep space and power-poor terrestrial locations such as arctic, subterranean, and deep ocean environments.

II. Chargeable Atomic Batteries (CABs)

Chargeable atomic batteries (CABs), a patent pending technology (PCTUS2116982, PCTUS2116980), are being developed by Ultra Safe Nuclear Corporation — Technologies (USNC-Tech) to meet this pressing need for an alternative to plutonium-based power generation. Like conventional plutonium devices, CABs produce heat via radioactive decay and can produce electricity with a thermocouple, but for orders of magnitude less cost and no proliferation concern.

II.A. Concept

The radioisotope within a CAB unit is created by exposing an uncharged CAB unit to neutron fluence in a fission reactor. This converts a non-radioactive precursor isotope into a desired radioisotope, selected for its power production and half-life, via neutron capture. As such, CAB units are initially manufactured in a conventional, non-radioactive setting and only require special handling procedures once neutronically activated. The optimal radioisotope may vary depending on power and duration requirements for a specific use case. The precursor isotopes currently under consideration for the wide range of half-lives and radiative performances their product radioisotopes provide are lithium-6, thulium-169, cobalt-59, and the two most stable europium isotopes (europium-151 and europium-153).

TABLE I. Precursor isotopes under consideration for use in CABs, their activated product radioisotopes, and radioisotope half-lives.

Precursor Isotope	Activated Isotope	Half-life [yr]
^{6}Li	^{3}H	12.3
^{169}Tm	^{170}Tm	29 days
^{59}Co	^{60}Co	5.7
^{151}Eu, ^{153}Eu	^{152}Eu, ^{154}Eu	11.0 (avg.)

An uncharged CAB unit is a layered ceramic pellet with an interior precursor region and an exterior encapsulation region surrounding it. The interior consists of the inert precursor isotope bound as a stable chemical compound and optionally mixed with an inert encapsulation compound. The exterior encapsulation layer consists exclusively of the encapsulation compound, which is itself chosen for producing only very short-lived isotopes upon neutron irradiation. Both compounds, purchased as powders, are pressed into a layered pellet and sintered to produce an uncharged CAB unit. The uncharged CAB unit later receives neutron irradiation within a fission reactor for approximately 30 days and is left to stand for another 30 days in order for all short-lived isotopes to decay. This leaves a charged CAB unit ready for integration.

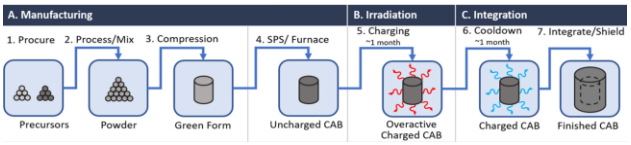

Fig. 2. Stages of CAB unit production process.

II.B. Prototyping

While the principal design choice for CABs is which precursor isotope to use, this choice is limited by the properties of the chemical compound that precursor is bound within. Considerations must be made for chemical stability, thermal conductivity, thermal expansion, mechanical strength, expansion under neutron irradiation, off-target radioisotope products, and sinterability. These considerations must also be made simultaneously for the encapsulation material so that the choices are fully compatible.

While many specific details of the CAB unit manufacturing process are patent-pending and must be undisclosed in this publication, an overview of the prototype production process can be given.

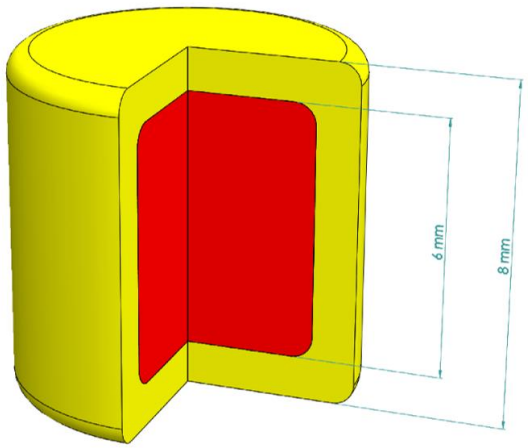

Fig. 4. Model of prototype CAB unit, showing interior precursor layer (red) and exterior encapsulation layer (yellow). Dimensions are approximate.

Initial prototypes are cylindrical sintered bodies approximately 8 mm in diameter and height. An interior region, approximately 6 mm in diameter and height, contains a mixture of the precursor compound and encapsulation compound while an outer layer, 1 mm thick, consists of only the encapsulation compound. The chosen precursor compound contained thulium-169 for initial experiments. The chosen encapsulation compound was alumina (Al_2O_3), selected for its chemical stability and excellent compatibility with the thulium compound and all other considered precursor compounds.

First, the precursor and encapsulation powders are weighed into appropriate quantities for producing the unsintered green form, which is made using a die and two specially designed punches in a hydraulic press. The first layer is made by pouring an appropriate quantity of encapsulation powder into an 8 mm ID die and compressing it with an 8 mm OD punch, forming a 1 mm thick base layer. A second, annular layer is formed by pouring more encapsulation powder into the die and compression with a 6 mm OD punch. A mixture of precursor and encapsulation powder is then poured into the cup-like annular layer and compressed with the 8 mm OD punch, followed by a final 1 mm thick encapsulation layer also compressed with the 8 mm OD punch.

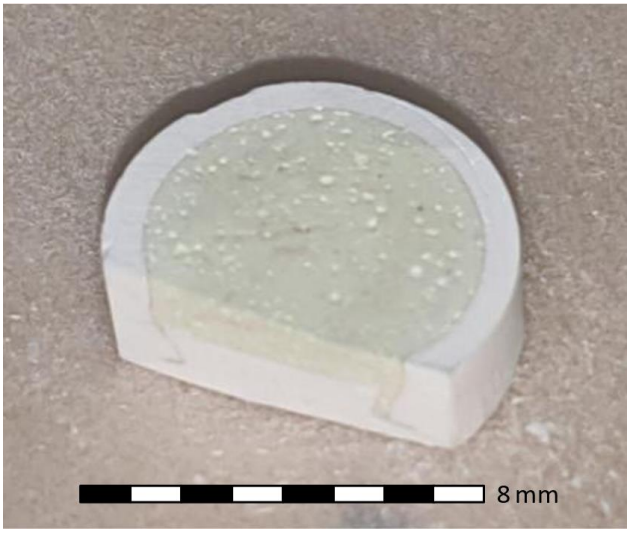

Fig. 5. Sectioned thulium CAB unit prototype after sintering, showing internal layered structure.

The result is a cylindrical green form with a concentric layered structure. Iteration of the punch designs was required to obtain a stable annular layer of encapsulation powder able to be filled with the precursor without collapsing. The green form is then carefully transferred to a crucible in which it is sintered, resulting in a durable, monolithic pellet.

II.C. Verification

Given the importance of containing the eventually radioactive interior of the CAB unit, it was crucial to verify that the precursor region was entirely contained by the inert encapsulation layer without any flow of precursor powder past the layer boundary during compression. This was verified by sectioning sintered pellets and examining the boundary with scanning electron microscopy (SEM). SEM images revealed a sharp visual contrast between the precursor region and encapsulation region along a distinct boundary line.

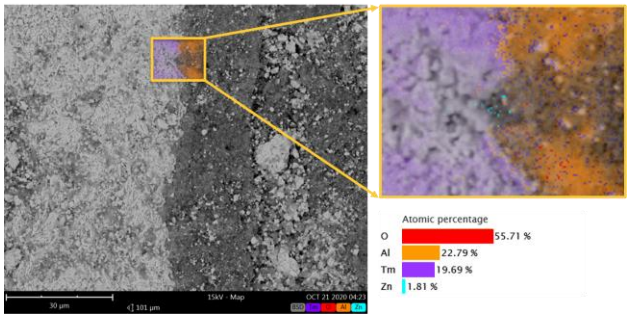

Fig. 6. SEM micrograph of boundary between precursor layer (left, light grey) and encapsulation layer (right, dark grey) of thulium CAB unit prototype. Magnified region displays EDS data plot for elemental distribution at boundary, showing minimal incursion of thulium precursor into encapsulation layer.

This was bolstered through the use of energy-dispersive x-ray spectroscopy (EDS), a technique used to reveal the elemental composition of the SEM specimens. As hoped, the precursor species remained confined to the inner region, demonstrating that the CAB unit manufacturing method can successfully produce layered pellets with uncontaminated encapsulation layers.

III. CONCLUSION

Current development efforts focus on introduction of prototype uncharged CAB units into fission reactors, which will allow for characterization of their power production over time. As USNC-Tech is currently working with partners to provide neutron irradiation, it seems that commercialization of CABs is imminent and will provide the first true alternative to plutonium-based RHUs and RTGs for both terrestrial and space use cases.

ACKNOWLEDGMENTS

The authors would like to thank the staff of the University of Washington Clean Energy Institute for use of the Washington Clean Energy Testbeds facility to support this research.

REFERENCES

1. Cataldo, Robert L., and Gary L. Bennett. "US space radioisotope power systems and applications: Past, present and future." Radioisotopes-Applications in Physical Sciences (2011): 473-496.
2. Werner, James, Kelly Lively, and Drake Kirkham. "A multi-mission radioisotope thermoelectric generator (MMRTG) for Mars 2020." 2017 IEEE Aerospace Conference. IEEE, 2017.
3. Bejczy, Antal K. "Robotic Rovers Aid Mars Surface Exploration." Budapest Tech Jubilee Conference. Óbuda University, 2004.
4. Miotla, Dennis. "Assessment of Plutonium-238 Production Alternatives." US Department of Energy, Briefing for Nuclear Energy Advisory Committee (NEAC) Meeting, Arlington VA.(21 Apr. 2008). 2008.
5. Cunningham, B. B., and L. B. Werner. "The first isolation of plutonium." Journal of the American Chemical Society 71.5 (1949): 1521-1528.
6. “Plutonium-238 Production for Space Exploration: A National Historic Chemical Landmark.” ACS National Historic Chemical Landmark program, 2018.
7. Depaoli, David W., et al. “Process Development for Plutonium-238 Production at Oak Ridge National Laboratory.” Oak Ridge National Lab (ORNL), 2019.

Nuclear and Emerging Technologies for Space
Sponsored by Oak Ridge National Laboratory, April 26th-30th, 2021.
Available online at https://nets2021.ornl.gov

CHARGEABLE ATOMIC BATTERIES – COMMERCIAL RADIOISOTOPE POWER SYSTEMS FOR SPACE AND TERRESTRIAL MISSIONS

Christopher Morrison

2356 W Commodore Way, Seattle, WA, 98199

(928) 925-3842, c.morrison@usnc-tech.com

Atomic batteries possess one-million times the energy density of state-of-the-art chemical batteries and fossil fuels. For locations that do not possess access to the sun or other energy sources, atomic batteries are enabling. Relevant use cases include small satellites operating far from the sun, electronics on the moon attempting to survive the lunar night, underwater vehicles to explore the depths of the ocean, and low-power heat in remote regions such as Canada and northern Europe and Asia. USNC-Tech is maturing a patented atomic battery concept and is actively engaging commercial companies, regulatory agencies, and production partners.

I. INTODUCTION

The challenges in production and the complexity of containing nuclear material have limited the application of atomic batteries. Traditional atomic battery solutions focus on the high performance but expensive special nuclear material Plutonium-238. The cost, necessarily controlled nature and limited supply of Pu-238 prevent widespread commercial production and application of systems that would otherwise benefit.

USNC-Tech has developed a patents pending (PCTUS2116982, PCTUS2116980) manufacturing method termed "pre-activation encapsulation" to reduce complexity and cost for atomic batteries as well as enable deployment by commercial companies. In this process, atomic batteries are manufactured using natural non-radioactive precursor material embedded within an encapsulation material. The precursor material is then activated or "charged" inside a radiation source such as a fission reactor and finally packaged. This concept is known as a Chargeable Atomic Battery or CAB.

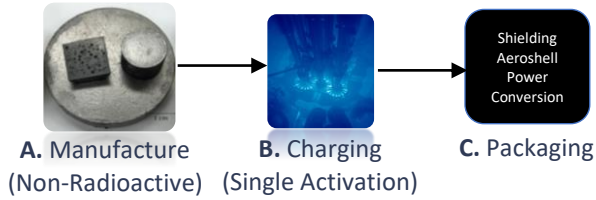

Fig 1. CAB Manufacturing Process

CABs can be manufactured in existing facilities and have a straight-forward path toward a prototype using available technologies and facilities. For watt-scale batteries, the process can be demonstrated to a TRL of 5-6 in the near-term.

II. SAFETY AND ENCAPSULATION

A CAB Unit is a cylindrical heterogeneous ceramic with an outer wall and a filling as shown in Figure 2. The wall is composed of an encapsulation material and the filling is composed of an activation target material known as a precursor material.

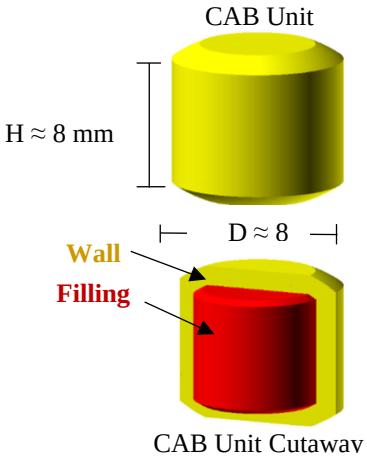

Fig 2. CAB Unit

The filling can be configured as show in Figure 3 with the different encapsulation configurations.

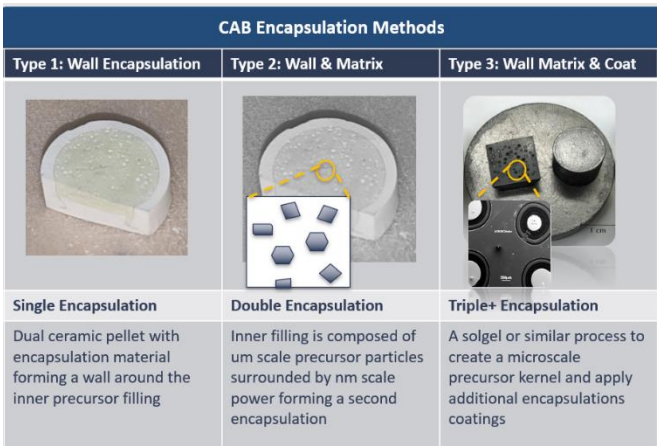

Fig 3. CAB Encapsulation Methods

The encapsulation layers provide additional intrinsic barriers to release of radionuclides into the environment. These barriers both increase operational safety and ease handling and manufacturing. This manufacturing method eases the production process, eliminating the need for expensive radiochemical processing. In addition, the encapsulation methods can be used with different types of isotopes and the CAB units can be tailed to meet the half-life, x-ray shielding, and power density needs of different customers. Table 1 displays a non-exhaustive list of precursors and activated isotopes of interest.

Precursor Isotope	Activated Isotope	Half-life [yr]
^{6}Li	^{3}H	12.3
^{169}Tm	^{170}Tm	129 days
^{59}Co	^{60}Co	5.7
^{151}Eu, ^{153}Eu	^{152}Eu, ^{154}Eu	11.0 (avg.)

Table 1. CAB Encapsulation Methods

III. CAB CHARGING

The CAB unit is compatible with radiation particle sources such ions in accelerators, high energy fusion neutrons, lower energy fission neutrons, spallation neutron sources, and high energy photon generators. The particle radiation source must penetrate the wall and into the filling containing the precursor. Higher energy radiation sources and neutral sources generally penetrate more deeply into a material and are more suitable for CAB unit charging. Fission reactors are attractive because of the high neutron flux capability, the availability of fission reactors facilities, and the similarity of the CAB charging process to existing medical and industrial radioisotope production. A charge cycle is a one-month irradiation in a typical megawatt scale reactor with a flux level of at least 1 x 10^{14} n/cm^{2}s. CABs can be charged for multiple cycles or in a higher radiation flux for higher performance levels.

IV. CAB POWER SYSTEM DESCRIPTIONS

The CAB unit in Figure 4 is a standardized form factor that can be adapted for many different commercial radioisotopes. The atomic battery stack in Figure 5 is a device that can hold multiple chargeable atomic batteries.

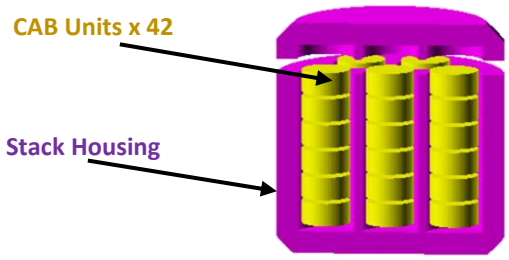

Fig 4. CAB Stack

The example CAB stack shown in Figure 2 has seven stacks of six CAB units, but different housings are available to package different stack configuration to meet power needs for various use cases. The atomic battery pack is shown in Figure 5.

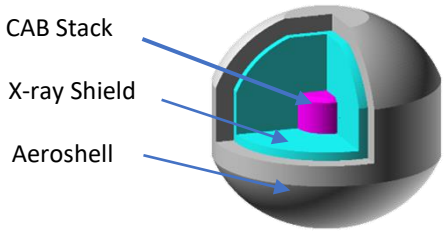

Fig 5. CAB Pack

The CAB pack contains the atomic battery stack along with supporting subsystems. It integrates mission-specific components such as an x-ray shield (for cases using beta or gamma emitting isotopes), thermal interfaces such as heat pipes, possible power conversion components, and an aeroshell for accidental launch failure/re-entry for space missions. Commercial customers can utilize these resources in their vehicles and missions for various purposes such as electrical power generation, thermal heating, remote sensing, propulsion, sanitization, etc.

V. X-RAY SHIELDING

Some CABs emit x-ray radiation which requires a radiation shield. For other types of CABs, no shield is required. Materials that require shielding have higher performance at higher power levels. For space applications the shield can double as an aeroshell. Table 1 show three example systems with different isotopes and power levels.

	Initial Power [W]	CAB Mass	5 mrem/hr Shield	100 mrem/hr Shield
LiCAB	0.1	105 g	0 kg	0 kg
TmCAB	30.5	250 g	23 kg	8.0 kg
EuCAB	1000	9 kg	1680 kg	1098 kg

Table 1. CAB Encapsulation Methods

Typically, the x-ray shield is the dominant mass in the system for isotopes that require x-ray shielding. For batteries which require shielding, two dose levels were evaluated: 5 mrem/hr and 100 mrem/hr. The 5 mrem/hr dose rate is below the NRC definition of a radiation area and is similar to the dose on the ISS. The 100 mrem/hour dose level is below the NRC definition of a high radiation area with controlled access but would be accessible to technicians for hour-long periods. This would be suitable for contact with electronics. For some applications (such as in space) a directional shield can be used to greatly reduce the mass of the shield by a factor of 4 or more. For other application such as underwater or underground the

environment can be used as shielding and in general mass is not a significant constraint.

VI. MISSIONS AND APPLICATIONS

A CAB pack can be designed to deliver thermal heat, electricity, or passive x-rays for user applications. There are a significant number of applications which can use the CAB technology and the applications are summarized in the following paragraphs.

For heating applications, the CAB can complement traditional battery systems. There are many locations such as on the moon or bottom of the ocean where temperatures can drop significantly impacting the operation of a traditional chemical battery. The batteries must use a significant amount of the stored energy for heating. A CAB unit can be used to provide a passive heat source to keep the chemical batteries warm, allowing the chemical batteries to be used for electric power.

Electric power is attractive, especially in locations where solar power is not an option, for example, in locations far from the sun, in permanently shadowed regions, in locations with significant dust or radiation. Static power conversion using thermoelectrics is a flexible near-term power conversion option. Higher efficiency dynamic power conversion technology is also a possibility.

The penetrating power of x-rays allows for characterization under the surface layer for material assay. The x-rays can also be used as passive beacons for devices up to kilometers away.

CAB technology can also be used for propulsion. Poodle thrusters were studied in the 1960s as a radioisotope thermal propulsion[1]. CAB technology could be adapted to a thruster and when combined with hydrogen could achieve a I_{sp} of 900 seconds or greater.

VII. REGULATORY

As of August 2019, a regulatory framework for commercial nuclear technology was authorized by National Security Presidential Memorandum-20 (NSPM-20)[2] that enables the deployment of CABs for space applications. USNC-Tech is currently engaging with NRC and FAA regulator in pre-application activities.

For terrestrial and oceanic usage, there are regulatory procedures vetted by existing medical and measurement industries.

VIII. CONCLUSIONS

CAB technology is not as high of a performance technology comparted to Pu-238. However, CAB technology can provide many of the same benefits to commercial customers who do not have access. USNC-Tech is investing significant internal funding into CAB technology because of a strong signal of customer interest. USNC-Tech is currently conducting customer development for CABs. The purpose of this solicit interest from different communities as well as customers to help determine the direction for future technology development. Interested parties are encouraged to reach out to the author.

REFERENCES

1. E. L. Nezgoda, Radioisotope Propulsion Technology Program (POODLE), TRW, Tech Report, STL-517-0049, April 1967
2. National Security Presidential Memorandum-20 (Launch of Spacecraft Containing Space Nuclear Systems), August, 2019

Nuclear and Emerging Technologies for Space
Sponsored by Oak Ridge National Laboratory, April 26th-30th, 2021.
Available online at https://nets2021.ornl.gov

NEXT GENERATION RADIOISOTOPE POWER FOR SPACE EXPLORATION

Robert D. Overy[1], Gerald G. Sadler[2], Jean-Pierre Fleurial,[3] and David G. Hall[4]

[1]NASA Glenn Research Center, 21000 Brookpark Road, Cleveland, Ohio, 44135
[2]Summit Technologies Solutions, 7686 Richmond Highway, Suite 110, Alexandria, VA 22306, [3]Jet Propulsion Laboratory, 4800 Oak Grove Dr., Pasadena, CA 91109, 818-354-4144
[4]ARES Corporation, 22800 Cedar Point Road, Cleveland, Ohio 44142, 216-433-8289
Robert D. Overy, Jr.: 216-433-8132 , Robert.D.Overy@nasa.gov

Radioisotope Thermoelectric Generators (RTGs) have been a key power source technology to enable NASA science and exploration missions exploring the surface of the Moon and Mars, the outer planets, and interstellar space since the 1960's. The Radioisotope Power Systems Program in partnership with the Department of Energy, plans to ensure that more capable RTGs are available to support future NASA missions to some of harshest, darkest, and dustiest destinations in the solar system and beyond. NASA plans to develop Next Generation RTGs through a multi-phase effort, building upon the reestablishment of the GPHS-RTG (General Purpose Heat Source-RTG) and providing a path for significant performance upgrades. The original GPHS-RTG qualification unit (Mod 0) should be refurbished and ready for fueling as early as 2024. The first new production unit (Mod 1), with capability akin to the heritage-design units, is planned by 2028. Infusion of advanced thermoelectric converter technology to make upgraded flight units (Mod 2), with greater performance than any previous RTG, would be available for possible flight missions by the early 2030's

I. INTRODUCTION

Many NASA missions given a high priority by the scientific community visit some of the harshest, darkest, coldest locations in the solar system, and these missions could not be possible or would be extremely limited, without the use of nuclear power. Radioisotope Power Systems–or RPS–harness the heat of the natural decay of plutonium-238, to produce continuous electric power for operating spacecraft systems and science instruments and have a proven record, providing the "Power to Explore" for the past 60 years.

The first two space flights that used RPS were the Navy's Transit 4A and 4B navigational satellites, launched in June and November 1961. A 3-watt Radioisotope Thermoelectric Generator (RTG) was flown on each spacecraft to prove the operational capability of the RTGs in a space environment.[1] Since then, RTGs have flown on such missions as the Apollo Lunar Surface Experiment Package (ALSEP), Viking 1 and 2 Mars landers, Pioneer 10 and 11, Voyager 1 and 2, Galileo, Ulysses, Cassini, and New Horizons.

The Mars Curiosity rover uses a newer RTG design called the Multi-Mission RTG, or MMRTG, that is based on RTG designs and converter technologies used for the Viking and Pioneer missions. The Perseverance rover that has just landed on Mars in February 2021 is powered by a MMRTG and the Dragonfly rotorcraft that is scheduled to start exploring the surface of Titan in the mid 2030's is also baselined to be powered by a MMRTG.

II. THE NEXT GENERATION RTG PROJECT

The NASA RPS Program is actively working to assure the availability of high power, vacuum-rated RTGs to enable future deep space missions. The Next Generation RTG (NGRTG) Project team is developing that capability by leveraging the GPHS-RTG (General Purpose Heat Source - RTG) design that powered the Ulysses, Galileo, Cassini and New Horizons missions (Ref #2). The New Horizons spacecraft is shown below with the GPHS-RTG visible on the left.

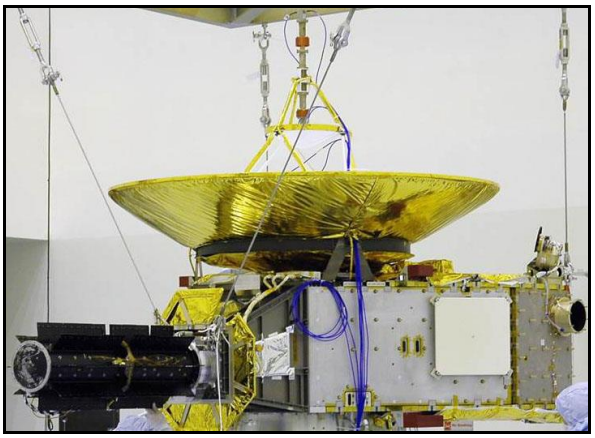

Fig. 1. New Horizons Spacecraft (JHU-APL)

The advantages of this approach include: a low risk building block development providing early mission capabilities (Mod 0), leveraging an existing RTG design, and allowing for a sustained, realistic "product improvement path" (Mod 1, Mod 2) for decades to come.

The multi-phased effort starts with the NGRTG Mod 0, which would deliver a refurbished, legacy GPHS-RTG qualification unit for use in the 2024 timeframe. The NGRTG Mod 1 campaign would re-establish the

production capability for the legacy RTG design and thermoelectric converter with required or necessary upgrades, including the use of Step-2 General Purpose Heat Sources (Step-2 GPHS), and technology updates to the silicon-germanium (SiGe) unicouple and multi-layer insulation converter technology for manufacturability and/or performance. NGRTG Mod 1 is planned for availability in the 2028 timeframe. Missions planned in the early 2030's could benefit from higher power and a more modular NGRTG Mod 2 capability. This design would be based on the Mod 1 however augmented with "retrofit-ready" higher performance thermoelectric converter technology that is currently under development.

I.A. Performance

The primary goal for the NGRTG Mod 0, Mod 1, and Mod 2 configurations is to maintain the exemplary record for system reliability and minimal, graceful performance degradation that stretches back to the Voyager missions of the 1970's (Ref. 2). The heart of any RTG is the thermoelectric converter, constituted by a series-parallel array of thermoelectric couples packaged with highly effective thermal insulation. The NGRTG Mod 0 and 1 will feature the SiGe unicouple design that was used in the Voyager missions, which are still producing power more than 40 years after launch. The reliability of this design has been further proven in multiple missions using the GPHS-RTG since the1980's. The Mod 0 and Mod 1 configurations are targeting power output performance on-par with the legacy GPHS-RTG design, with up to 295 W_e at beginning-of-life (BOL) and up to 210 W_e at end-of-design-life (EODL), 17 years after BOL including up to 3 years of ground storage. The Mod 2 configuration is targeting 290 W_e at EODL, which, assuming a similar total performance degradation that is comparable to Mod 0 and Mod 1, would translate to at least 400 W_e at BOL.

I.B. Uses

The NGRTG is being developed to provide power to deep space science missions, and its design would allow operation on earth during the pre-launch phase, in the vacuum of deep space, in-transit, and in extreme temperature variations on the lunar surface. With an EODL power requirement of 17 years, the NGRTG could accommodate a long cruise time to the outer planets, or long duration missions to icy worlds, including powering flyby missions, landers, and rovers operating in vacuum environments.

The development of NGRTG for space science missions can also benefit lunar exploration. The first application for NGRTG may be for a lunar surface resource exploration rover at the south polar region, where photovoltaic power is not practical. Other uses could include electrical and thermal energy for an in-situ resource utilization (ISRU) pilot plant. In addition, prior to large fission reactor deployment, NGRTG could be used for auxiliary human habitation support. NGRTG Mod 0 could support a mission in the mid 2020's.

III. EXPLORATION OF URANUS/NEPTUNE

Exploration of at least one ice giant system (Uranus or Neptune) has been identified as a high priority science target to advance our understanding of the solar system, its exoplanetary systems, and to advance our understanding of planetary formation and evolution. The NGRTG project is well positioned to support mission concepts that have been proposed to explore one or both of these fascinating planetary systems.[3]

IV. PROJECT MANAGEMENT APPROACH

The NGRTG project is being structured to follow the same pattern that was a success in past efforts to deliver GPHS-RTG flight units: forming a cross-cutting consortium of government, industry and academic partners, led this time by the NASA RPS Program office and with NASA's Glenn Research Center providing the core of the management team. Other key organizations that are part of the NGRTG Team include NASA's Jet Propulsion Laboratory (JPL), Idaho National Laboratory (INL), Johns Hopkins University Applied Physics Laboratory (JHU-APL), Oak Ridge National Laboratory (ORNL) and the University of Dayton Research Institute (UDRI).

The plan is to have INL conduct the Mod 0 work, since they are the keepers of the legacy hardware and have the in-house expertise to refurbish the existing qualification-unit generator. INL will also take the lead in awarding a prime industrial development contract for Mod 1. In parallel, NASA's Jet Propulsion Laboratory, through the RPS Program's Technology Management, will lead the Mod 2 technology development work.

The RPS Program is also sponsoring two independent groups to provide support to the project. First, a Technical Advisory Team has been formed, composed of experts in thermoelectric technology and engineering, to provide advice, recommendations, and counsel to the Project Management Team. Secondly, a SiGe task force was commissioned in May 2020, to assess risks related to reestablishing the capability to manufacture the heritage SiGe unicouples, including the exploration of obsolescence and, or enhancement-driven options relative to materials and processes. Members include subject matter experts from JPL, APL, ORNL, INL, and UDRI. This group has been made available to support the prime contractor that will be down selected in Mid-2021 to begin work on Mod 1 development. They are also tasked with providing risk mitigation support to the NGRTG Project management team. These groups will provide

critical expertise and facilitate long term success as the project team re-establishes the capability to manufacture SiGe unicouples and the GPHS-RTG system.[4]

ACKNOWLEDGMENTS

The authors wish to gratefully acknowledge the ongoing support from the Radioisotope Power Systems Program, NASA's Headquarters, NASA's John H. Glenn Research Center, the U.S. Department of Energy, the NASA's Jet Propulsion Laboratory at Caltech, the Johns Hopkins University Applied Physics Laboratory, and many others.

REFERENCES

1. SPACE DEPARTMENT (1978) *Artificial Earth Satellites Designed and Fabricated by the Johns Hopkins University Applied Physics Laboratory*, SDO-1600 (Revised).
2. G.L. Bennett and J.L Lombardo (2006) *Mission of Daring: The General-Purpose Heat Source Radioisotope Thermoelectric Generator*, AIAA 2006-4096.
3. M. Hofstader, A. Simon (2017) *Ice Giants Pre-Decadal Study Final Report*, JPL D-100520.
4. R. Overy, et al. (2021) *Radioisotope Power for Scientific Exploration.* 52nd Lunar and Planetary Science Conference (LPSC), USRA-2770.

Nuclear and Emerging Technologies for Space
Sponsored by Oak Ridge National Laboratory, April 26th-30th, 2021.
Available online at https://nets2021.ornl.gov

Spark Plasma Synthesis of SiGe Materials and Performance of Unicouples

Jonathan Pierce[1], Richard Ung[1], Meiyong Himmtann[1], Joseph Poon[2], and Rama Venkatasubramanian[1#]

[1]Johns Hopkins University Applied Physics Laboratory, Laurel, MD
[2]University of Virginia (UVa), Charlottesville, VA

rama.venkatasubramanian@jhuapl.edu

We will discuss the developments on Spark Plasma Sintered (SPS) synthesis of SiGe materials, their characterization and performance of unicouple devices made from these materials. These are relevant to Next Gen GPHS-RTG systems. SPS SiGe materials were characterized by ZEM3 for electrical resistivity and Seebeck coefficient from 300K to ~1100K. The 300K data for the $Si_{78}Ge_{22}$ N-type and $Si_{78}Ge_{22}$ P-type SPS materials are close to the legacy/heritage materials acceptance criteria. The initial ZT values estimated for N-type $Si_{78}Ge_{22}$ material made by SPS appear significantly better than legacy SiGe materials, which is consistent with several previously published work. A significant risk to the fabrication of heritage GPHS-RTG SiGe couples is the ability to carry out diffusion bonding between various layers – (i) between SiMo and $Si_{78}Ge_{22}$ and (ii) between $Si_{78}Ge_{22}$ and $Si_{63}Ge_{37}$ layers. We have investigated SPS as a potential method to show in-situ diffusion bonding between $Si_{78}Ge_{22}$ and $Si_{63}Ge_{37}$ layers; essentially, the two-layer stack is prepared in-situ, thus avoiding lower-yield diffusion bonding steps in the heritage process. In order to validate the SPS SiGe materials, we built 15 mm-tall SiGe unicouples and tested them upto T_{hot}~985°C and T_{cold}~100°C. We estimate an efficiency of ~9% in these SiGe couples. The V_{oc} and power output from these SiGe unicouples appear good as a function of T_{heater} and we obtained a peak power ~425 mW. These results are of likely value to the Next Gen project tasked with SiGe unicouple production for building a GPHS-RTG system.

I. Introduction

There is considerable interest in the synthesis of SiGe materials – in particular the $Si_{78}Ge_{22}$ N-type and $Si_{78}Ge_{22}$ P-type alloys and the $Si_{67}Ge_{33}$ alloys, with similar P-type and N-type doping, for building GPHS-heritage unicouples as shown in **Figure 1** and described by Bennett at al. [1].

However, there has not been much recent work in the synthesis of GPHS-like SiGe materials or building P-N unicouples with them and their testing in the last two decades. In this reported work, we will describe our recent efforts to look at the SPS route to making SiGe materials. Specifically, $Si_{78}Ge_{22}$ N-type and $Si_{78}Ge_{22}$ P-type materials were prepared in a 10-ton SPS unit, with desired doping levels to target acceptance criteria used in GPHS-RTG SiGe P-N couples [2]. To put into context-pulverization and blending to produce SiGe alloy powders, from vacuum-cast materials, and isostatic hot-pressing has been the route for producing heritage SiGe materials. However, there are significant concerns today if vacuum-cast SiGe materials can be produced in the true heritage fashion and even if produced, whether the typical composition and dopant non-uniformities can be preserved. Further, there have been reproducibility issues in the heritage SiGe materials production in the past that need to be overcome. It is in this context, we observe that several researchers in the US and in around the world, have successfully demonstrated exciting increases in thermoelectric figure-of-merit (ZT) enhancement in SPS SiGe materials with important potential benefits for NASA RTG missions.

There have been multiple validation (published reports) by various teams [3, 4, 5, 6] of enhanced thermoelectric figure of merit (ZT) in both P-type and N-type $Si_{78}Ge_{22}$ made by SPS, compared to heritage NASA RTG heritage SiGe materials. However, to our knowledge, nobody has validated the higher performance (i.e., higher conversion efficiency of SiGe uni-couples made with SPS SiGe materials) in a systematic way. In this reported work, we discuss the APL device results made with SPS SiGe materials.

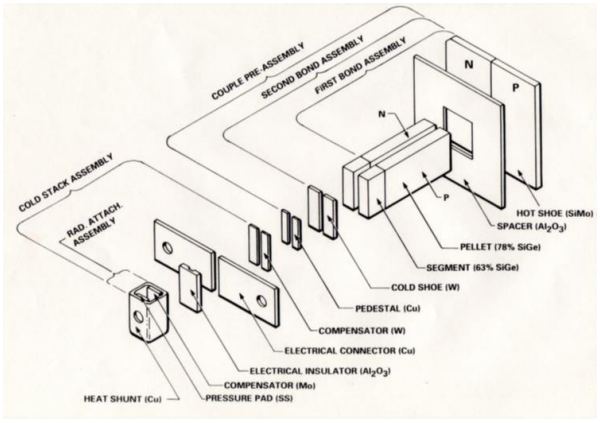

Figure 1 Exploded view of SiGe alloy thermoelectric elements and unicouple architecture as used in the GPHS-RTGs and the MHW-RTGs [1].

2. Experimental Results and Discussion

SPS $Si_{78}Ge_{22}$, both P- and N-type for this study were prepared using a SPS system at UVa, using mechanical alloying procedures [3] with inputs on composition, doping levels, and thickness specified by APL. SPS SiGe materials were characterized by ZEM3 for electrical resistivity and Seebeck coefficient from 300K to ~1100K. These data were compared to measurements made at UVa. The data for $Si_{78}Ge_{22}$ N-type and $Si_{78}Ge_{22}$ P-type alloy materials is shown in **Figure 2**. The 300K data for the $Si_{78}Ge_{20}$ N-type and $Si_{78}Ge_{22}$ P-type alloys are compared with legacy/heritage materials, specifically for the acceptance criteria [2] in **Table 1**. The initial ZT values estimated for N-type $Si_{78}Ge_{22}$ material made by SPS appear significantly better than legacy SiGe materials as shown in **Figure 3**.

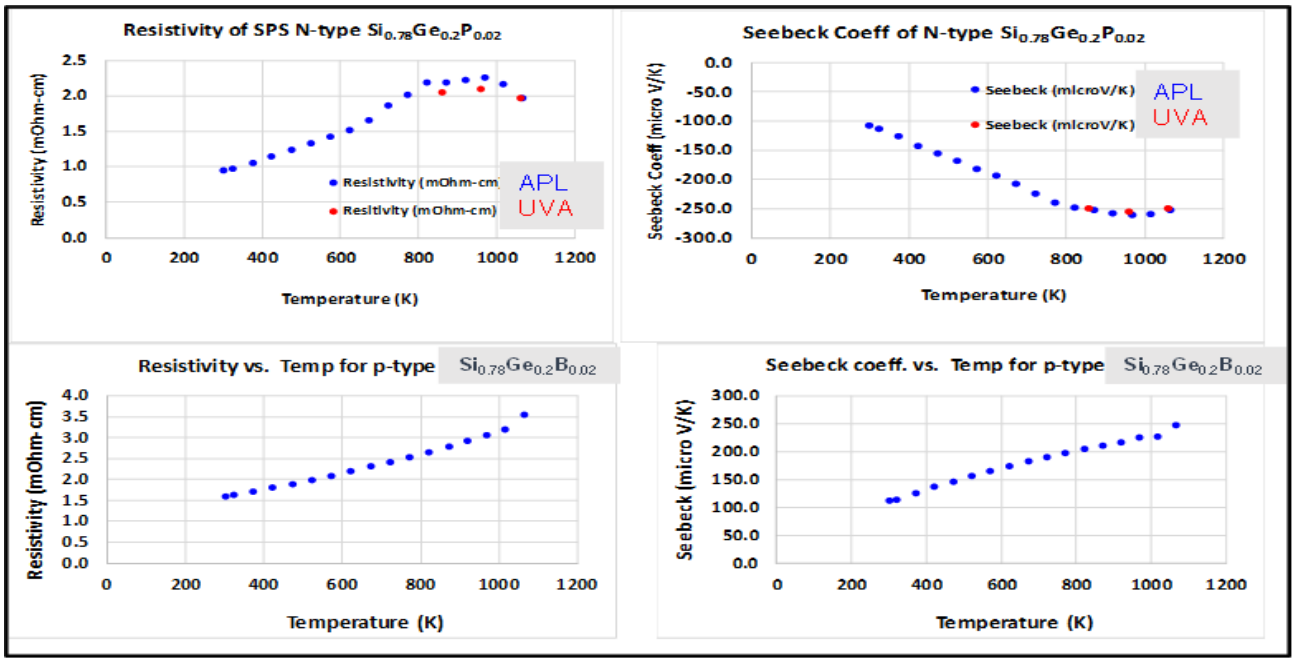

Figure 2 ZEM3 electrical resistivity and Seebeck of N-type $Si_{78}Ge_{22}$ and P-type $Si_{78}Ge_{22}$ alloy materials prepared by SPS

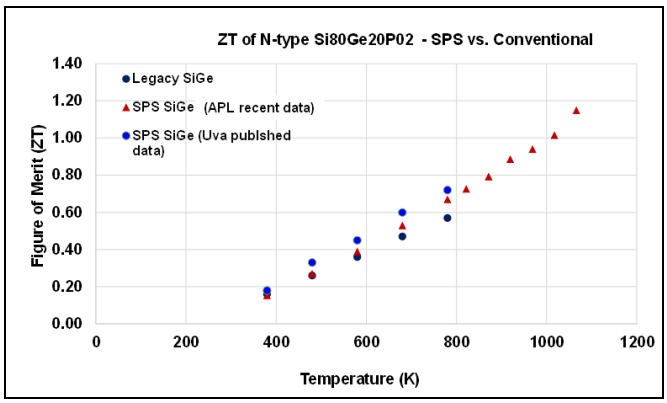

Figure 3 Figure of merit (ZT) in $Si_{78}Ge_{22}$ N-type alloy made by SPS, based on electrical resistivity and Seebeck as a function of temperature from Fig. 2; known lattice thermal conductivity values and Wiedemann-Franz law were used for electronic thermal conductivity

Material (N-type)	Resistivity (mOhm-cm)	Seebeck Coeff (micro V/K)
Legacy $Si_{0.78}Ge_{0.2}P_{0.02}$	0.7 - 1.0 0.9 (Nominal)	-90 to -125
SPS $Si_{0.78}Ge_{0.2}P_{0.02}$	0.947	-108.1

Material (P-type)	Resistivity (mOhm-cm)	Seebeck Coeff (micro V/K)
Legacy $Si_{0.78}Ge_{0.2}B_{0.02}$	0.85 – 1.10 1.0 (Nominal)	100 to 130
SPS $Si_{0.78}Ge_{0.2}B_{0.02}$	1.58	112.7

Table 1 ZEM3 data for $Si_{78}Ge_{22}$ N-type alloy and $Si_{78}Ge_{22}$ P-type alloy materials made by SPS and compared to legacy/heritage acceptance criteria; the SPS data was cross-checked at two labs for the N-type SPS materials; but done only at APL for P-type materials.

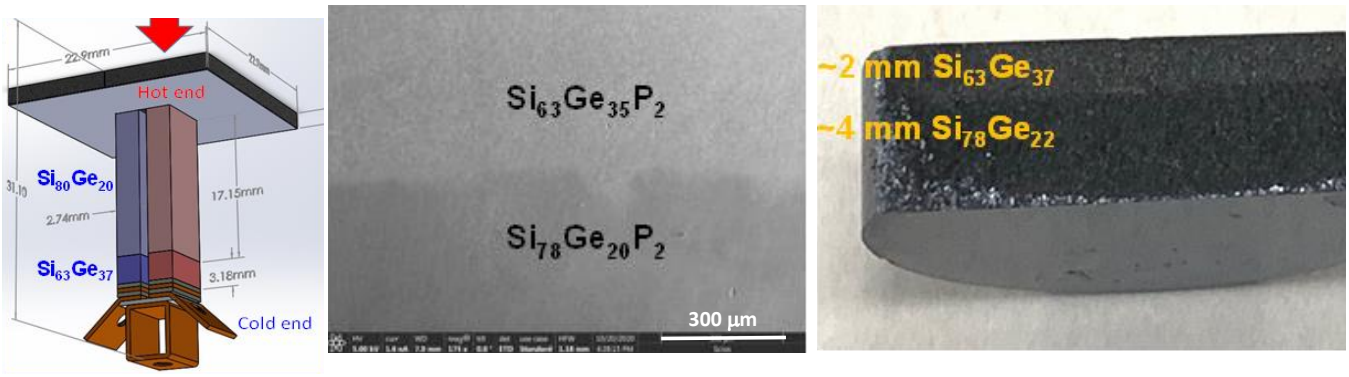

Figure 4 (Left) Schematic of a GPHS-RTG SiGe heritage uni-couple with diffusion bonding between $Si_{80}Ge_{20}$ and $Si_{63}Ge_{37}$ layers; (center) APL approach to in-situ diffusion bond; (right) SEM cross-sectional image of the SPS in-situ two-layer stack The scale for the SEM image (center) represents 300 µm.

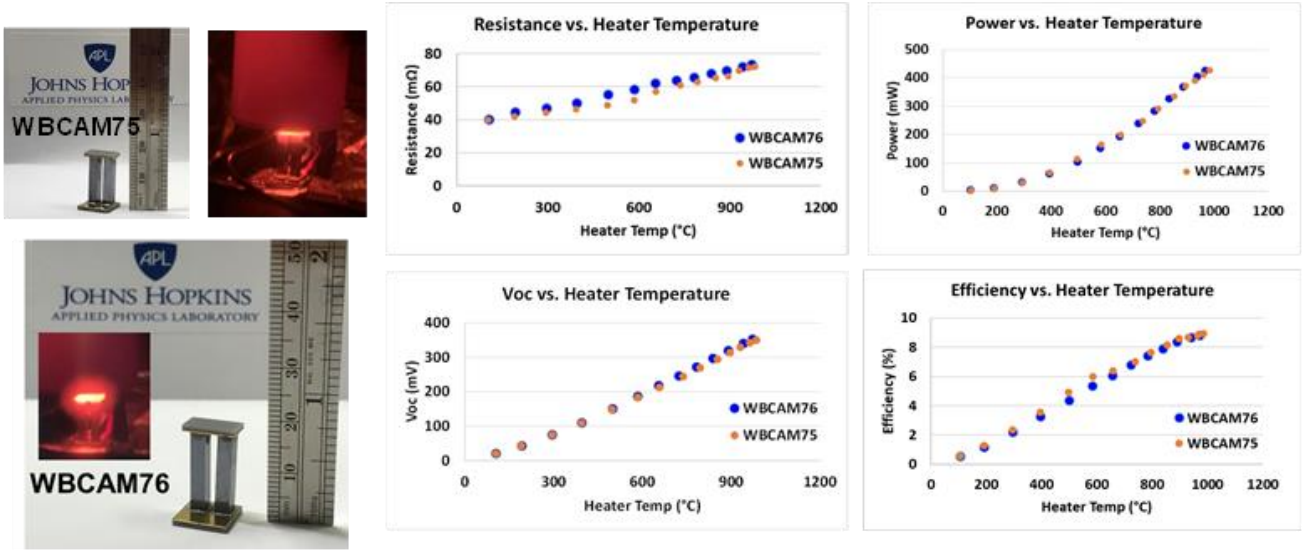

Figure 5 Reproducible resistance, V_{oc}, power output and efficiency of SPS SiGe uni-couples as a function of T_{heater}; data shown for two15-mm-tall $Si_{78}Ge_{22}$-$Si_{78}Ge_{22}$ P-N couples

A significant risk to the fabrication of heritage SiGe couples, like shown in **Fig. 4 (left)**, is the ability to carry out reproducible diffusion bonding between various layers – (i) SiMo and $Si_{78}Ge_{22}$ and (ii) $Si_{78}Ge_{22}$ and $Si_{63}Ge_{37}$ layers. A significant loss in yield and reproducibility issues have been noted in the past, with conventional diffusion bonding processes during the fabrication of heritage uni-couples. **Fig. 4 (center)** shows a schematic of how we are investigating SPS for in-situ diffusion bonding between $Si_{78}Ge_{22}$ and $Si_{63}Ge_{37}$ layers; essentially, the two-layer stack is made in-situ thereby avoiding lower-yield subsequent diffusion bonding steps as in the heritage process. A hi-resolution image of the in-situ diffusion-bonded $Si_{63}Ge_{37}$/$Si_{78}Ge_{22}$ interface is shown in **Fig. 4 (right)**. While several studies have been carried out in SiGe SPS materials synthesis, production and their characterization, the work done here by APL is the first demonstration of unicouple level performance of direct relevance to the NASA Next Gen project. We first looked at shorter (~ 3 mm tall) SiGe couples – using P-type $Si_{78}Ge_{22}$ and N-type $Si_{78}Ge_{22}$ materials. To validate the higher efficiency, by operating the SiGe couple at higher T_{hot} where the higher materials ZT (**Fig. 3**) can be taken advantage of, we built taller couples, about 15 mm high although not same as the 20-mm height of heritage SiGe couples. These unicouples were evaluated between T_{hot}~985ºC and T_{cold}~100ºC. The summary of the data is displayed in **Figure 5**. The V_{oc} and power output as a function of T_{heater} appear good and a peak power ~425 mW was observed. The heat-to-electric conversion efficiency was estimated to be ~9% in good agreement with calculated efficiency based on material properties.

It is noteworthy that we estimate an efficiency of ~9% in the SiGe couples, reproducibly from successive devices.

We note that the power output of ~425 mW, in spite of higher predicted efficiency from higher ZT, is due to less heat flow in these couples from the lower aspect ratio (area/length) and thermal conductivity of the SPS SiGe materials. The aspect ratio of the couples studied here were lower than that typical GPHS-heritage SiGe couples; also the lattice thermal conductivity of the SPS SiGe materials are lower than those of heritage SiGe materials [3]; these two factors lead to less heat flow in the SPS SiGe couples. In the future, we plan to adjust the aspect ratio of the couples to be same as the GPHS-unicouples and study them for power production.

The well-behaved resistance of SiGe couple during testing from room temperatures to ~985ºC is noteworthy. The change in electrical resistance of the device with temperature is consistent with materials properties as a function of temperature and comparable to those of heritage SiGe devices.

4. Summary

We have shown that SPS SiGe materials, both P- and N-type, have thermoelectric properties that are attractive for GPHS-RTG applications. We have shown first device level demonstrations with the SPS SiGe materials. It is noteworthy that the initial estimates of efficiency of SPS-made SiGe couples could be in the range of 9% when measured between T_{hot} of ~985ºC and T_{cold} of ~100ºC. These can be compared to heritage SiGe unicouple devices with an efficiency in the range of 7.5%, when measured between T_{hot} of ~1025ºC and T_{cold} of ~290ºC. These efficiency values have to be viewed in concert with the differences in cold-side temperatures in these two cases and so no direct comparison can be drawn at this point; we are in the process of measuring the efficiency of SPS SiGe couples with T_{cold}~290ºC. Once successful lifetime assessments of SPS SiGe materials and unicouple devices are completed, they could potentially offer a near-term pathway to build SiGe unicouples required for near-term GPHS-RTG systems. Further, when the higher ZT and device efficiencies with SPS SiGe materials are validated, they could be a potential route for achieving higher Beginning of Life (BOL) and End of Mission (EoM) power outputs in GPHS-RTG power systems.

5. References:

[1] G. Bennett et al., Mission of Daring: The General-Purpose Heat Source Radioisotope Thermoelectric Generator, 4th IECEC 26-29 June 2006, San Diego, California.

[2] GPHS-RTG SiGe Couples, Report from GE/Lockheed Martin (1988).

[3] Ali Lahwal, S. Bhattacharya, Jian He, Di Wu, A. Peterson, S. J. Poon, L. Williams, A. Mehdizadeh Dehkordi, and T. M. Tritt, Impact of yttria stabilized zirconia nanoinclusions on the thermal conductivity of n-type Si 80 Ge 20 alloys prepared by spark plasma sintering, Journal of Applied Physics 117, 145101 (2015).

[4] S. Bathula, M. Jayasimhadri, N. Singh, A.K. Srivastava, J. PUlikotil, A. Dhar and R.C. Budhani, Enhanced Thermoelectric figure-of-merit in spark plasma sintered nanostructured n-type SiGe alloys, Appl. Phys. Lett. 101, 213902 (2012).

[5] Jing Li , Jun Han, Tao Jiang, Lili Luo, and Yongchun Xiang, Effect of Synthesis Procedure on Thermoelectric Property of SiGe Alloy, Journal of Electronic Materials, Vol. 47, No. 8, (2018).

[6] K. Romanjek, S. Vesin, L. Aixala, T. Baffie, G. Bernard-Grainger, and J. Dufourcq, High-Performance Silicon–Germanium-Based Thermoelectric Modules for Gas Exhaust Energy Scavenging, Journal of Electronic Materials, Vol. 44, No. 6, (2015).

Acknowledgement: The authors acknowledge the support of NASA Next Gen RTG Project and NASA/RPS Program Office for the development of SPS SiGe/SiMo materials and carrying out early unicouple device tests.

Nuclear and Emerging Technologies for Space
Sponsored by Oak Ridge National Laboratory, April 26th-30th, 2021.
Available online at https://nets2021.ornl.gov

MITIGATION OF ^{208}TL GAMMA DOSE FROM ^{236}PU DECAY CHAIN VIA CHEMICAL REMOVAL OF ^{232}U

Joshua Rhodes[1], Emory Colvin[2], Teyen Widdicombe[3], and Brad Kirkwood[4]

[1]*University of Tennessee Knoxville, jrhode19@vols.utk.edu*
[2]*Oregon State University, colvinem@oregonstate.edu*
[3]*University of Idaho, widd8527@vandals.uidaho.edu*
[4]*Idaho National Laboratory, brad.kirkwood@inl.gov*

Many spacecraft use radioisotope thermal electric generators containing ^{238}Pu to provide power to spacecraft systems and scientific instruments. Originally a byproduct of plutonium for weapons, new domestic production sources are being investigated. The High Flux Isotope Reactor is already producing some ^{238}Pu, but more is needed to meet NASA requirements. The Advanced Test Reactor is being considered. However, ^{236}Pu is produced as a contaminant, which has daughter isotopes that produce high-energy gammas. The SCALE 6.2 ORIGEN module was used to simulate mitigation of the hazards of ^{236}Pu through radioactive decay and chemical processing after aging.

I. INTRODUCTION

Most Radioisotope Thermoelectric Generator (RTG) powered spacecraft flown by NASA in the last few decades were powered by a GPHS (General Purpose Heat Source) RTG (Ref. 1). A stockpile of ^{238}Pu exists from these "golden days", which may be used for new fuel for the Multi-Mission RTG (MMRTG) (Ref. 2) but has decayed over the decades to around 80% ^{238}Pu, and so must be blended up with fresh (up to 95% ^{238}Pu) (Ref. 3) material to produce a fuel with a Beginning of Life (B.O.L.) power density consistent with the future requirements of the generator. The fresh material will contain a significant amount (parts-per-million) of ^{236}Pu as an impurity, which controls the gamma radiation dose rate from an RTG. The level of ^{236}Pu increases with the hardness of the flux used to transmute the neptunium source material. The prominent neutron reaction pathways of ^{237}Np are shown in Fig. 1.

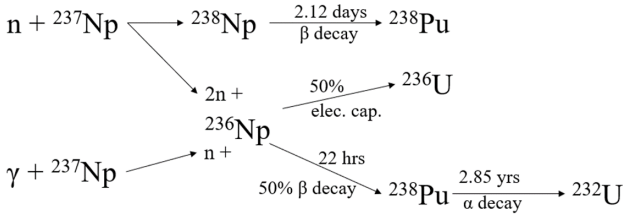

Fig. 1. Neutron Reactions with ^{237}Np. Note the (n,2n) reaction that leads to ^{236}Np, which decays to ^{236}Pu (Ref. 4).

The High Flux Isotope Reactor is already producing some ^{238}Pu, but more is needed to meet NASA demands. In order to meet NASA demand for ^{238}Pu, the Advanced Test Reactor (ATR) at the Idaho National Laboratory is being considered. The ATR has numerous core positions at differing flux levels which are to be used to produce the fresh ^{238}Pu, so it is at a variety of impurity levels when it leaves the reactor. Following the fresh ^{238}Pu extraction from the neptunium target, the ^{236}Pu impurity will decay over time to ^{208}Tl, which delivers a larger than acceptable gamma dose from 2.62 MeV gamma rays, and so poses a time-dependent risk to fuel handlers. In order to mitigate the dose from ^{208}Tl, the buildup of ^{208}Tl can be limited by chemical removal of the longest-lived daughter products of ^{236}Pu, ^{232}U and ^{228}Th.

I.A. Analytical approach

The Bateman equations are the traditional tool for finding secular equilibrium in decay chains (Ref. 5). However, they are cumbersome even for the simplest case of a single actinide decay chain with no initial daughters. The ^{236}Pu decay chain is shown in Fig. 2.

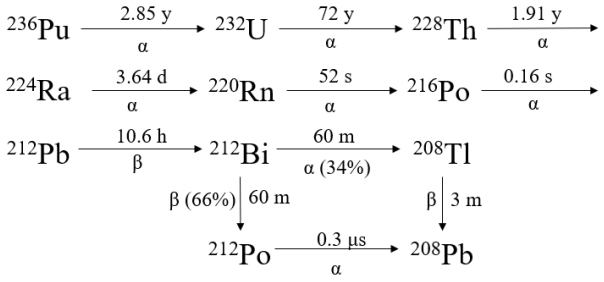

Fig. 2. ^{236}Pu Decay Chain (Ref. 6).

Though a case with zero initial daughters is easily tractable analytically, in the case of finite quantities of daughter isotopes the equations for an 11-member decay chain require about an order of magnitude more terms to describe. The complexity of this problem warrants the use of specialized software.

I.B. Computational Approach and Methodology

In order to simulate the decay and chemical processing of the ^{238}Pu fuel, the ORIGEN module of SCALE 6.2.3 was chosen. ORIGEN allows for the user to

model point irradiation, depletion, and decay calculations of several isotopes at once for varying time durations. Chemical processing can be simulated in ORIGEN by specifying how much of an element is retained between decay cycles (Ref. 7). For this work, each ORIGEN run will start with one gram of plutonium.

I.C. Simulated Processing Regimen and Variables

For this project, the following processing procedure will be considered. After the neptunium targets are removed from the ATR, the plutonium is separated and allowed to age for 150 days. The plutonium will then undergo the first processing for removing uranium and thorium. The plutonium will then be allowed to age again for a variable amount of time before undergoing a second removal process identical to the first.

The variables to be tested are the initial ^{236}Pu concentration, the aging time between the first and second processing, and the decontamination factor used for the removal of uranium and thorium. The ^{236}Pu concentration was varied from 1 ppm to 12 ppm. Aging times for the second processing range from one to eight years in one-year increments.

Anion exchange processes for separating out plutonium are capable achieving a decontamination factor of upwards of $2*10^4$ (Ref. 8). As chemical processing in ORIGEN is handled by specifying elemental fractions retained after processing, it is more convenient to discuss processing in terms of fraction removed. Higher removal may be necessary for achieving specifications. This project tests the removal fractions of 97%, 99%, and 99.99% removal of uranium and thorium Both processings were assumed to only remove uranium and thorium, retaining all other elements.

For this work, it is important to note that the specifics of the relevant chemistry and the necessary procedures were outside the scope. It is assumed that relevant facilities such as REDC at ORNL are able to achieve the removal fractions simulated in this project, such as the 99.99% removal for both uranium and thorium, as simulated here. Removal fractions of 97% and 99% are modeled to explore the importance of how much uranium and thorium are removed affects the ^{208}Tl activity in the final product.

I.D. Objectives

Using the above procedure, this project aims to find a combination of initial ^{236}Pu concentration, second aging time, and decontamination factor that produce a suitable product. The criteria for a suitable product are that the plutonium must have less than 1.7 µCi of ^{208}Tl per gram of plutonium, and the ^{208}Tl activity must stay below this threshold for at least two years. It is at this activity of ^{208}Tl that the 2.62 MeV gamma emissions are deemed excessive; staying below this activity for two years provides a two-year working window. A baseline material used for comparison is plutonium initially containing 2 ppm of ^{236}Pu that underwent only one processing with 97% removal. This material is shown in Fig. 3.

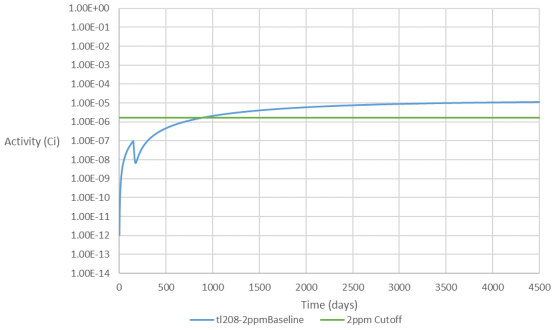

Fig. 3. 2 ppm ^{236}Pu Baseline

II. RESULTS AND OBSERVATIONS

Once each combination of variables was run in ORIGEN, the combinations of variables that provide at least two years of ^{208}Tl less than 1.7 µCi per gram of plutonium needed to be determined. In this section, the effects of ^{236}Pu concentration, the aging time for the second processing, and the removal fractions will be examined. Each of these parameters can affect the ^{208}Tl activity and how this activity changes over time.

II.A. Effects of ^{236}Pu Concentration

For a given aging time and removal fraction, as the concentration of ^{236}Pu is increased, the ^{208}Tl activity increases. This may seem obvious, but it is important to know the ^{208}Tl activity after the second processing in relation to the 1.7 µCi ^{208}Tl limit. If the activity of ^{208}Tl is above the 1.7 µCi limit before two years has elapsed after the second processing, then the aging time between the two processings was increased. These effects can be observed in Fig. 4 and Fig. 5.

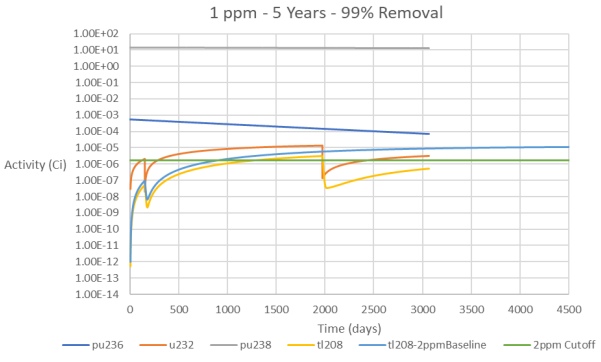

Fig. 4. 1 ppm Concentrations

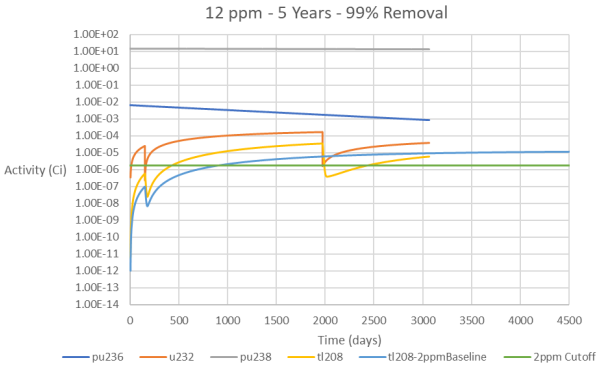

Fig. 5. 12 ppm Concentrations

II.B. Effects of Aging Time Before Second Processing

When observing the effect of aging time, it can be seen that as the plutonium ages, the isotope concentrations approach secular equilibrium. As the ^{208}Tl activity approaches secular equilibrium, the rate of increase in the concentration slows. Because of this, increasing the aging time for the second chemical processing may result in a slower ^{208}Tl increase, and result in a longer working window below the 1.7 µCi ^{208}Tl limit. These effects can be observed in Fig. 6 and Fig. 7.

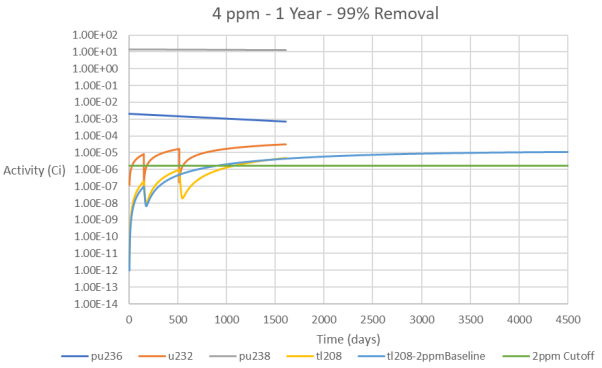

Fig. 6. 1 Year Aging Time

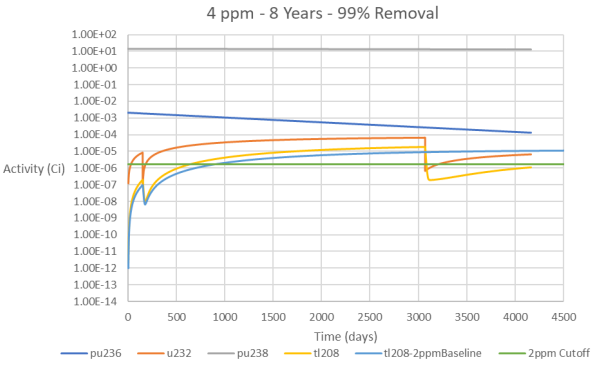

Fig. 7. 8 Years Aging Time

II.C. Effects of Increasing Uranium and Thorium Removal

Increasing the processing efficiency removes more ^{232}U and ^{228}Th, resulting in a lower ^{208}Tl activity in the final product. This is demonstrated when comparing the 97% and 99.99% removal factors. It can be seen that the 99.99% removal factor results in a lower remaining ^{208}Tl activity. It is also seen that the 99.99% removal factor results in the ^{208}Tl activity crossing the 1.7 µCi ^{208}Tl limit at a later time. These effects can be observed in Fig. 8 and Fig. 9.

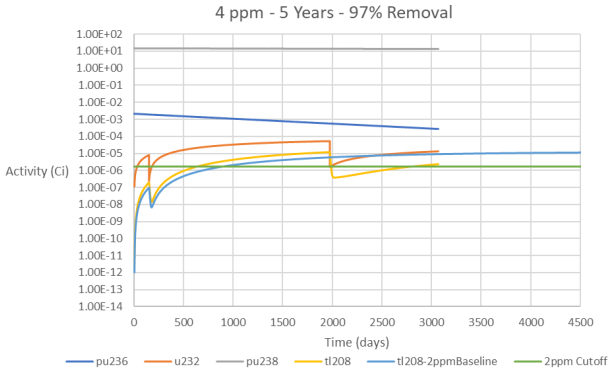

Fig. 8. 97% Removal of Uranium and Thorium

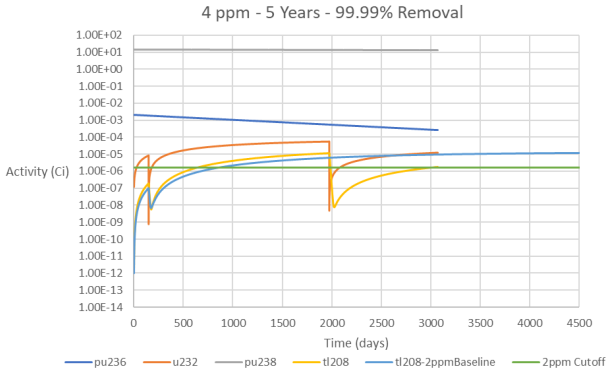

Fig. 9. 99.99% Removal of Uranium and Thorium

II.D. Analysis

When bringing the effects of these variables together, the results can be seen in Fig. 10. Notice that for a given ^{236}Pu concentration, increasing the decontamination will allow for a shorter aging time for processing. For a given aging time, increasing the processing efficiency will make higher ^{236}Pu concentration materials usable earlier. The highest ^{236}Pu concentrations (10 and 12 ppm) remained below the two-year 1.7 µCi limit only when using the 99.99% removal, and only after aging times of seven and eight years respectively.

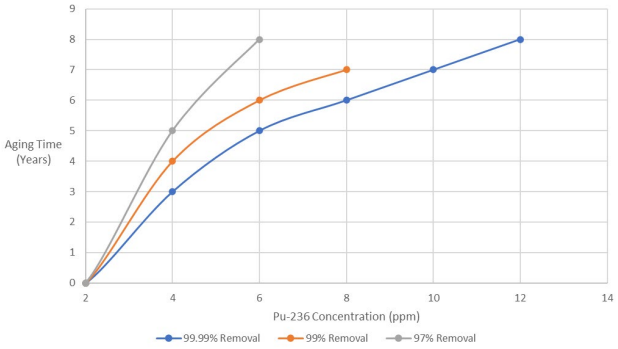

Fig. 10. Aging Time and Removal Fraction Required to make ^{238}Pu material Gamma Dose Acceptable.

III. CONCLUSIONS

After using ORIGEN to study the effects on ^{236}Pu concentration, processing aging time, and processing efficiency, it can be concluded that a higher processing efficiency and longer aging time are both important for ensuring that a given material has a two-year working window. This is important due to the potentially higher ^{236}Pu concentrations that are produced in positions of the ATR where the fast portion of the neutron spectrum is significant (Ref. 9). However, if the ^{236}Pu concentration is high enough, even with higher decontamination factors, the willingness to allow the plutonium to age for several years is a limiting factor. Quicker options may be preferred. Since the reactor facilities previously used to produce high purity ^{238}Pu are no longer available, and with limited availability of existing reactors, the use of a combination of two separation steps and appropriate aging time is the way to meet NASA's needs.

ACKNOWLEDGEMENTS

We would like to thank Dr. Steve Herring of CSNR for his assistance with this work. We would also like to thank the previous members of CSNR that contributed to this project.

REFERENCES

1. G. Bennett, J. Lombardo, R. Hemler, G. Silverman, C. Whitmore, W. Amos, E. Johnson, A. Schock, R. Zocher, T. Keenan, et al., "Mission of daring: the general-purpose heat source radioisotope thermoelectric generator," in 4th International Energy Conversion Engineering Conference and Exhibit (IECEC), p. 4096, 2006.
2. R. Bechtel, "Multi-mission radioisotope thermoelectric generator (MMRTG)," NASA Facts, 2013.
3. B. Burt, L. Carpenter, E. Colvin, S. Ercanbrack, J. Freilich, R. Herner, T. Kajihara, and J. Magnusson, "Optimization of Pu-238 production in the advanced test reactor," *Proceedings of Nuclear and Emerging Technologies for Space,* 2020, Oak Ridge, Tennessee.
4. J. E. Jones, "Process for Producing Ultra-Pure Plutonium-238". United States of America Patent US 6,896,716 B1, 2005.
5. H. Bateman, "The solution of a system of differential equations occurring in the theory of radio-active transformations," Proc. Cambridge Phil. Soc., 1908, vol. 15, pp. 423– 427, 1908.
6. G. Matlack., and F. Metz, "Radiation Characteristics of Plutonium-238," 1967. Los Alamos Scientific Laboratory.
7. B. T. Rearden, and, M. A. Jessee (Eds.). (2018, March). SCALE Code System. Oak Ridge National Laboratory.
8. J. D. Navratil and Y. Wei, "Actinide ion exchange technology in the back end of the nuclear fuel cycle," *Nukleonica*, **46**, 75-80 (2001).
9. INL/EXT-08-14709, "Advanced Test Reactor National Scientific User Facility User's Guide, Idaho National Laboratory, FY 2009.

Nuclear and Emerging Technologies for Space
Sponsored by Oak Ridge National Laboratory, April 26th-30th, 2021.
Available online at https://nets2021.ornl.gov

ONLINE MONITORING OF RADIOCHEMICAL PROCESSING STREAMS FOR THE PLUTONIUM-238 SUPPLY PROGRAM

Luke R. Sadergaski[1], Steven S. Schwengels[1], Lætitia H. Delmau[1], Dennis E. Benker[1], David W. DePaoli[1], and Robert M. Wham[1]

[1]*Oak Ridge National Laboratory, P.O. Box 2008, Oak Ridge, TN, 37831-6234: 865-574-1167, sadergaskilr@ornl.gov*

Online monitoring with spectrophotometry is being developed to improve the timeliness of analytical measurements for the Plutonium-238 Supply Program at Oak Ridge National Laboratory. A commercially available online monitoring software was used to calculate and view process data in real time to help identify process deviations and optimize system performance. Monitoring detailed process data will improve processing efficiency and help technicians make decisions during hot-cell operations.

I. INTRODUCTION

Plutonium-238 is being produced at Oak Ridge National Laboratory (ORNL) for National Aeronautics and Space Administration (NASA) space applications. Neptunium- (Np-) containing targets are irradiated at the High Flux Isotope Reactor (HFIR) to produce ^{238}Pu. Radiochemical separations such as liquid-liquid extraction and ion exchange chromatography are used to purify the ^{238}Pu product.[1] The program is scaling up production efforts to meet the NASA's need, which is 1.5 kg of plutonium(IV) dioxide (PuO_2) per year on average by 2025. The effort focuses on developing spectroscopic and real-time monitoring tools for rapid analysis and process feedback during radiochemical separations used for Np processing and purification of the Pu product.[2, 3]

Spectrophotometry, or absorption spectroscopy, is a technique that quantitatively measures the amount of light absorbed by a molecule as a function of wavelength. Absorbance is proportional to the concentration of a light-absorbing species and can be quantified using Beer's law when the optical pathlength and molar absorptivity of the substance is known.[4] This univariate approach breaks down in complex systems with overlapping absorption bands, shifting baselines, and dependencies on solution conditions.[5, 6] Multivariate data analysis (e.g., partial least squares regression [PLSR]) can be used to describe complex systems by correlating the entire spectrum (instead of a single wavelength) to the concentration of species in solution.[3, 7]

Spectrophotometry and the appropriate regression analysis can be used for timely analytical measurements in harsh environments, such as heavily shielded hot cells.[3, 8] Fiber-optic cables can transmit light for hundreds of meters and allow ultraviolet/visible/near infrared (UV-Vis-NIR) absorption measurements to be made in cells while personnel operate equipment in a control room. This enables spectroscopic measurements of materials located in the hot cells at the Radiochemical Engineering Development Center at ORNL without transferring samples out of the cells.[3]

The Unscrambler by Camo Analytics is a powerful software tool useful for multivariate data analysis. It can also be used to apply a variety of preprocessing methods (e.g., derivatives, smoothing, scaling) to spectral data to improve the analysis.[9] Multivariate models and spectral data transformations developed using the Unscrambler are automated with Process Pulse II (PP) by Camo Analytics, a commercially available online monitoring software. PP is compatible with numerous data sources and accessible to all users, including process engineers and technicians. In production Campaign 5, PP was evaluated during two full-scale Np monoamide solvent extraction (P5MX) and three plutonium anion exchange (P5AXPu) runs. A brief description of the software, key findings, and future work is discussed herein.

II. EXPERIMENTAL

The Unscrambler X (version 10.4) software package was used to develop a PLSR model. Spectra were mean normalized before PLSR analysis to equalize the influence of each variable. The model was optimized by minimizing the root mean square error of the cross validation. A Savitsky-Golay first derivative algorithm was applied to the spectra to remove baseline offsets and smooth the data.[9] The PP Multivariate Statistical Process Monitoring system by Camo Analytics (version 5.60) was used to automate univariate and multivariate calculations, view process variables, and notify staff when certain process conditions were reached. Ocean Insight spectrophotometers QE Pro and NIRQuest were used for UV-Vis and NIR absorption measurements, respectively. Spectral data were acquired as ASCII files using OceanView software (version 2.0.7). Hellma UV-Vis dip-probes with varying pathlengths (220 mm) and an Avantes 5 mm in-line flow cell were used. The halogen light (HL-2000 by Ocean Optics) and transmitted signals

were directed into and out of the hot cell using nearly 20 m of ThorLabs multimode SMA fiber patch cables (FG550LEC-Custom). Chemical reagents were commercially obtained (ACS grade).

III. PP DEMONSTRATION

Spectrophotometry is an important component of the ^{238}Pu Supply Program and is well-suited for determining Np and Pu concentrations in various oxidation state(s) in feed solutions and for monitoring separations. UV-Vis-NIR spectrometers collect spectra at relatively rapid intervals (e.g., 10 - 1,000 ms) and contain a wealth of information. The data are more intuitive for users to understand when converted to process variables, such as concentration. Converting spectra to process variables in real time assists users monitoring complex systems.

Most software/programing online monitoring options require a large investment upfront (i.e., mostly for customizing to a specific application) and extensive updates. PP is an "off-the-shelf" software package designed specifically for online process monitoring. The software has configurable dashboards where results are displayed in a choice of plots and alarms that are used to alert users of potential issues or action items. Software configurations were set up by research and development staff to monitor both P5MX solvent extraction and P5AXPu anion exchange column runs. Configurations included combinations of data sources, models, notifications, and output settings that can be used later by technicians to monitor these processes.

III.A. Neptunium Monoamide Extraction

During Campaign 5, the ^{238}Pu Supply Program used a monoamide-based extractant for the first time to separate recycled Np from most of the fission products. The recycled ^{237}Np will be refabricated into targets to make more ^{238}Pu. Spectroscopic measurements of the aqueous phase were used to ensure that Np was extracted into and stripped from the organic phase before exiting with the raffinate and unloaded organic solvent. Both UV-Vis and NIR spectral data were recorded using multiple dip-probes placed in the settlers of a mixer-settler liquid-liquid extraction system. Data from the entire run, which spanned multiple days, were viewable in interactive charts using the PP main view.

In this example, Np(V) and Np(VI) concentrations were measured in the stripped aqueous product stream (see Figure 1). A dip-probe was left primarily in one location to monitor the aqueous phase composition of the product stream to inform how Np was being stripped from the loaded solvent and to evaluate the system dynamics over time. The product concentration profile changed near the beginning of the run when process conditions were adjusted (see Figure 1). Periodically, the probe was moved to other stages to obtain bank profiles. These data are shown at discrete times in Figure 1 at concentrations above and below the relatively stable product profile. Concentration profiles were significantly different than expected based on calculations from a solvent extraction model. This further justified the need for a monitoring tool and revealed opportunities for studies to improve elements of the process model.

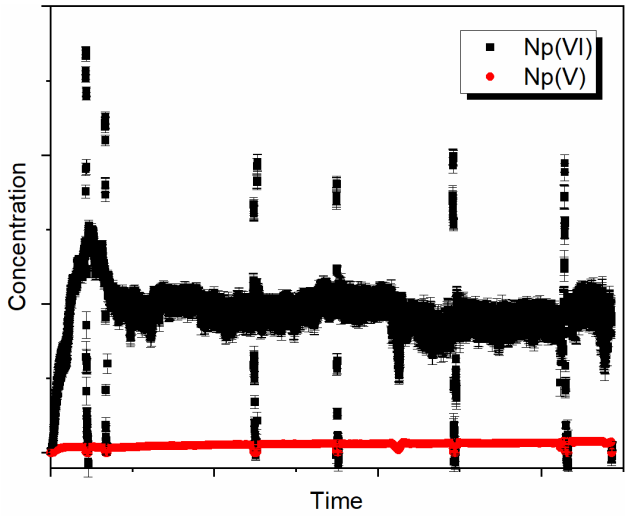

Fig. 1. Np(VI) and Np(V) strip bank concentration profiles. High- and low-concentration points correspond to stage profiles taken at discrete times during the operation.

The spectral data were corrected for baseline offsets using a linear baseline transformation and converted to concentration using Beer's law. The concentration of Np(V) and Np(VI) were determined using the 980 nm peak and the shoulder of the 1,220 nm peak, respectively. Molar absorptivity values were determined by comparing spectroscopic measurements at a given time with grab samples analyzed by inductively coupled plasma mass spectrometry (ICP-MS), which provided a pseudo-calibrated system. The absorptivity values agreed with published data.[6] Comparing the Np concentration measured by spectroscopy with the ICP-MS data revealed that this approach may have the potential to provide more than just trends and qualitative profiles, if desired.

Based on the feedback provided by online monitoring, flow rates were adjusted during the run to minimize Np loss to the raffinate and ensure complete stripping of Np from the organic solvent. This demonstrated the ability to evaluate and optimize the performance of solvent extraction runs. Future iterations of the software configuration will include notifications and action items to inform users when/if changes are needed.

III.B. Plutonium Anion Exchange

Plutonium anion exchange (AXPu) column runs are used to purify the Pu recovered by solvent extraction from the dissolved targets. AXPu runs remove phosphorus-containing contaminants (e.g., solvent degradation products), thorium, fission products, and most of the Np from the ^{238}Pu product. Np(IV) and Pu(IV) are converted to anionic complexes in high-concentration nitric acid, loaded onto a large column filled with anion exchange resin, and eluted with dilute nitric acid. Key analyses include identifying the Pu(VI), Np(V), and Np(IV) in the effluent and determining the appropriate time to collect the eluate as a Pu product cut. Determining the best time to begin collecting the Pu product is challenging and arguably the most important task. The decision is based on opposing factors: (1) maximizing the yield of Pu product per run, while (2) simultaneously minimizing the carryover of Np in the product. This allows the subsequent cation exchange runs to proceed efficiently and helps meet the heat source PuO_2 product specifications (i.e., Np in the total Pu product <0.5 wt%).

An in-line, flow cell was used to monitor the AXPu column with UV-Vis and NIR absorption spectroscopy. The concentrations of Np and Pu were predicted using a PLSR model. A multivariate approach was necessary to distinguish each analyte in the convoluted spectra. The PLSR model was developed using a representative set of training samples acquired from historical data from production Campaign 4. Spectra were manually deconvoluted by applying scaling factors to historical reference spectra and minimizing the residual difference between the sum of each contribution and the actual spectrum. This method assigned concentration values for each species and comprised the "concentration" response matrix (Y) while the unaltered spectral data represented the independent matrix (X). PLSR analysis was used to correlate the convoluted spectra to concentration by iteratively maximizing the covariance between these two data matrices. The explained variance, regression coefficients, and overall metrics suggested that it was performing well and could be used to describe the system. The prediction performance improved when a first derivative was applied to the spectra.

The Np(IV), Np(V), Pu(III), Pu(IV), and Pu(VI) concentration profiles were calculated and viewed in real time during each AXPu column run in Campaign 5. Examples from two of the runs are shown in Figure 2. The elution profiles for Np and Pu vary from run to run, with most of the Np eluting before the Pu. However, a significant portion of the Np tail is present while the Pu front elutes, which makes it challenging to optimize the product cut.

The software helped identify the appropriate time to start collecting the Pu product. The criteria for this decision limit were based on two parameters: (1) a predefined calculated Np/Pu ratio and (2) the total amount of Pu, such as Pu(III) and Pu(IV). Notifications appeared on the monitoring screen when process limits were exceeded and included relevant action items. These were also sent by text/email to staff members. The predicted Pu concentration results matched alpha spectroscopy results from the analytical group within ~10%. Models will be refined with data obtained at different acidities to match radiochemical analyses more closely.

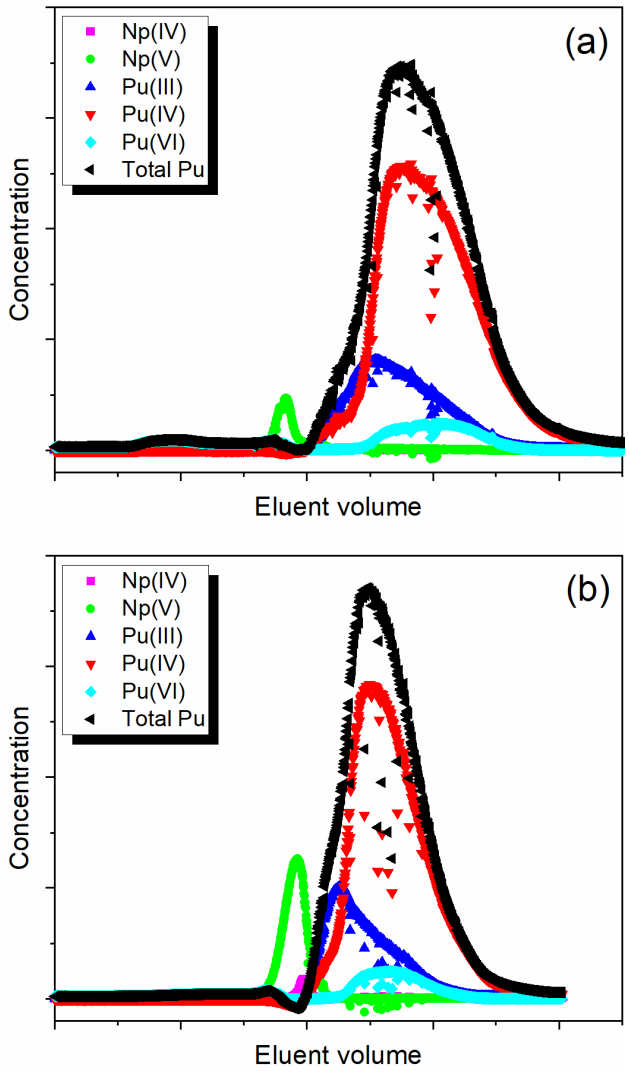

Fig. 2. Predicted Np(IV), Np(V), Pu(III), Pu(IV), and Pu(VI) and total Pu concentration profiles for the first (a) and third (b) column run.

IV. CONCLUSIONS

This work highlights a major improvement toward establishing an online monitoring capability for the ^{238}Pu Supply Program at ORNL. Spectroscopic measurements prompted operational adjustments to optimize run performance during solvent extraction runs and helped identify an optimal product cut decision in anion exchange column runs during hot-cell operations. The results indicate that real-time monitoring adds value to an essential part of the overall process and enhances the control of the radiochemical processing streams. Fully integrating PP will help close the gap between research and development and production by automating spectroscopic analyses. Future work will focus on optimizing configurations and training staff members who support processing to use this capability for routine analysis.

ACKNOWLEDGMENTS

Funding for this program was provided by NASA's Science Mission Directorate and administered by the US Department of Energy, Office of Nuclear Energy, under contract DEAC05-00OR22725. This work used resources at HFIR, a Department of Energy Office of Science User Facility operated by ORNL.

The authors wish to thank Nonreactor Nuclear Facilities Division technicians for their assistance with hot-cell operations and Chris Wightman for ICP-MS data.

REFERENCES

1. D. W. DEPAOLI, D. E. BENKER, L. H. DELMAU, E. D. COLLINS, and R. M. WHAM, "Progress in Chemical Processing for Production of Plutonium-238 from Irradiated Neptunium Oxide Cermet Targets," *ANS NETS*, Las Vegas, Nevada, February 26–March 1, American Nuclear Society (2018).
2. L. R. SADERGASKI, K. G. MYHRE, L. H. DELMAU, D. E. BENKER, D. W. DEPAOLI, and R. M. WHAM, "Spectroscopic and Multivariate Analysis Development in Support of the Plutonium-238 Supply Program." *ANS NETS*, Knoxville, Tennessee, April 6–9, 2020, DOE/ORNL (2020).
3. L. R. SADERGASKI, D. W. DEPAOLI, and K. G. MYHRE, "Monitoring the Caustic Dissolution of Aluminum in a Radiochemical Hot Cell by Raman Spectroscopy," *Appl. Spectrosc.*, **74**, 1252–1262 (2020). DOI:10.1177/0003702820933616
4. M. H. LEE, Y. J. PARK, and W. H. KIM, "Absorption Spectroscopic Properties for Pu(III, IV and VI) in Nitric and Hydrochloric Acid Media," *J. Radioanal. Nucl. Chem.*, **273**, 375–382 (2007). DOI:10.1007/s10967-007-6848-1
5. D. KIRSANOV, A. RUDNITSKAYA, A. LEGIN, and V. A. BABAIN, "UV-Vis Spectroscopy with Chemometric Data Treatment: An Option for On-Line Control in Nuclear Industry," *J. Radioanal. Nucl. Chem.*, **312**, 461–470 (2017).DOI:10.1007/s10967-017-5252-8
6. S. CHATTERJEE, S. A. BRYAN, A. J. CASELLA, J. M. PETERSON, and T. G. LEVITSKAIA, "Mechanisms of Neptunium Redox Reactions in Nitric Acid Solutions," *Inorg. Chem. Front.*, **4**, 581–594 (2017). DOI:10.1039/C6QI00550K
7. K. R. BEEBE, R. J. PELL, and M. B. SEASHOLTZ, *Chemometrics: A Practical Guide*, John Wiley and Sons, New York (1998).
8. R. LASCOLA, P. E. O'ROURKE, and E. A. KYSER, "A Piecewise Local Partial Least Squares (PLS) Method for the Quantitative Analysis of Plutonium Nitrate Solutions," *Appl. Spectrosc.*, **71**, 12, 2579–2594 (2017). DOI:10.1177/0003702817734000
9. J. GERRETZEN, E. SZYMANSKA, J. J. JANSEN, J. BART, H.-J. VAN MANEN, E. R. VAN DEN HEUVEL, and L. M. C. BUYDENS, "Simple and Effective Way for Data Preprocessing Selection Based on Design of Experiments," *Anal. Chem.*, **87**, 24, 12096–12103 (2015). DOI:10.1021/acs.analchem.5b02832

Nuclear and Emerging Technologies for Space
Sponsored by Oak Ridge National Laboratory, April 26th-30th, 2021.
Available online at https://nets2021.ornl.gov

HIGH ENERGY DENSITY TRTIUM BETAVOLTAICS FOR MEMS AND SENSOR DATA GATHERING APPLICATIONS

Chris Thomas[1], Marc Litz[1], and Third Author[2]

[1]*950 Danby Road, Suite 139, Ithaca, NY, 14850, 607-319-0268*
[2]*Some Other Street Address or Affiliation, City, State, Postal Code, Phone*

Primary Author Contact Information: 607-279-1065 and cthomas@widetronix.com

Betavoltaics are a significant power source alternative to Li-ion batteries, providing a pathway to higher energy densities and higher lifetimes per unit volume. In this report, we will give an update on the development of betavoltaics at Widetronix with emphasis on the use of tritium gas and titanium tritide as sources. We fabricate our own convertors using silicon carbide (SiC) and have designed and fabricated both planar and textured betavoltaic versions. Widetronix's planar betavoltaics have demonstrated 18% device efficiency. We will also present information on betavoltaic powered sensor data gathering circuits.

I. INTRODUCTION

Since the 1960's, semiconductor device evolution has been on a steady march towards smaller and smaller devices, first following Moore's Law, then More than Moore to get to today's die stacking technologies like 2.5D, 3D-IC, and, the latest, Chiplet stacking. Along the way, we have uncovered the techniques to fabricate MEMs sensors and to realize design ideas in nanotechnology and 2D materials. The semiconductor industry has also developed the skills to drastically reduce the power required for the operation of microcontrollers, of various sensors in infrastructure monitoring and cubesat monitoring, and for application specific integrated circuits (ASIC) in medical implants like pacemakers, hearing aids, and glucose meters. It is the ability to create these small, low power sensors and control circuits that is enabling the internet of things (IOT), the grand interconnection of all wired electronics, intelligent appliances, and anything that is controlled by software.

These mobile and embedded sensor systems have to be powered locally, and Li-ion batteries have mostly shouldered the burden of powering the initial evolution of these technologies. To fully realize the potential of networked sensor systems, however, higher energy density power sources will have to be matured or invented. While the rate of innovation of semiconductor devices and sensors has been rapid, a commensurate development of chemical battery technology has not been realized.

Betavoltaics are a unique power source alternative to Li-ion batteries. The titanium tritide ($TiT_{1.4}$) powered silicon carbide (SiC) betavoltaics made by Widetronix, Inc. have the potential to realize energy densities between 3.21×10^5 Wh/kg and 1.83×10^5 Wh/kg for 10 to 20 years lifetimes respectively. In this paper, I will report on the state of development of Widetronix, Inc. siC betavoltaics for the tritium gas source, the titanium tritide source, and the Ni-63 source.

II. TRITIUM GAS BETAVOLTAIC

Silicon carbide planar betavoltaic devices were designed and fabricated. The parameters of the planar betavoltaics have been described elsewhere in another publication. Two of the planar devices were mounted in a customized glass enclosure and two wires were bonded to each of their positive and negative contacts (Figure 1). The dark current-voltage (I-V) measurement was then made and the glass enclosure was fill with tritium gas at atmospheric pressure. Next, the I-V curves were measured to record the power produced by the device.

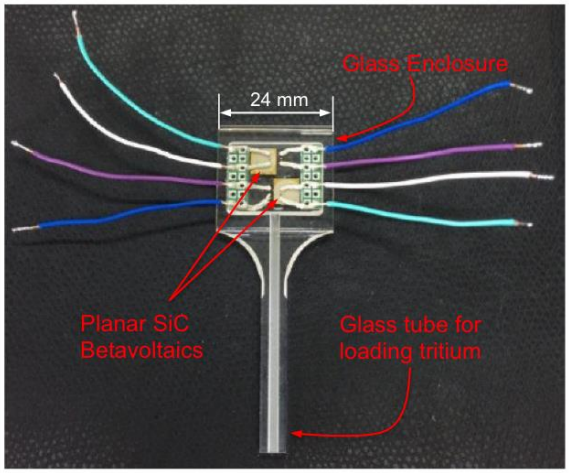

Fig. 1. Two Widetronix planar SiC betavoltaics were enclosed in a customized glass package. Tritium gas was then loaded at atmospheric pressure and I-V curve measurements were made.

The power output of the planar device due to betas from the tritium gas is shown in figure 2. The short circuit current is 50nA and the open circuit voltage is 2.01V.

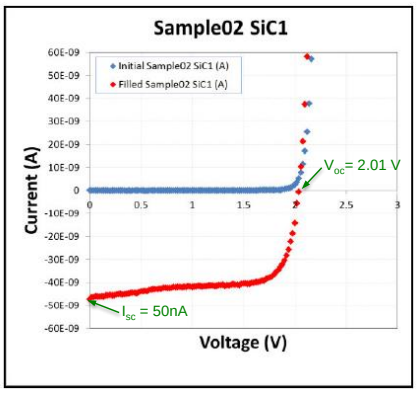

(a)

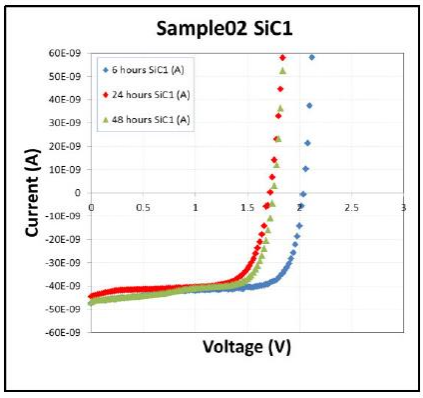

(b)

Fig. 2. Widetronix planar SiC betavoltaic (a) dark I-V and initial tritium power output and (b) the I-V measurements after 6, 24, and 48 hours. The open circuit voltage droped from 2.01V to avbout 1.7 V.

The I-V measurement were then repeated 6, 24 and 48 hours after the first one and the open circuit voltage was seen to shift form 2.01V to about 1.7 V. We will discuss why we believed this happened.

II. TITANIUM TRITIDE PLANAR BETAVOLTAIC

Planar betavoltaic device were mated with titanium tritide foils to produce power. The power output produced by a single 6mm x 6mm die with the foil is shown in figure 3. The foil used with this device was loaded with about 35mCi of tritium and the beta flux measured to determine the semiconductor efficiency. Widetronix routinely produces devices that are 18% efficient. These individual planar devices can be connected in series and parallel to produce larger power output devices as shown in figure 4. This device, DB-010, in the inset image has an open circuit voltage of 4.15V and a short circuit current of 326nA.

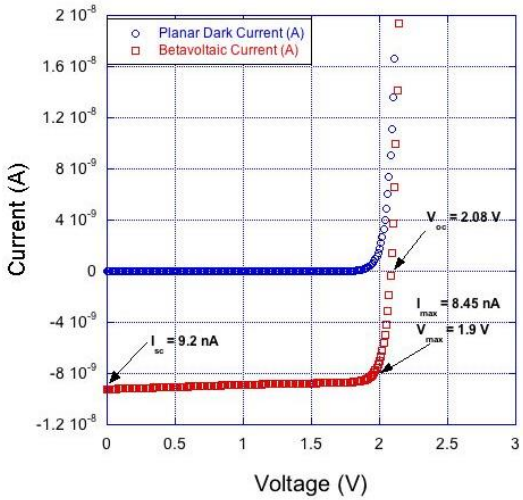

Fig. 3. Widetronix planar SiC betavoltaic with titanium tritide foil. The short circuit current is 9.2 nA and the open circuit voltage was 2.08V

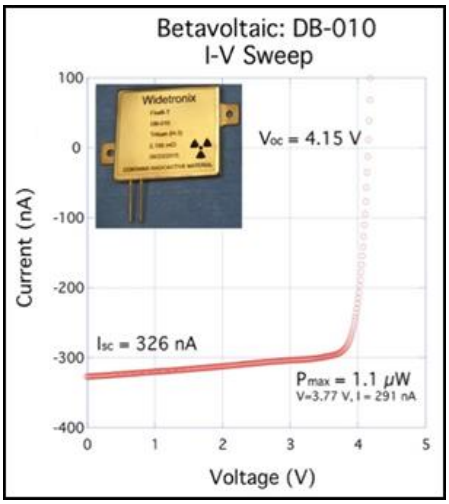

Fig. 4. Widetronix planar SiC betavoltaic packed in series and parallel to produce a battery that delivers 326nA short circuit current and a 4.15V open circuit voltage.

We will discuss the manufacture process for producing these devices.

III. TITANIUM TRITIDE TEXTURED BETAVOLTAIC

We will also talk about the current state of the textured betavoltaic development at Widtronix. Figure 5 shows the cross section of one of the devices.

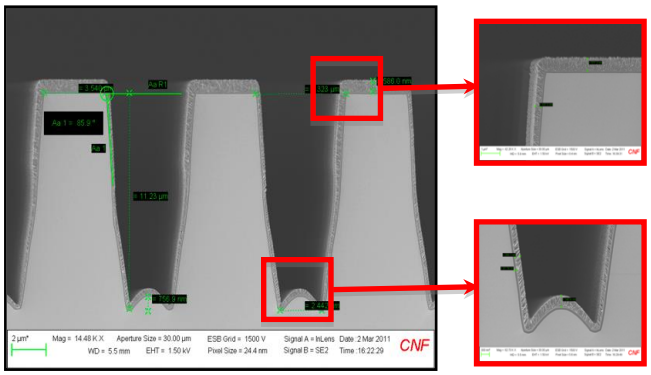

Fig. 5. Textured SiC betavoltaics with titanium metal deposited. The metal is subsequently loaded with tritium to make an active betavoltaic.

IV. TITANIUM TRITIDE PLANAR BETAVOLTAIC

We will introduce the sensor data board shown in figure 6. A 200nW betavoltaic is used to make a temperature measurement every 10 minutes and store the data on board. The data can then be retrieved by connecting a laptop to the board.

Fig. 6. Widetronix FireFli betavoltaic. It is made up of tritium isotope sources and SiC convertors.

Nuclear and Emerging Technologies for Space
Sponsored by Oak Ridge National Laboratory, April 26th-30th, 2021.
Available online at https://nets2021.ornl.gov

OVERVIEW OF RECENT PU-238 PRODUCTION ACTIVITIES AT IDAHO NATIONAL LABORATORY

Andrew Zillmer, William Green, Craig Tyler, Brian Gross, Erik Rosvall, Austen Fradeneck, Joshua Fishler, David Reeder, Ryan Marlow, Jagoda Urban-Klaehn, Michael Reichenberger, Mark Hill and Richard Howard

[1]*PO Box 1625, Idaho Falls, ID 83415*

Primary Author Contact Information: 208-533-7634; Andrew.zillmer@inl.gov

The Plutonium Fuel Services (PFS) program at Idaho National Laboratory (INL) is active in the qualification of irradiation targets containing Np-237 for irradiation in the Advanced Test Reactor (ATR) to produce Pu-238 for future NASA missions. INL qualified and loaded 7 targets in ATR's South Flux Trap (SFT) for cycle 169A, which occurred in Spring 2021. This program was reinitiated after two baseline production targets in three positions validated significant production of Pu-238 [ref.1]. The validation model was followed by the PFS-1 experimental test in the ATRC (Critical) facility [ref.2]. This paper outlines the progress and status of the PFS program. The qualification effort, safety analysis, hardware status, and future activities for qualification of an updated target design for use in the ATR will be discussed.

I. ATR IRRADIATION POSITION OVERVIEW

The INL team has qualified the I-7 and SFT (see Fig. 1) positions for the insertion of Np-237 targets. Both positions are large enough to accommodate 7 targets each. The current targets design is shorter than the length of the core and spacers are used to align the center of the targets with the center of the core and maximize Pu-238 yield.

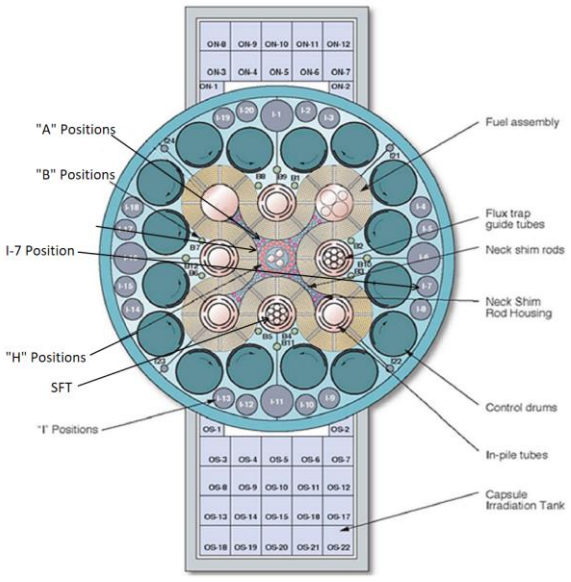

Fig 1. Section view of ATR

The "I" positions are outside of the main core and have a lower thermal flux of 1 to 9 x 10^{12} n/cm^2-s compared to 4.4 x 10^{14} n/cm^2-s flux traps [ref. 3]. This reduction in available flux negatively impacts the plutonium production rate, making in-core positions attractive from a programmatic standpoint. To achieve sufficient production from "I" positions the targets must be irradiated for approximately six cycles. The higher flux of the in-core SFT requires a single 60-day irradiation cycle to achieve production. This reduction in irradiation time is beneficial for achieving higher production of Pu-238 per reactor cycle. Therefore, more in-core positions will be pursued for qualification to support future production campaigns.

II. IRRADIATION QUALIFICATION DESCRIPTION

II.A Design Support

The ATR contains multiple irradiation sites with variable flux magnitudes and physical size constraints, making it a versatile and flexible facility for supporting PFS target irradiations. Many of these positions require an initial irradiation in a low power facility known as the ATR Critical (ATRC) Facility for safety. ATRC testing supplements analytical models to satisfy rigorous safety requirements. These and myriad other considerations, including availability and requirements for specialized tooling to handle targets down to 30 feet of water, led the project to first consider the medium I-7 position. This position has a relatively low flux outside the serpentine fuel core region and did not require preliminary ATRC irradiation. Therefore, limited irradiation assembly and tooling design was required to qualify the I-7 position. Later, the SFT position became available and was used with an existing housing, which also reduced new hardware design and fabrication efforts. SFT irradiations enable higher production rates than that of the I-7 position. Figure 2A shows the relative locations of these two positions. The SFT positions are partially surrounded by the serpentine fuel elements, which provide closer proximity and better exposure of this target position to the neutron flux.

Target qualification was initiated using existing target designs and, as feasible, existing hardware. Targets used for these initial irradiations are those developed for Oak Ridge National Laboratory's (ORNL's) High Flux Isotope Reactor (HFIR) [ref. 4]. Handling and axial location of the targets was accomplished by modifying

common basket designs and using spacers to axially align targets to the core midplane. Figure 2B shows an image of seven production targets installed in the SFT, preparing for irradiation in ATR cycle 169A in Spring 2021.

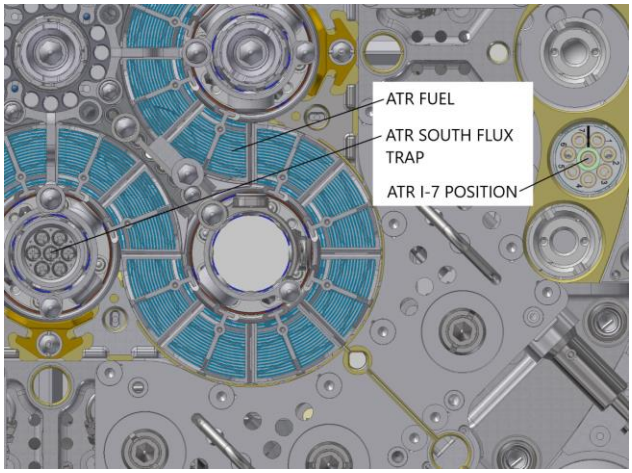

Fig. I-1. Relative Location of I-7 and South Flux Trap Positions

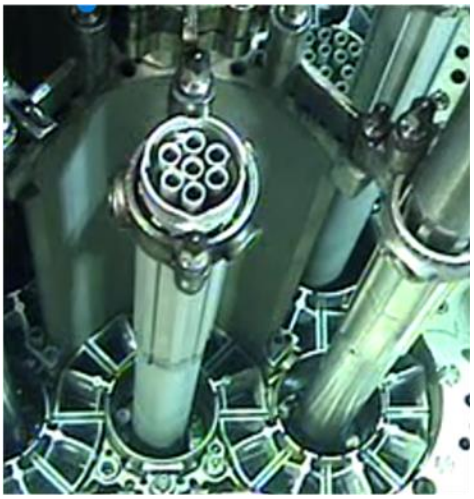

Fig. I-2. Photo, Installed South Flux Trap Assembly

All current and future target designs intended for ATR irradiation will require baskets, and specialized tools must be developed to carry out reactor insertion/removal, canal handling, storage, and transportation cask loading operations. Complete production and handling capabilities were developed in parallel with the initial I-7 and SFT irradiation hardware, including fabrication of a dedicated Battelle Research Reactor (BRR) cask and associated payload licensing to enable shipment of irradiated Pu-238 to ORNL for post-irradiation processing.

II.B Neutronics Qualification

Qualifying experiments for irradiation in ATR require the integration of various teams to create the appropriate models and analyses. This process begins with a neutronics analyst building a model (see Fig. 2) that reflects the computer aided design (CAD) rendering developed by a design engineer. The expected ATR operational parameters must be assumed to estimate the irradiation induced heating and reactivity generated by the experiment because ATR operational time and power varies from cycle to cycle. These assumptions are generally decided to bias the model in a more conservative (safer) manner because they yield derived parameters that demonstrate experiment compliance with the ATR safety analysis report (SAR). Monte Carlo N-Particle (MCNP) is the analysis tool used to perform these calculations. Material activation and depletion calculations are performed with ORIGEN and use MCNP generated neutron flux and cross section data as ORIGEN inputs.

A baseline requirement of a 60-day cycle was used for the PFS target assembly simulation. In the SFT case, the amount of Pu-238 yield from the seven targets was estimated to be on the order of 30 grams total. This amount is slightly more than twice the amount estimated to be produced in seven targets in the I-7 position of ATR in one fifth the time. Irradiation of all fourteen targets is expected to be completed in April 2021.

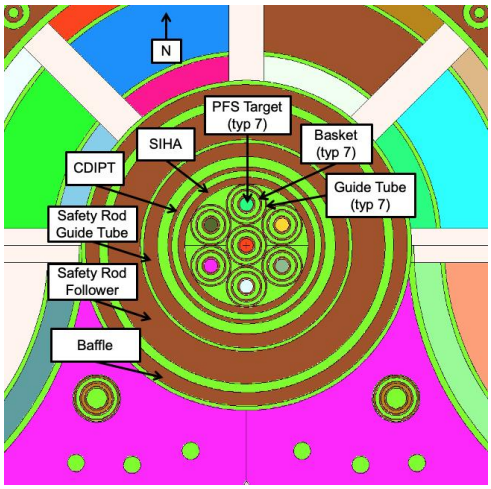

Fig. 2. Cross-sectional view of MCNP model of PFS assembly in ATR south flux trap

II.C Thermal Qualification

Thermal qualification was dependent on the neutronic qualification and involved several iterations to assure safety. The goal of the iterative analysis was to prevent capsule failure from overheating and to calculate the minimum required cooling time post-irradiation. This analysis was executed using RELAP5-3D and ABAQUS. RELAP5-3D simulates thermal and hydraulic phenomena using a finite volume methodology, whereas ABAQUS employs finite element analysis.

The RELAP model (see Fig. 3) describes the hydraulic volumes through which coolant flows. Energy generated/input into the system is accounted for via heat

structures attached to these flow volumes (see Fig. 4). Heat generation rates (HGRs) resultant from the neutronics analyses for fuel, structural, and coolant materials are modeled using a one-dimensional conduction model. Energy is then advected into the coolant flow volumes. A similar model was built to describe thermal and hydraulic behavior during flow stagnation and reversal.

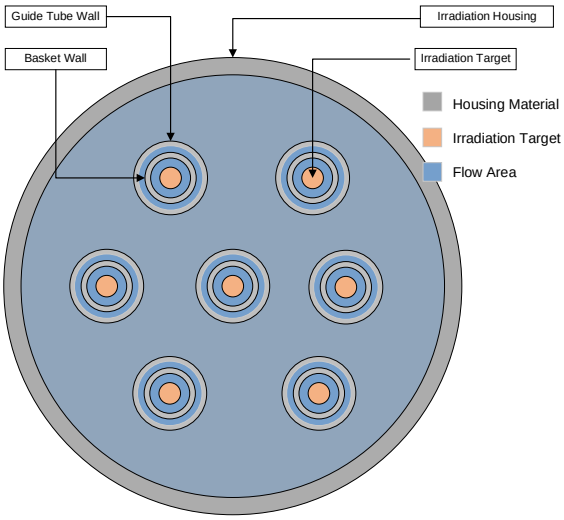

Fig. 3. Cross sectional view of the hydrodynamic system modeled using RELAP4-3D.

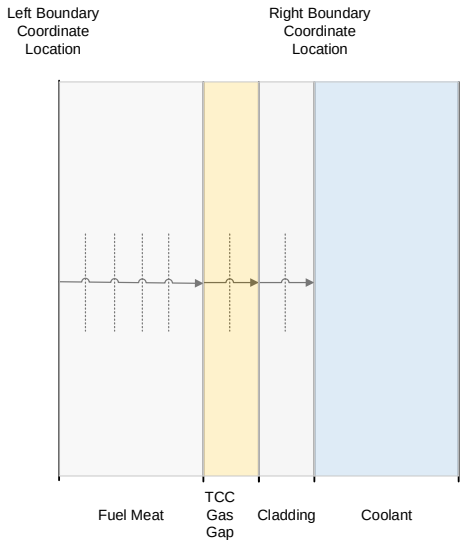

Fig. 4. Radial view of the conduction network modeled in RELAP5-3D.

Several finite-element models were developed in ABAQUS to assess the thermal performance of the PFS experiment in the SFT of the ATR. Component heat generation rates and flow conditions for each model are provided from preceding reactor physics (MCNP) and hydraulic (RELAP) analyses, respectively. Uncertainties in the modeled heating rates due to operational lobe power, instrument measurement error and outer shim control cylinder rotation are accounted for with a safety factor multiplier. The thermal/hydraulic conditions for each model are modified to represent normal operation and possible accident scenarios in the ATR. To meet the safety requirements for operation in the ATR, the minimum departure from nucleate boiling ratio (DNBR) and flow instability ratio (FIR) for each scenario must be greater than 2. In addition, the peak temperatures of the irradiated components must remain below their respective melting points. The limiting thermal case is a reactivity insertion accident caused by a large pipe break (RIA4). The resulting temperatures from the finite-element model in the case of a RIA4 event are shown in Fig. 5. The maximum temperatures of the NpO_2-Al cermet pellets and Al-6061 cladding are maintained below their respective melting points (estimated conservatively at 660 and 585°C), while the minimum DNBR and FIR values are 2.2 and 3.9, respectively.

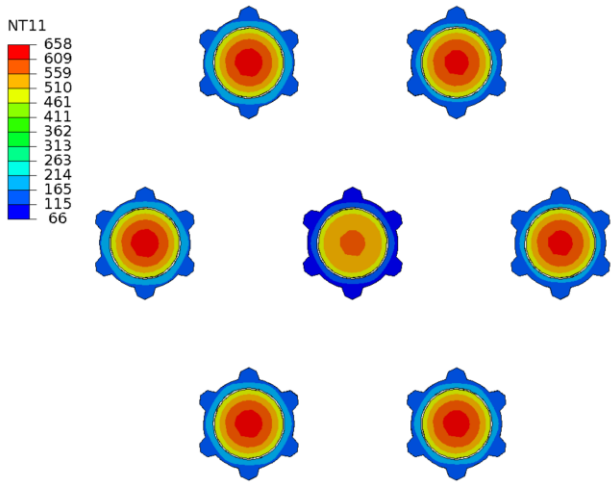

Fig. 5. Radial distribution of nodal temperature values of the NpO_2-Al cermet pellet and Al-6061 during a condition 4 reactivity insertion accident (RIA4).

II.D Structural Qualification

The purpose of the structural safety analysis was to evaluate the target and its associated hardware under various potential loading scenarios to ensure the safety of operational personnel and the public. The loadings considered in this evaluation while within the ATR included the following: internal pressure within the target due to the release of fission gas, external pressure, external pressure differential acting on the length of the assembly, pressure and skin friction drag forces due to coolant flow velocities, flow induced vibrations, thermal

loads, and cyclical loads. Other loadings, such as handling loads from transferring components to and from the reactor, were also considered. The decision for which loading scenarios had to be evaluated in the structural analysis was based upon the probability of the event occurring and the desired state of the structural components after each event. These events include: normal reactor operation, a flow coastdown event due to loss of commercial power, a reactivity insertion accident for in-pile tube voiding, overpressure, and a loss of coolant accident. Events with extremely low probability of occurrence and those where the loss of pressure boundary integrity meet the safety limits, defined by INL's SAR, were excluded from the structural evaluation.

The response of each structural component (i.e., stress, strain, deformation, etc.) under the various loading conditions was calculated using, where simplifications could be made, hand calculations or, where simplifications could not be made, the finite element software *Abaqus*. These responses were compared to acceptance criteria. For the non-pressure retaining components, this criterion was typically the yield strength of the material at given temperature. Due to the potential of fission gas release, the target was treated as a pressure vessel. Acceptance criteria limits defined in the American Society of Mechanical Engineers (ASME) Boiler and Pressure Vessel (B&PV) Code were used. Though other acceptance criteria could be used, this code was used because it provides a nationally accepted design/analysis approach which INL has applied and adapted to various nuclear experiments. Based on the low internal pressure of the target (240 psig), the requirements of ASME Section III, Class 3 vessels were used as a guide. This code defines these limits based on Design and Service Levels. Following the design specification of the ATR, which categorizes these loading scenarios into Service Levels, the response of the target resulting from each load scenario was compared to the corresponding limit in the code. Each structural component met the safety requirements and was permitted for irradiation in the ATR.

II.E. ATRC Planning

Initial irradiation testing of Np-237 was carried on NpO_2 sensors in the ATRC (Critical) reactor, which is a low power copy of the ATR at 600 W vs 110 MW. The Pu-238 production was estimated from the intermediate short-lived product Np-238, which produces characteristic gamma rays in the range 900 – 1040 keV. The measurements of these gamma rays after 20 minutes of irradiation showed production rate at 10% higher than predicted from modelling at 1.01×10^{-2} μCi/mg. This value is in agreement with an earlier trade study that predicted assay value (Pu-238/total Pu) as high as 98% for "I" positions after one year [ref.2]**.**

II.F SAFETY ANALYSIS AND DOCUMENTATION

An experiment safety analysis (ESA) was developed for both the PFS experiment in the I-7 and SFT positions. Both ESAs demonstrate the PFS experiments' irradiation in the ATR is in compliance with the requirements of technical safety requirements and the approved authorization basis established by ATR's Safety Analysis Report. The ESAs were developed and authorized under an ATR Complex procedure that addresses experiment receipt, reactor loading, irradiation, discharge, storage, preparing for shipping from ATR, and waste disposal. The PFS ESAs concluded that operation of the PFS experiments were in accordance with the restrictions identified in the ESAs and within the authorization basis of the ATR.

III. OPERATIONS

III.A ATRC Irradiation

PFS targets was irradiated at extremely low power in the ATRC facility to ensure safety of the targets prior to full power irradiation in ATR and is shown in Fig. 6.

Fig. 6. ATRC facility personnel remove and arrange irradiated flux wires for analysis

III.B. Target Unloading

PFS-3 Targets are shipped from Oak Ridge National Laboratory to INL's Advanced Test Reactor Complex individually in drums. The targets were then unloaded from the shipping drums and taken the ATRC facility for preliminary irradiation. This activity is shown in Fig.7.

III.C Target Assembly & Loading

After completion of the ATRC test run, the targets were then transferred to the ATR canal for configuration prior to insertion in ATR, shown in Fig 8. The assembly is then transferred under water by ATR Canal Operators to the ATR drop chute. ATR reactor top operators are then able to retrieve the assembly from the inner vessel side of the drop shute. The PFS target assembly is then inserted into the south flux trap and inventoried to ensure that it is properly seated into the chopped dummy in-pile tube.

Fig. 7. ATR Personnel remove a PFS-3 target from the shipping drum while monitoring radiation levels.

Fig. 8. ATR Canal Operators load a basket containing a PFS target into the South Irradiation Housing Assembly

IV. FUTURE WORK

The INL team is currently working to qualify several ATR positions with an updated target design. This new target design will have a full length of the ATR core, but it will be comprised of two targets stacked on top of each other Having a top and bottom target is desirable because it simplifies processing of the Pu-238 from the targets in hot cells at ORNL.

INL plans to initially qualify the Northeast Flux Trap (NEFT), Inner A positions, and H positions. Later, the B positions, South Flux Trap, and East Flux Trap will be qualified. The low flux in the I-Positions results in a low production rate, which makes them the lowest priority position to qualify.

TABLE I. ATR Locations and Number of Positions

Column Header	Positions in Target	# of Locations in ATR
NEFT	23	1
Inner A	1	8
H Position	1	14
B Position	1	8
South Flux Trap	7	1
East Flux Trap	7	1
I Position	1 to 7	23

II. CONCLUSIONS

INL's work on Pu-238 production in ATR has qualified the South Flux Trap for ORNL supplied targets and will significantly speed up the production process. Seven targets were characterized by an ATRC run and inserted into the SFT for irradiation in ATR cycle 169A These targets, as well as several targets being irradiated in the ATR I-7 position are expected to produce several 10s of grams of Pu-238. This material will be sent to ORNL for post-irradiation processing in 2021. The recovered Pu-238 will be ultimately used to fuel for radioisotope thermal generators in future space exploration missions.

ACKNOWLEDGMENTS

This work was funded through DOE & NASA Interagency Agreement # NNH19OB05A and DOE contract DE-AC05-00OR22725.

The authors would like to thank Trevor Skeen and Kurt Lombard for their operational support; Doug Crawford for initial thermal engineering support, Joshua Peterson-Droogh for technical check support, Misti Lilo for technical management, and Nathan Manwaring for help with preparing qualifying ATRC experiments.

REFERENCES

1. J. Navarro, C. Biebel, et al Trade Study to Access Pu-238 production in ATR Large-I, Medium-I, and NEFT Positions Using 20% Np-Al or Pure Np. Oxide Targets. INL/LTD-17-41273
2. J. Urban-Klaehn, D. Miller, B. J. Gross, C. R. Tyler, C. D. Dwight, "Initial Phase of Pu-238 Production in Idaho National Laboratory", *Applied Radiation and Isotopes*, 169 (2021).
3. W. Skerjanc, William & G. Longhurst. Gas Test Loop Facilities Alternatives Assessment Report. (2021).
4. R. Howard. Overview of the Plutonium-238 Supply Program's CERMET Production Target. United States: N. p., 2019. Web.